ANNALES
UNIVERSITATIS SCIENTIARUM BUDAPESTINENSIS DE ROLANDO EÖTVÖS NOMINATAE

SECTIO GEOLOGICA

TOMUS XIX.
1975

REDIGUNT
B. GÉCZY
J. KISS
L. STEGENA

BUDAPEST
1975

ANNALES
UNIVERSITATIS SCIENTIARUM BUDAPESTINENSIS DE ROLANDO EÖTVÖS NOMINATAE

SECTIO BIOLOGICA
incepit anno MCMLVII

SECTIO CHIMICA
incepit anno MCMLIX

SECTIO GEOLOGICA
incepit anno MCMLVII

SECTIO GEOGRAPHICA
incepit anno MCMLVII

SECTIO HISTORICA
incepit anno MCMLVII

SECTIO IURIDICA
incepit anno MCMLIX

SECTIO LINGUISTICA
incepit anno MCMLXIX

SECTIO MATHEMATICA
incepit anno MCMLVIII

SECTIO PAEDAGOGICA ET PSYCHOLOGICA
incepit anno MCMLXX

SECTIO PHILOLOGICA
incepit anno MCMLVII

SECTIO PHILOSOPHICA ET SOCIOLOGICA
incepit anno MCMLXII

METHOD FOR A COMMON EVALUATION OF PETROGRAPHICAL AND PALEONTOLOGICAL INVESTIGATION OF DETRITAL SEDIMENTARY FORMATIONS

J. ANDÓ

(Department of Petrography and Geochemistry, L. Eötvös University, Budapest)
Received: 10 October 1975

РЕЗЮМЕ

Состав некоторого пространства отложений, свойства его отдельных составляющих и петрологические характеристики накопившихся отложений определяются в основном теми же самыми физическими и химическими параметрами. Этот факт обусловит принципиальную основу для совместной интерпретации результатов петрологических и палеонтологических исследований фаций. В качестве основы для совместного исследования можно взять выявление гидродинамического характера среды переноса и отложение вещества и физического состояния области отложения. В качестве петрологического метода может быть применено исследование диаграмм логарифмической вероятности распределениы зёрен. С помощью этого метода легко могут быть определены свойства движения обломков, характерных для более ранных районов накопления, размеры по разному накопившихся зёрен, а также и их количественные пропорции. Эти характеристики обосновывают выводы относительно характера и интенсивности движения воды а также и консистенции области отложений. Палеонтологический метод исследования опрается также на определение в основном этих характеристик, следовательно, два упомянутых метода могут быть применены параллельно. В работе приводится совместная интерпретация двух методов исследования фаций, на примере обработки материала с профилей обломчатых отложений третичного периода в районе гор Черхат (Северная Венгрия).

Introduction

Existence and development of living organisms is inseparable from the physical-chemical state of their environment. These factors determine by and large also the processes taking place after their fading away and after their embedment. In the case of hydrobiosphere the lifeless environment is mostly represented by the sediment-collecting terrain and/or by the medium transporting and depositing the sedimentary matter. So the composition of the biocenosis, the features of the individual member as well as the petrographical character of the matter accumulated within the environment of the given biotope, respectively of the matter deposited out of the given medium will be influenced by and large by the same characteristics of state. Thus we may well expect a close connection between faunistical, floristical and sedimentological features and this is supported also by the study of sediment-collecting terrains, respectively life-spaces of tody.

Salinity, temperature, as well as the transillumination are influencing significantly the biocenosis, thus usually they can be well reconstructed from the analysis of the latter. The connection between these factors and the petrographical features of the detrital formations is rather loose and it is more difficult to be investigated. For the structure of the surrounding dry land as well as for its crustal constructional state one can get information from the mineral composition and from the shape and size of grains. Such immediate informations are seldom provided by the paleontological material, thus in

this connection a parallel study of paleontological as well as petrographical features presents certain difficulties. Organic life as well as the sediment accumulation is significantly influenced by the life space, respectively the *hydrodynamical, energetical* features of the detritus depositing or transporting medium. Since it is in immediate connection with the water depth, with the distance from the shore and with the morphology, i.e. with the factors basically influencing the paleontological and petrographical character of a sedimentary formation developing at a given place, the investigations of facies particularly emphasize the reconstruction of this characteristics.

The paleoecology – investigating the features of form, frame structure, feeding, positioning and change of place of the one-time biocenoses – draws conclusions – among others – to the water movement, the consistency of the sediment, the intensity of transport of detritus and in way this to the mentioned environmental conditions. A similar aim is pursued by the petrographical facies-investigating methods making use also of these characteristics in connection with the hydrodynamical-energetical features.

Neither the paleontological, nor the petrographical facies investigations are able to eliminate certain sources of error stemming either from principle or practice, which can weaken the value of the conclusions drawn in various manner. The effectivity could be improved by a simultaneous application of several paleontological and petrographical facies investigating methods taking into account various aspects and so complementing each other. Nevertheless, very little progress has been made up to now in this direction, especially concerning detrital sedimentary formations. Paleoecologists are attributing a great significance to the petrographical features, but in the course of their works they seldom go beyond such general statements, as "sandy", "clay", "slity" etc., or beyond a mechanical documentation of grain distribution investigations. The cause for this is lying in the imperfections of the possibilities provided by the petrographical investigating and evaluating methods. Thus far, no such evaluation method has been gaining ground, which could easily be implemented, consequently could have a widespread application and which would support the paleoecological partial results by means of individual sedimentological data. The petrographical methods used thus far – providing often rigid results of final conclusional character – are hardly to be used for such a purpose.

Basic principles of the possibility of joint paleontological and petrographical facies-investigations with common point of view

On the basis of what was outlined above it is clear that common aspect of paleontological and petrographical facies analysis may be the investigation of the hydrodynamical character of the transporting and depositing medium and that of the physical state of the sediment collecting terrain. A grain distribution investigating method well to be used for this purpose was discussed earlier by the author (J. Andó, 1973), so that here only ist basic principles will be given.

Based on a detailed investigation of the grain-size distributions Doeglas, D. J. (1964), then Pettijohn, F. J. (1949) realized that these can be broken up into two or more partial distributions – populations – formed by different transportand sedimentational conditions. The explanation of this connection by physical and hydrodynamical notions is due to Inman, D. L. (1949). He stated that the transport of detrital grains has three main forms: a surface slipping-rolling, a saltatory and a suspension – form. The individual grain groups representing the single transport-deposition- forms show lognormal distributions, so that on the distribution diagram showing lognormal probability values they present themselves as straight sections of the composit distribution curve. This sections are characterized by different slopes

– due to the different energetical and classifying features of the factors forming the individual populations – thus they can well be separated (Fig. 1.).

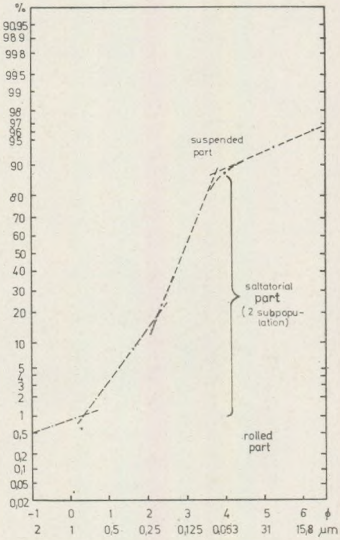

Fig. 1. Log-probability distribution of transport-sedimentary grain components

In the domain of greatest dimensions we find the population representing the material transported by rolling. This portion – being absent in cases – is usually represented by a single section of straight line. Within the domain of smaller dimensions the distribution section represents the grains transported by saltations and this classifies itself into one or two subsections. The bipartite saltatory population is characteristic to the littoral flat-shore terrain. Its development can be explained – also according to the recent experiments of K o l m e r J. R. (1973) – by the periodically changing direction of the water movement prevailing here, which is – as it is widely known – of a variable transporting and classifying capacity. The sedimentary material in suspension produces a straight line section of distribution in the domain of fine grains (Fig. 1.).

Thus using this method one can determine the character of the movement of detritus corresponding to the environment of the one time accumulation terrain and the dimension of the grains deposited in the various ways, as well as their shares in quantity. (V i s h e r, G. S. 1969) From these indicators we can draw conclusions regarding the character of water movement, its intensity, the consistency of the sedimentary terrain and its debrismaterial content. The paleontological investigation

methods also largely rely on the determination of environmental conditions (L. Bogsch, 1968, T. Báldi, 1973).

For the appearence of *epifauna* a relatively rigid bedding is needed, the development of which is possible only above a certain grain size. Water flowing with a critical speed corresponding to this greater grain size (J. Bogárdi, 1971) transports away most part of this detrital material, so the rate of sediment accumulation becomes lower. In a water with strong mobility the material transported by suspension and partly also that transported saltatorily is of uniform distribution, the concentration of the detrital grains – indicating a tendency towards deposition – is slight. All this results in a clear water enabling at the same time an alimentation with *filtering of suspension*. These conditions are indicated on the log-probability cumulative grain distribution curve by the prominent appearence of the section corresponding to the rolled component.

For the existance of *infauna* the presence of a more loose, finely grained sediment is necessary which enables the living beings to dig themselves in to the basement. In this framework we can make further refinements regarding the environment of the one-time living-space basing on the analysis of the way of feeding. The presence of the suspension-filtering infauna is characteristic of a flowing, clear water environment. Under such conditions the basement is made of a sediment with medium grain size and eminently rolled as well as saltated parts the role of the suspension grain population, however, is becoming more and more apparent.

To the way of life of the silt devouring infauna a sediment rich in organic matters is necessary. The accumulation of this may take place in a slightly aerated and moved water from a very fine grained suspension. Thus these formations are characterized by a grain distribution with high proportion of suspension parts.

The organisms digging themselves into the sediments and especially the silt devouring ones in the course of their life-functions are stirring up and intermixing the debris deposited in the various levels (bioturbulence). Owing to this the grain distribution being originally corresponding to the existing hydrodynamical features may be distorted and a mixing up of the single grain populations can be observed. This is indicated by the rounded off parts of the curves at the intersections of the straight sections representing the various types. In case of a more strong mixing and reaccumulation – e.g. in case of a drastic matter-rearrangement characteristic to the turbidites – one can not draw any conclusion to the primary accumulation terrain on the basis of the grain distribution. In that case the facies investigations may rely first of all on characteristics of the rockstructure and stratification.

With these we have outlined the general connections only; for the solution of paticular problems detailed, individual analysis are needed. According to the above discussed principles the method can be applied of course only in case of a simultaneous paleographical and petrographical sampling. We have to make efforts – especially in case of finely or

rhitmically layered sedimented complexes – to provide samples with as small a time unit as possible, i.e. samples representing as homogeneous developing conditions as possible.

Complex facies investigation of the loose sandstone series of Iliny

The possibility of a common valuation of paleontological and petrographical points of view will be shown on the example of the investigation of the fine sand complex from the surroundings of Iliny. Regarding the stratigraphical conditions of this formation – as well as regarding all the sedimentary series of the Northern–Cserhát – no uniform attitude has been taken for a long time in the relevant technical literature (I. Ferenczi, 1939, F. Horusitzky, 1939, J. Noszky sen., 1940). The removing of contradictions has been made possible only by the recent faunistical- stratigraphical (T. Báldi – M. Horváth, 1971, M. Horváth, 1972, T. Báldi, 1973) as well as by the petrographical invetigations (I. Kubovics – J. Andó, – Mrs. Nagy, J. Balogh–Mrs. PécsiÉ. Donáth–J. Rózsavölgyi, 1971). According to T. Báldi the upper Oligocene (Egerian) containing in the Western–Cserhát mostly shallows sublittoral, reduced salt-watery and littoral intercalations towards east turns step by step into a medium-deep-sublittoral, shallow bathyal facies. Westwards, after the development of a fine-grained as well as coarse-grained, aleuritic sandstone of the Oligocene a turning into continental land is encountered – owing to regressional tendencies – while Eastwards – on the deeper parts of the sedimentary basin we can see a continuous sedimentation up to the end of the lower Miocene. Corresponding to this the lower section with finer grains of the so called "streaks" (of Szécsény) which developed on the deepest basin parts accumulated in the upper Oligocene, while the somewhat coarser grains forming the upper section accumulated in the lower Miocene (Eggenburgian). On the areas of the sedimentary basin nearer to the shore (Westwards) the continuous Oligocene-lower Miocene sedimentation resulted in layers of variegated development connected laterally with the "streak" – series. A characteristic representative of these formation is the loose sandstone series of Iliny of some 100 m thickness; its layers have been deposited in the deep gorge southwards of Iliny on the lower parts of the streaks of Szécsény with continuity of sedimentation (Fig. 2.). The overlying rock is probably the continental-paralic coal bed series (I. Ferenczi, 1939), which had been one time explored towards SE. Thus, following the development of the lower section of the streak of Szécsény the gradual regression developed through the sandy-aleuritic series up to the full emergence.

The biostratigraphical investigation of the series has been made by T. Báldi and M. Horváth, 1971: in the course of my studies I took all the faunistical, biofaciological basic data from this work. According to the above mentioned authors besides the gradual petrographical development of the series from the streak of Szécsény the development

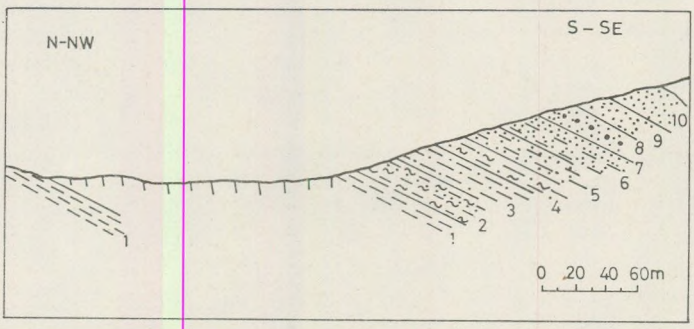

Fig. 2. Geological profile of the Iliny-gorge (after T. Báldi, 1971)
Legend: 1. Lower section of the fine grain, aleuritic Szécsény-streak series; 2. "Transitional layers" between the Iliny-sandstone and Szécsény streak series: fine-grain ed sandy, clayey aleurite with sandstone embedments; 3. Yellow fine-sandstone-aleurolite; 4. fine-sand aleurolite; 5. layered loose sandstone-aleurolite; 6. fine-grain loose sandstone, with 1 cm aleurolit embedments; 7. whitish grey aleuritic , fine grained loose sandstone; 8. gravely fine-grained loose sandstone; 9. fine-grained sandstone; 10. yellow, aleuritic fine-grained loose sandstone

of the fauna shows also similar transitions. The first layer of Fig. 2. proved to be also faunistically the bathysyphonic section of the streak of Szécsény. But the layer 2. is "transitional on the one hand between the streak of Szécsény and the sand of Iliny, and on the other hand between the Egerian and Eggenburgian". The above mentioned authors consider the "transitional fauna provisionally as the uppermost part of Egerian" and so they set the "frontier of the Egerian and Eggenburgian, i. e. of the Oligocene and Miocene" between the layers 2. and 3.

In the bathysyphonic streak (layer 1.) forming the deepest part of the studied profile silt devouring fauna prevails. This indicates the presence of a "soft, silty basic layer" and of a very weakly moved sedimenting medium. The frequency of euryoxibiontic forms and the absence of herbivorous organisms indicate the existence of a greater water depth and larger distance from the shore. According to the grain size investigations this formation consists of a saltatory population of a relatively low frequency (20 – 30%) and restricted to the fine grain domain, and in the most part of a suspension grain component which is very steep (Fig. 3.). This characteristics – in agreement with the faunistic results – point to a very weak bottom flow and to a sediment accumulation consisting of grains mostly floated in a hardly moving medium. On the grain distribution diagram we can see a double break which can be attributed to the mixing influence of the silt devouring organisms.

The so called "transitional layers" (Fig. 2., 2.) can not be separated on the basis of their external appearence from the streak of Szécsény forming the basement. The prevalence of the silt devouring infauna indicates also a biotope basically similar to the earlier ones. To the chang- of physical factors we can conclude from the appearence of popula-

tions indicating the presence of a smaller sea depth of 30 – 50 m. This change can be traced also on the basis of grain size distribution investigations (Fig. 3., 2.): the quantity of saltatory grains has increased significantly (80%) but ist weaker classification and the still significant suspension part indicate the weak influence of water movements (waves, flowing). On the basis of these characteristics as well as owing to the absence of rolled grains no smaller sea depth than that of a sublittoral one can be supposed.

The macrofauna of the ensuing levels (Fig. 2:3 – 10) deviates signifacantly from those discussed above, both in stratigraphical, as well as in faciological character. But "the difference was not formed at once ..., going upwards one can observe the staying out of the latest streak faunas." The gradual change of the sediment-accumulating terrain becomes apparent also on the basis of grain-distribution studies. Within the grain distribution of the 3. layer (Fig. 3.) – although to a small extent at first – the slipping population has also developed. The saltatory grain component is well classified and gives 90% of the distribution. The lower dimension limit of the floated grains is 40 μm, their quantity is only 10%. These characteristics indicate definitely an enlivened water movement. But the dimensional domain of the saltatory population bears witness to an accumulation environment with a relatively distant shoreline and to a somewhat greater depth than that of the shallow-sublittoral, coarsegrained zone.

A vigorous change of the fauna picture sets in within the layer 4. (Fig. 2.). The appearence of supension-filtering molluscs en mass indicates

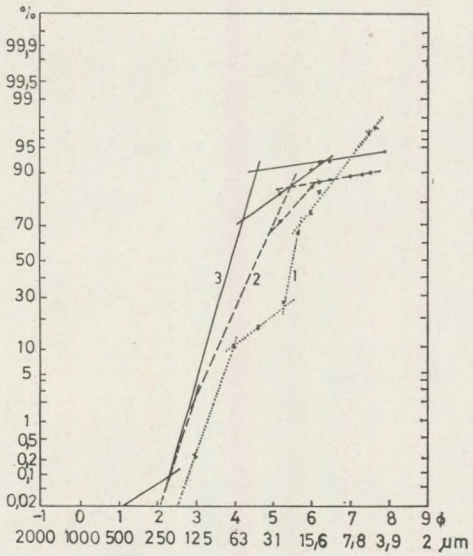

Fig. 3. Log-probability grain distribution of the formations exposed on the lower part of the Iliny-gorge (denotations as on Fig. 2.)

a well defined water movement. The "infauna" characteristics as well as the further presence of "silt devouring streak formes" point to a soft basement. This later phenomenon proves also the graduality of the change of sedimentation terrain and that of the exchange of the fauna. According to the grain distribution investigations the gradual change took place through smaller oscillations of energy conditions and thus, of the debris-transporting and sedimenting conditions. In the layer-components of the above discussed level 3. and of the somewhat deviating level 4. – as regards their composition – the very characteristic form of the curve does not change, although we can observe differences in the average grain size, the quantity of the suspension population as well as in the appearence of the slipping grain component (Fig. 4.). This variability – being very characteristic for the lower part of the sublittoral zone in general – is in agreement with the paleontological observation outlined earlier. The significant quantity of saltatory population and its dimensional domain of 0,25 – 0,03 mm shows a vivid water movement, but a still soft, fine grained basement. This duality can also be established from the appearence of a small amount of rolled grains besides of the still significant suspension component. The lability of sedimentational conditions is extremely apparent in the layers 5. and 6. – in form of micro-layering. The grain distribution of layer 6. shows (Fig. 4.) a broad mixing interval, as well as a restricted steepness of the saltatory component, which can be explained by the mixing of the single microlayers in the course of sedimentation, or – owing of the work of silt-digging

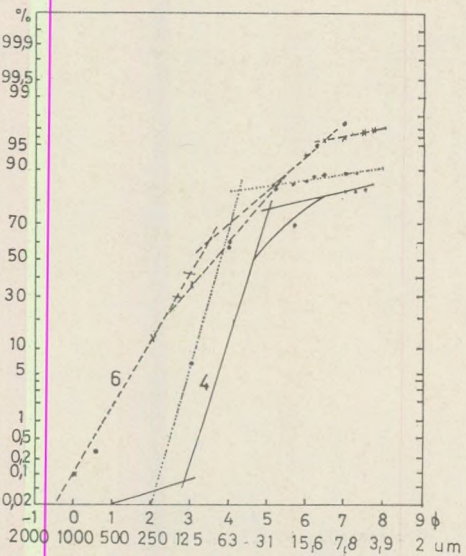

Fig. 4. Log probability grain distribution of the formations exposed on the middle part of Iliny-gorge (denotations as on Fig. 2.)

organisms — immediately after it (partly, however, by the difficulties of analysing rocks of such facies).

According to the investigations of T. Báldi and M. Horváth (1971) the "silt-devouring forms ore completely absent already in the upper levels of the spot explored. The tendency of strengthening the flows and the richess in oxygen in connection with it has made less possible the mixing of organic matter with the sediment". Nevertheless, the presence of suspension-filtering organisms digging themselves into the basement points to a still prevailing softness of the bottom. Arder surfaces and slow sedimentation periods could develop only occasionally, which is proved also by the scarcity of epifauna. The form of the grain-distribution curves of these yellow loose sandstone layers reflects the influence of strong wave-motions (Fig. 5.). The increase of the significance of sliding population and the turning point of the saltatory and suspension grain components falling into the domains of coarse grains point to the higher regions of shallow sublittoral zone. Within the saltatory population no break can be observed, thus excluding a shoaling up to the tidal zone. The significant amount of the suspension component indicates a rich material supply. The rollingly transported grains, however, are of relatively smaller dimensions and their amount dos not exceed 25%. This points to a loose (not soft!) basement, which is easily to be stirred over and so it was unfavourable to the development of epifauna. The only exception is presented by the fine-gravelly level of the layer 8. This component represents that formation of the studied series, which has sedimented nearest to the shore.

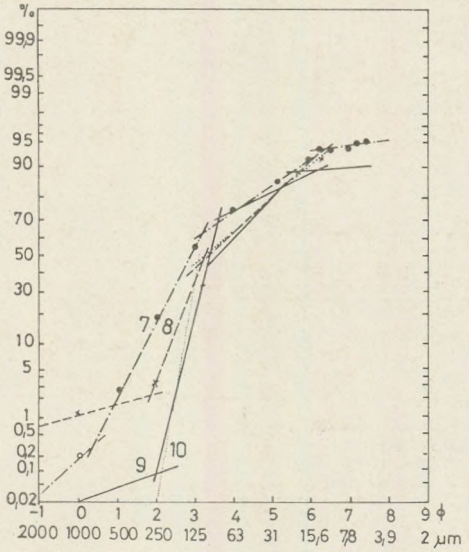

Fig. 5. Log-probability grain-distribution diagrams of formations exposed on the upper part of the Iliny-gorge (denotations as on Fig. 2.)

In the uppermost layers of the series a slight decrease of the average energy characteristic to the sedimentation is observed. The dimensional domain of the grains deposited out of the suspension, however, ist almost unchanged. This phenomenon may indicate that the sediment accumulating spot has become more protected, more closed. In that case, namely, the intensity of terrigenous material supply may remain similar to the previous one also with a weaker water movement, due to the relative nearness of the shore. This process may further lead to a gradual seclusion of the sedimentary basin as well as to its filling in. Though this can not further be investigated in the profile, this concept is supported also by the cover formation of terrestrial character with coal beds mentioned earlier.

On the basis of these consideration one can state that the paleographical and petrographical methods furnish results being in agreement with and completing well each other. The analysis along the profile (Fig. 6.) shows that parallel to the increase of the ratio of saltatory component, respectively of the decrease of the quantity of the matter deposited from suspension (layers 1 – 4.), the silt devouring forms gradually fall into the background against the suspension filtering ones. In the upper levels of the exposure the share of the saltatory component diminishes, but the prevailing role of the suspension filtering ones remains unchanged. This phenomenon can be explained by the change of average size of the individual grain populations. In the course of our studies we used for the characterisation of the average grain size of the individual populations – as a first approximation – the mean value of the size interval.) The characteristic mean grain size for the Szécsény – streak consisting of sal-

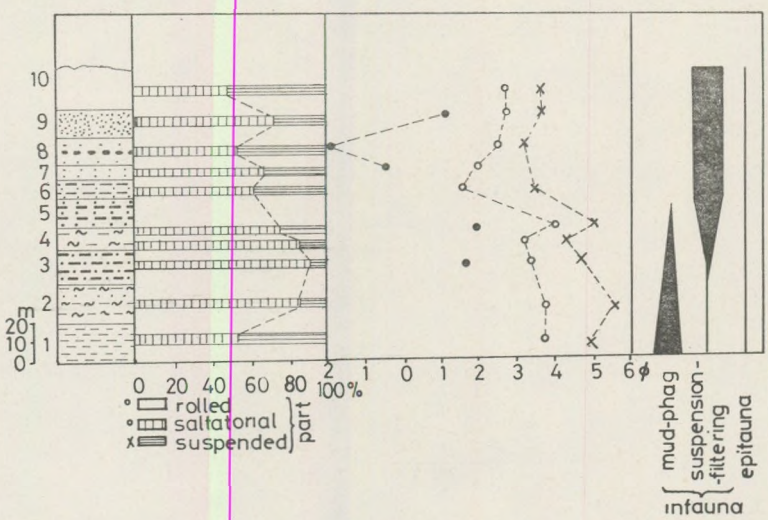

Fig. 6. Connection between sedimentary petrological and faunistical characteristics on the profile of the Iliny-gorge

tation and suspension components in a 50–50% ratio is shifting towards the coarser domains in the younger layers – in some places with sharp changes. Together with change of the grain dimension of the two components the saltatory population gains weight in the layers 2. and 3., then upwards from the 4th level the original ratio of 50–50% comes gradually back again. Inbetween – as we have indicated – the mean grain size of the saltatory component changes from 3,6 to 2,6 Φ, while that of the suspension component goes from 5 Φ to 3,6 Φ, i. e. to the size of the saltatory population of the Szécsény-streak. Thus, the one time accumulation terrain was characterized by a relatively clear water because in spite of the higher ratio of the suspension component there was stable sedimentary basement corresponding to the way of living of suspension filtering organisms and proved by the coarser grain size. In the continuation of the series, however, it may be assamed by geological analogies, that the filling in tendency went on, thus leading to a possible basic change of the living space and of the fauna.

REFERENCES

Andó, J. (1973): Study of transport-sedimentation terrain based on the analysis of log-normal grain populations, Földtani Közlöny 103, pp. 355–363. (in Hungarian)

Báldi, T.–Horváth, M. (1970): Report on the stratigraphical investigations in the Cserhát in 1970. Manuscript. Document store of the Hungarian State Geological Institute, Budapest. (in Hungarian)

Báldi, T. (1973): Mollusc Fauna of the Hungarian Upper Oligocene (Egerian). Publishing House of the Hung. Acad. of Sciences, Budapest. (in Hungarian)

Bogárdi, J. (1971): Alluvial transport of water courses. Publishing House of the Hung. Acad. of Sciences, Budapest. (in Hungarian)

Bogsch, L. (1968): General paleontology. Educational Publishers, Budapest.

Doeglas, D. J. (1964): Interpretation of the results of mechanical analyses. Journ. of Sedimentary Petrology 16., pp. 19–40.

Ferenczi, I. (1939): Contributions to the geological knowledge of the parts of the Ipoly-basin between Sóshartyán–Karcaság, respectively Balassagyarmat. Annual Report of the Hung. State Geological Institute from 1933–35., 2. pp. 734–775. (in Hungarian)

Horusitzky, F. (1939): Upper Oligocene and lower Miocene Faunas from the Ipoly-basin. Annual Rep. of the Hung. State Geological Institute from 1933–35. 2. pp. 775–778. (in Hungarian)

Horváth, M. (1972): Microfauna of the Szécsény amussium streak (upper part). Földtani Közlöny 102. pp 163–175. (in Hungarian)

Inman, D. L. (1949): Sorting of sediment in light of fluvial mechanics. Journ. of Sedimentary Petrology 19. pp. 51–70.

Kolmer, J. R. 1(973): A wave tank analysis of the beach foreshore grain size distribution. Journ. of Sedimentary Petrology 43. 1.

Kubovics, I.–Mrs. Pécsi Donáth, É.–Rózsavölgyi, J.–Andó, J.–Mrs Nagy Balogh, J. (1971): Complex petrological, geochemical and volcanological investigations of the volcanological and sedimentary formations of the Cserhát mountains. Manuscript. Data store of the Hung. State Geological Institute Budapest. (in Hungarian)

Noszky, J. (1940): Geological conditions of the Cserhát mountains. Geological description of Hungarian regions. Budapest. (in Hungarian)

Visher, G. S. (1969): Grain size distributions and depositional processes. Journ of Sed. Petr., 39. p. 1074–1106.

ВЛИЯНИЕ ВЯЗКОСТИ И НАГРУЗОК НА РАСПРЕДЕЛЕНИЕ НАПРЯЖЕНИЙ В ЛУНЕ

by

B. BODRI

(Department of Geophysics, Roland Eötvös University, Budapest)
Received: 15 October 1975

SUMMARY

Observations evidently have shown that the figure of the Moon significantly departures from the hydrostatic case, and these departures raise stresses in its interior. The investigation of these stresses strongly depends on the mechanical model applied to our satellite. We have considered different probable mechanical models and analised the stresses and strains arising for each case. If the interior of the Moon has relatively low temperature and the relaxation time is greater than the interval needed for significant changes of the elements of its orbit, than the model can be determined as an elastic, nearly homogeneous sphere. On the other hand, if the Moon's interior has high temperatures than the conditions will be similar to those taking place in the upper mantle of the Earth, the energy dissipation will increase by about of 1 – 2 orders of magnitude and therefore it will be necessary to include in the theory viscosity too. Finally, the existence of mascons induced extensive mass loads strongly affecting the distribution of stresses. For each of the above mentioned models there have been carried out computations of stresses and of the phase lag of deformations and on the bases of the results the true mechanical model of the Moon can be clearly obtained.

Можно считать почти бесспорным, что недра Луны находятся в сильно напряженном состоянии. Исследования гравитационного поля и фигуры Луны показывают, что фигура Луны заметно отклоняется от гидростатически равновесной. Эти отклонения приводят к напряжениям в теле Луны. Немаловажным источником напряжений в Луне являются также приливы и, возможно, температурные неоднородности. Существование масконов, по-видимому, дает возможность постулировать наличие на Луне значительных нагруженных зон. Возмущение гравитационного поля, вызванное нескомпенсированной поверхностной плотностью может привести к значительному изменению напряжений в нагруженной области.

Вязкость Луны изменила бы не только амплитуду, но и фазу напряжений, поэтому ее также необходимо учитывать при расчетах. О вязкости Луны пока можно судить лишь по косвенным данным. Существование масконов, то есть больших концентраций вещества под центрами всех пяти круглых морей на видимой стороне Луны, можно объяснить либо тем, что наш спутник обладает весьма значительной твердостью, которая много выше твердости внешних частей Земли

и способна бесконечно долго выдерживать напряжения, дызываемые масконами; либо тем, что масконы размещаются в очень вязкой жидкости, и время, прошедшее с момента их образования, недостаточно для выравнивания. В этом случае по расчетам U r e y and M a c D o n a l d (1971) вязкость Луны должна составлять 10^{26} пуаз, то есть на четыре порядка превышать эффективную вязкость поверхностных областей Земли. В первом случае диссипация энергии в Луне, по-видимому, буд т весьма малой ($Q \sim 1000-10\,000$), что приведет к чрезвычайно малым углам запаздывания деформаций, во втором же случае диссипация может сильно превышать диссипацию энергии в Земле, что соответственно увеличит угол запаздывания.

Цель настоящей работы исследовать распределение напряжений в Луне и определить влияние на них поверхностных нагрузок и вязкости.

В качестве модели Луны в данной работе использовалась почти однородная модель, расчитанная A r k a n i-H a m e d (1973), которая представлена в таблице 1.

Таблица I.

Модель Луны, A r k a n i - H a m e d (1973)

Table 1.

Model of the Moon, A r k a n i - H a m e d (1973)

r (км)	G (см сек$^{-2}$)	ϱ (г см$^{-3}$)	λ (10^{11} дин см$^{-2}$)	μ (10^{11} дин см$^{-2}$)
300	28.2801	3.374	6	4
500	47.1335	3.374	6	4
700	65.9869	3.374	6	4
900	84.8403	3.374	6	4
1100	103.6937	3.374	6	4
1200	113.1204	3.374	6	4
1300	122.5470	3.374	6	4
1400	131.9737	3.374	6	4
1500	141.4004	3.374	6	4
1600	150.8271	3.374	6	4
1685	158.8398	3.374	6	4
1735	162.8709	3.200	4	3

Отправной точкой данного исследования послужила задача о распределении напряжений в идеально упругой Луне при отсутствии напряжений на свободной поверхности. Уравнения упругого равновесия, использованные при расчете, имели следующий вид:

$$M - r^2 \mu \left(T' + H - \frac{2T}{r} \right) = 0$$

$$N - (\lambda + 2\mu) H' - \lambda \left[\frac{2H}{r} - \frac{n(n+1)}{r^2} T \right] = 0$$

$$L - r^2 (R' - 4\pi f \varrho H) = 0$$

$$N' - \frac{n(n+1)}{r^4} M + \frac{\varrho}{r^2} [L - 4V' rH + n(n+1) TV'] +$$

$$+ \frac{2\mu}{r} \left[2H' - 2H/r + \frac{(n+1)\, n}{r^2} T \right] = 0 \qquad (1)$$

$$M' + Nr^2 + \varrho r^2 (R + V' H) - 2\mu [H' r^2 - Hr + (n^2 + n - 1) T] = 0$$

$$L' - n(n+1)(R - 4\pi f \varrho T) = 0$$

, где

f	–	гравитационная постоянная,
$G = -V'$	–	ускорение силы тяжести,
r	–	текущий радиус Луны,
ϱ	–	плотность,
λ, μ	–	параметры Лямэ,
H, T	–	соответсвенно, радиальное и тангенциальное смещения,
N, M	–	радиальное и тангенциальное напряжения,
R, L	–	потенциал и его градиент,
n	–	поряадок прилива.

Мы не останавливаемся подробно на формулировке задачи в, целом ссылаясь на работы Молоденского (1953) и Bodri (1974).

Граничные условия на поверхности Луны брались следующие

$$M = 0$$

$$N = 0$$

$$L + (n+1) rR = 0. \qquad (2)$$

Они были выведены в предположении отсутствия напряжений на свободной поверхности и непрерывности потенциала и его производной.

Граничные условия в центре Луны

$$M = 0$$

$$N = 0$$

$$L = 0 \qquad (3)$$

предполагали регулярность соответствующих функций в нуле.

Система уравнений (1) интегрировалась численно методом Рунге-Кутта. В результате интегрирования были получены следующие числа Лява

$$h = 0.0639$$

$$l = 0.0173$$

$$k = 0.0383 \qquad (4)$$

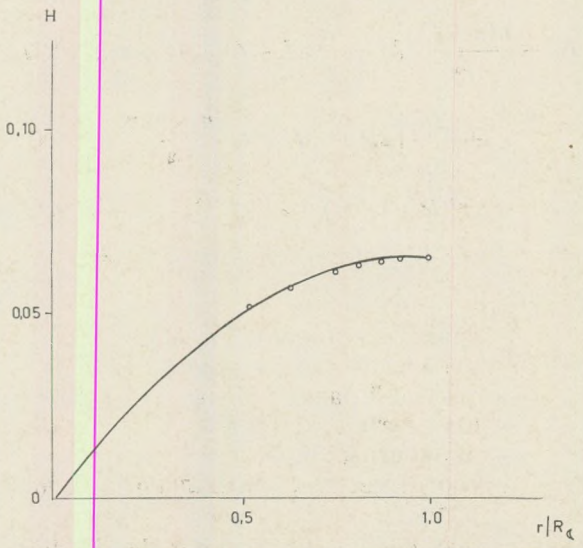

Рис. 1.а. Зависимость радиального смещения от радиуса при отсутствии напряжений на поверхности Луны

Fig. 1.a. The dependence of the radial displacement on the distance from the centre of the Moon. Surface loads do not exist

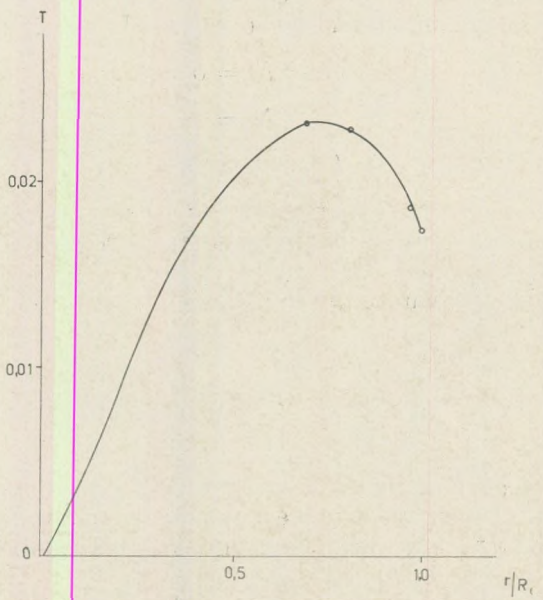

Рис. 1.b. Зависимость тангенциального смешения от радиуса при отсутствии напряжений на поверхности Луны

Fig. 1.b. The dependence of the tangential displacement on the distance from the centre of the Moon. No surface loads

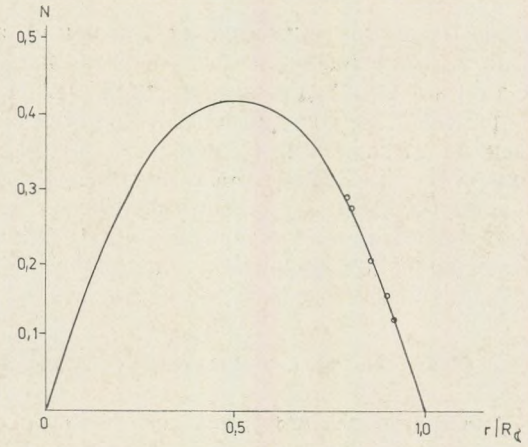

Рис. 1.c. Зависимость радиального напряжения от радиуса при отсутствии напряжений на поверхности Луны

Fog. 1.c. The dependence of the radial stress on the distance from the centre of the Moon. No surface loads

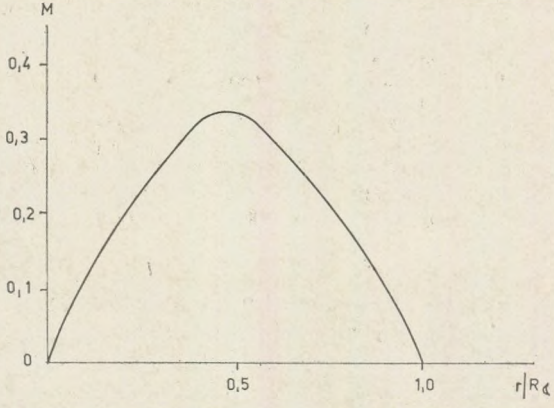

Рис. 1.д. Зависимость тангенциального напряжения от радиуса при отсутствии напряжений на поверхности Луны

Fig. 1.d. The dependence of the tangential stress on the distance from the centre of the Moon. No surface loads

Следует отметить хорошее согласие полученных нами чисел Лява с расчитанными Harrison (1963) для однородной Луны. Числа Лява, примерно, на порядок ниже земных, что вероятно, весьма затруднит возможность изучения лунных приливов непосредственно на поверхности Луны, поскольку потребует приборов значительно более точных, чем любые из применяемых в настоящее время на Земле.

В таблице 2 представлены общие решения системы (1), и, наконец, на графиках 1 a, b, c, d отложены соответственно распределения с

радиусом радиальных и тангенциальных смещений и напряжений. Для сравнения на тех же графиках отложены аналогичные функции, полученные Kaula (1964) для однородной Луны с плотностью 3.34 г см$^{-3}$, твердостью 7.38 10^{11} дин см$^{-2}$ и модулем сжатия 1.23 10^{12} дин см$^{-2}$. Последние два значения соответствуют эффективным значениям для верхней мантии Земли. Поскольку мы использовали почти в два раза меньшую твердость, смещения и напряжения, полученные нами, превышают расчитанные Kaula (1964). Максимум напряжений сильно смещен к поверхности и располагается, примерно, на расстоянии 0.6 $R_(\,$ от центра. Здесь $R_(\,$ – радиус Лунн.

Таблица 2.

Общее решение системы уравнений (1).

Table 2

General solution of the equation system (1).

$r/R_(\,$	H	M	T	R	N	L
1.0000	0.06389	0.00000	0,01732	1.03830	0.00000	1.88510
0.9712	0.06408	0.02291	0.01804	0.97945	0.04704	1.71971
0.9222	0.06405	0.05262	0.01876	0.88321	0.12228	1.46243
0.8646	0.06343	0.07379	0.01890	0.77650	0.20199	1.19536
0.8069	0.06225	0.08333	0.01838	0.67685	0.27103	0.96365
0.7493	0.06059	0.08438	0.01736	0.58429	0.32759	0.76446
0.6916	0.05855	0.07960	0.01595	0.49887	0.36872	0.59476
0.6340	0.05624	0.07119	0.01426	0.42067	0.38947	0.45173
0.5187	0.05148	0.04567	0.01058	0.28681	0.33960	0.23479
0.4035	0.04776	0.02115	0.00745	0.18606	0.12376	0.09213
0.2882	0.04474	0.00033	0.00608	0.13332	0.04145	0.00046
0.1729	0.00000	0.00000	0.00000	0.09837	0.00000	0.00000

Для сравнения на графиках 2 a, b, c, d приведено распределение соответствующих величин для мантии Земли, расчитанное Молоденским (1953), Kaula (1964) и Bodri (1974). Как видим, картина зависимости смещений и напряжений от радиуса сильно отличается от лунной. Максимум смещений расположен на расстоянии 0.65 $R_\oplus$ от центра Земли ($R_\oplus$ – радиус Земли), картина напряжений имеет более сложный вид. Поскольку диссиация энергии пропорциональна произведению напряжения на деформацию, можно сразу сказать, что максимальное выделение энергии в результате приливных деформаций на Луне будет близко к поверхности, а на Земле будет находиться на глубине нескольких десятых приведенного радиуса. То есть энергия приливных деформаций в Луне, скорее всего, рассеивается в пространство и вряд ли способствует нагреванию Луны.

В дальнейших расчетах задача была усложнена. Уравнения равновесия оставались прежними, точно так же, как и предположения о регулярности всех функций в нуле, но граничные условия

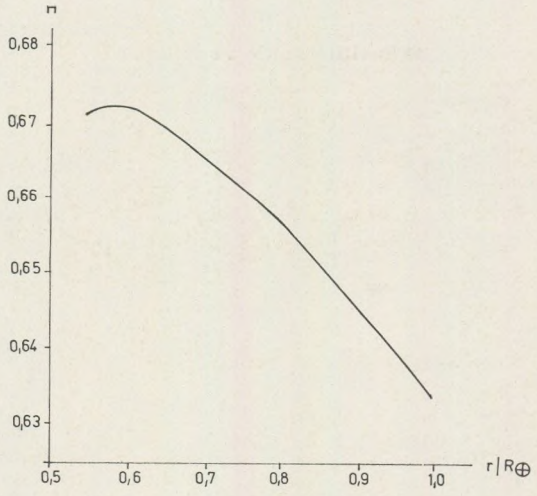

Рис. 2.а. Радиальное смещение в упругой мантии Земли
Fig. 2.a. The radial displacement in the elastic mantle of the Earth

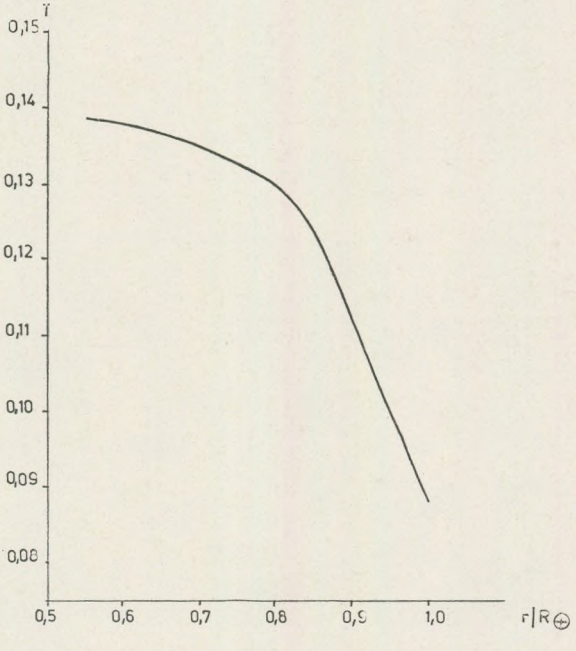

Рис. 2.ь. Тангенциальное смещение в упругой мантии Земли
Fig. 2.b. The tangential displacement in the elastic mantle of the Earth

на поверхности были изменены. Предполагалось, что на поверхности существует нескомпенсированный избыток массы плотности ϱ, который вызывает поверхностную нагрузку A и возмущение гравитационного поля g.

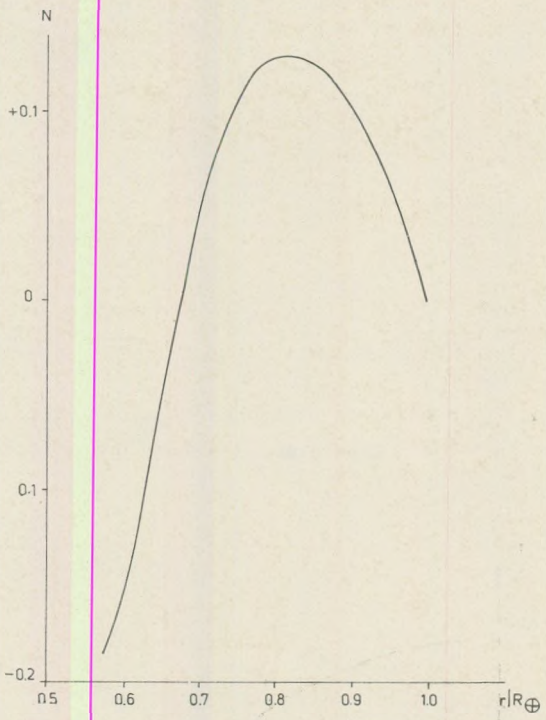

Рис. 2.c. Радиальное напряжение в упругой мантии Земли
Fig. 2.c. The radial stress in the elastic mantle of the Earth

Пусть γ — единица массы, однородно распределенная по диску радиуса α. Пользуясь разложением по полиномам лежандра (F a r r e l 1972), имеем:

$$\gamma = \sum_{n=0}^{\infty} \Gamma_n P_n(\cos \Theta)$$

$$\Gamma_n = [P_{n-1}(\cos \alpha) - P_{n+1}(\cos \alpha)]/[4\pi R_\zeta^2 (1 - \cos \alpha)]$$

$$\Gamma_0 = 1/4\pi R_\zeta^2 \qquad (5)$$

Возмущение гравитационного поля можно разложить в аналогичный ряд

$$g = \sum_{n=0}^{\infty} G_n(r) P_n(\cos \Theta), \qquad (6)$$

,где для точечной массы, то есть при $\alpha \to 0$,

$$G_n = \frac{4\pi f R_(}{2n+1} \Gamma_n .$$

При такой постановке задачи граничные условия на поверхности будут следующими
$M = 0$ (отсутствие тангенциальных напряжений)

$$N = -(2n+1)\, A\,, \qquad A = [G(Rc)]^2/4\pi f$$

(наличие радиальной поверхностной нагрузки A)

$$L+(n+1)\, R_(\, R = -4\pi f \Gamma_n$$

(учтен возмущающий потенциал).

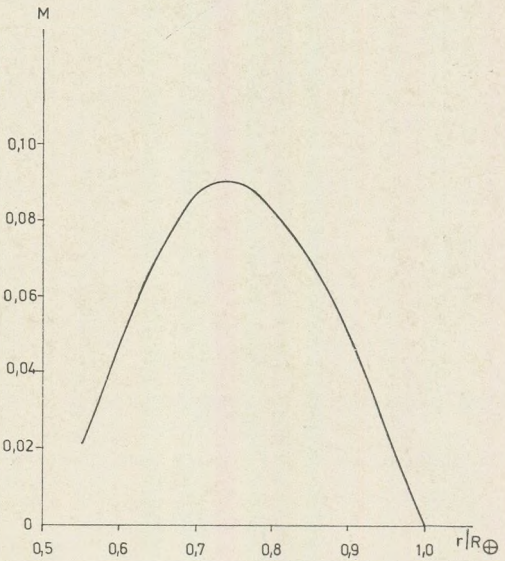

Рис. 2.д. Тангенциальное напряжение в упругой мантии Земли

Fig. 2.d. The tangential stress in the elastic mantle of the Earth

Эта задача решалась аналогично предыдущей численным интегрированием на ЭЦВМ для $n = 2$. Были получены следующие числа Лява, обусловленные деформациями от нагрузки

$$h = -0.0761$$

$$l = -0.0025$$

$$k = -0.0274\,. \qquad (8)$$

Отрицательные значения чисел Лява говорят о том, что поверхность опускается при положительной нагрузке, что и следовало ожидать.

На графиках 3 a, b, c, d, как и в предыдущей задаче, представлено распределение тангенциальных и радиальных деформаций и напряжений в теле Луны для случая поверхностной нагрузки. Для сравнения на графиках 4 a, b, c, d представлены аналогичные величины для нагруженной мантии Земли, расчитанные нами для модели Земли. Как видим, и здесь картины распределения напряжений и деформаций сильно различаются.

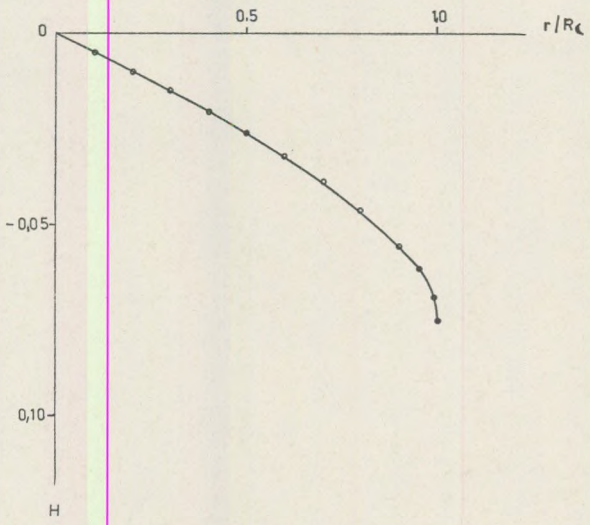

Рис. 3.а. Зависимость радиального смещения от радиуса на нагруженной поверхности Луны

Fig. 3.a. The radial displacement versus distance from the centre of the loaded Moon

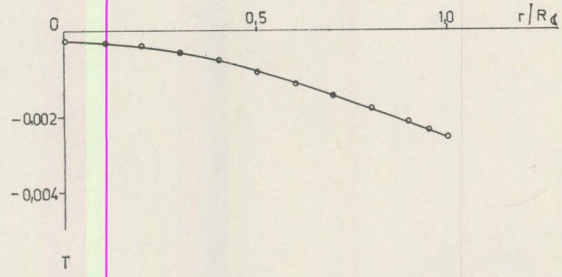

Рис. 3.b. Зависимость тангенциального смещения от радиуса на нагруженной поверхности Луны

Fig .3.b. The tangential displacement versus distance from the centre of the loaded Moon

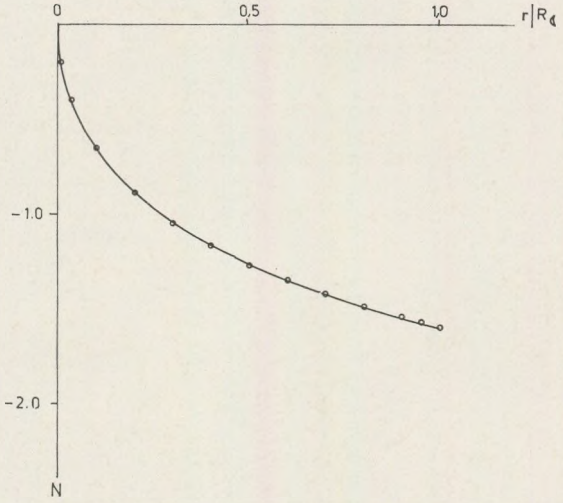

Рис. 3.с. Зависимость радиального напряжения от радиуса на нагруженной поверхности Луны

Fig. 3.c. The radial stress versus distance from the centre of the loaded Moon

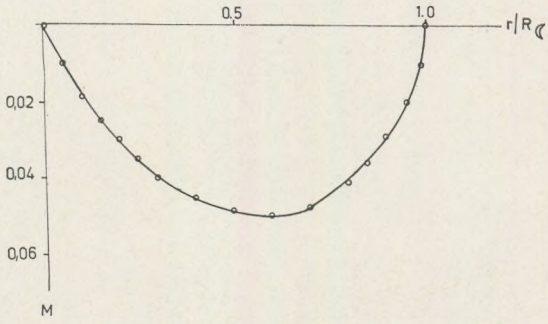

Рис. 3.д. Зависимость тангенциального напряжения от радиуса на нагруженой поверхности Луны

Fig. 3.d. The tangential stress versus distance from the centre of the loaded Moon

Для $n = 2$ наибольшая разность напряжений существует в центре Луны. Разность напряжений в центре Луны по нашим вычислениям составляет около 20 бар. Это указывает на то, что глубокие недра Луны должны быть в настоящее время исключительно прочными и что они были таковыми с тех пор, как Луна приобрела свою неправильную форму, поскольку за этот период не произошло изостатического выравнивания. Для гармоник более высокого порядка максимум напряжений будет смещаться вверх, например, при $n = 3$ максимальная разность напряжений существует на глубине, приблизительно, $0.4R_{(}$.

Судя по гармоникам низкого порядка, мы делаем вывод, что вещество, составляющее Луну, способно выдержать разность напряжений от нескольких бар до 10—20 бар на всех глубинах. Можно сделать определенный вывод, что Луна много тверже и находится при более низких температурах, чем Земля.

Тем не менее следует заметить, что подобный вывод справедлив лишь для однородной Луны. U r e y et al. (1959) показали, что если плотность Луны меняется с угловыми координатами, то при некоторых законах изменения плотности разность напряжений в центре можно сделать близкой к нулю. Однако эти же авторы показали, что нагрузку на изостатически уравновешенной поверхности нельзя использовать

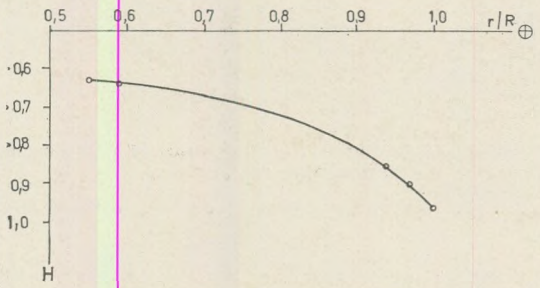

Рис. 4.а. Радиальное смещение на нагруженной мантии Земли
Fig. 4.a. The radial displacement in the loaded mantle of the Earth

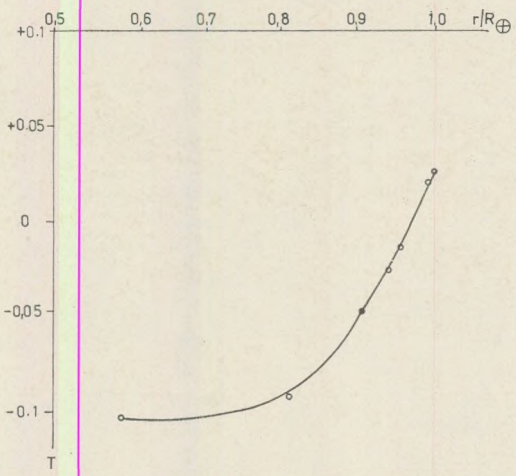

Рис. 4.б. Тангенциальное смещение на нагруженной мантии Земли
Fig. 3.b. The tangential displacement in the loaded mantle of the Earth

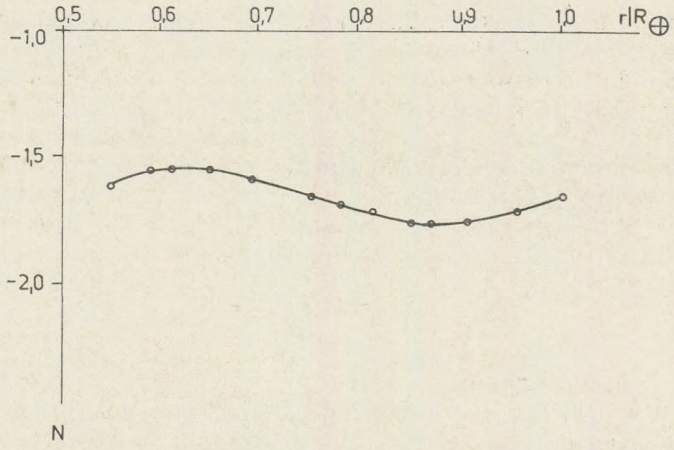

Рис. 4.с. Радиальное напряжение на нагруженной мантии Земли

Fig. 4.c. The radial stress in the loaded mantle of the Earth

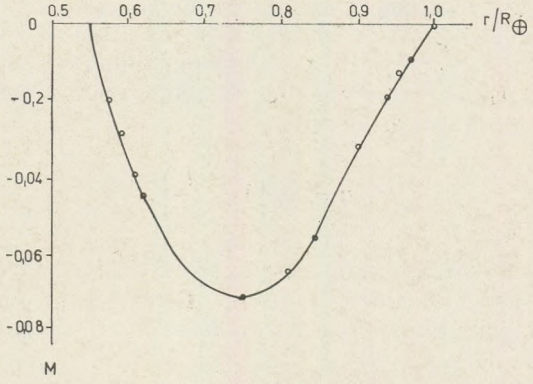

Рис. 4.д. Тангенциальное напряжение на нагруженной мантии Земли.

Fig. 4.d. The tangential stress in the loaded mantle of the Earth

для объяснения наблюдений гравитационного поля, если в центре Луны нет напряжений. Полытка обойтись без напряжений, выбрав для этого некоторый закон изменения плотности от координат, представляется нам несколько искусственной, поскольку анализ коэффициентов разложения в ряд по сферическим функциям гравитационного потенциала Луны указывает на то, что распределение плотности в Луне не очень отличается от однородного и что, во всяком случае, Луна значительно более близка к однородности, чем Земля.

Следующим шагом был учет вязкости при вычислении деформаций и напряжений в теле Луны. Как известно, неидельная упругость Луны вызывает запаздывание фаз деформаций по оношению

к деформирующему потенциалу, которое принято характеризовать углом запаздывания φ. Метод вычисления угла φ подробно описан в работах Bodri (1974, 1975), в данной работе мы остановимся лишь на его принципах. Как известно, упругая изотропная среда характеризуется двумя упругими модулями: K — модуль сжатия и μ модуль сдвига, или постоянными Лямэ. Предположим, что диссипация при всестороннем сжатии значительно меньше, чем при сдвиговых процессах. Математически это можно выразить, оставив модуль K действительным, а μ заменив комплексной величиной

$$\mu = \mu_0(1 + i\psi), \quad \psi \ll 1, \tag{9}$$

где

i — мнимая единица,

ψ — комплексная часть модуля сдвига, малая для малого поглощения.

Наконец, особое распространение среди геофизиков получило положение, согласно которому диссипативная функция Q не зависит от частоты возмущающей силы. Обосновать это положение теоретически в рамках теории линейного поглощения трудно. Ломнитц показал, что оно будет приближенно выполняться в широком интервале частот для определенных логарифмических функций крипа. Введение этой гипотезы в уравнения теории упругости принадлежит Кнопову, который показал, что

$$\mu = \mu_0\left(1 + \frac{i}{Q}\right). \tag{10}$$

При этом учтено отсутствие микрокрипа при всестороннем сжатии.

В случае комплексности модуля сдвига, очевидно, и функции H, T, R, L, N, M, фигурирующие в уравнениях системы (1), также будут комплексными. То есть

$$\begin{aligned} H &= H_0 + H^* i \\ T &= T_0 + T^* i \end{aligned} \tag{11}$$

и так далее. Здесь звездочки обозначают комплексную часть соответствующей функции. Подставляя (10), (11) в систему дифференциальных уравнений (1) и приравнивая нулю отдельно реальные и комплексные части, мы получим две системы дифференциальных уравнений, в которых разделены реальные и комплексные части функций. Проинтегрировав эти системы, мы будем знать вид функций (11), а отношение комплексных частей к реальным на поверхности и даст нам, очевидно, углы запаздывания по соответствующим деформациям и напряжениям.

Некоторую трудность в решении данной задачи представляет лишь вопрос о виде используемой в расчетах функции Q. Для Земли

распределение Q с радиусом получают обычно методом свободных колебаний. Некоторую информацию о величине Q может дать также наблюдение затухания чандлеровского периода свободных колебаний Земли и запаздывания приливных деформаций. Применение этих методов для Луны, естественно, невозможно, так что о вязкости Луны мы можем судить лишь по косвенным фактам. Поскольку при расчетах нами использовалась почти однородная модель Луны, естественно было положить и диссипативную функцию почти практически постоянной. О величине ее можно сказать следующее. Если физические условия в большей части лунных недр близки к условиям в верхней мантии Земли, то в качестве оценки Q можно принять $Q \sim 100$ (Жарков, 1960), если же, как мы упомнали выше, недра Луны характеризуются гораздо большей твердостью, то диссипативная функция может изменяться в пределах $1000 \div 10\,000$. Для обсуждения вероятности той или иной гипотезы мы имеем пока еще слишком мало данных, поэтому в нашей работе были расчитаны углы запаздывания для трех возможных величин Q : 100, 1000, 10 000. Результаты вычислений углов запаздывания представлены в таблице 3. Индекс у φ показывает по какому виду напряжений или смещений берется запаздывание.

Как видим, при $Q = 100$ результаты довольно неожиданны, поскольку углы запаздывания почти на два порядка превышают соответствующие для Земли. Если дальнейшими исследованиями этот факт подтвердится, то это может привести к полному пересмотру теории эволюции ситтемы Земля-Луна. Как показали расчеты Bodri (1973), диссипация энергии системы Земля-Луна, а следовательно и изменение элементов орбиты Луны, скорости вращения Земли и т. п., сильно зависит от принятого нами значения угла запаздывания φ_R. До сих пор болшинством исследователей углы запаздывания считались равными, примерно, $\sim 2°$ и для Земли, и для Луны. Из этого следовал вывод о том, что перераспределение энергии диссипации между Луной и Землей зависит только от соотношения их чисел Лява k (Kaula, 1964), и таким образом, диссипация около 70% всей энергии считалась происходящей в Земле. Если Q для Луны действительно порядка 100, то предыдущий вывод, скорее всего, неверен, по-видимому, большая часть энергии в этом случае будет диссипировать в Луне. Таким образом создается возможность для заметного приливного нагрева Луны в прошлом.

При $Q = 1000$, 10 000 углы запаздывания слишком малы для того, чтобы привести к какой-либо заметной эволюции орбиты Луны за последние 4.5 млрд. лет. На рис. 5 a, b и представлено соответственно изменение большой полуоси a и эксцентриситета орбиты Луны e в предположении, что угол запаздывания для Земли и для Луны равен 1'. Алгоритм, согласно которому производился расчет, подробно описан в работе (Bodri, 1973). Как видим, за 4.5 млрд. лет (предполагаемый возраст системы Земля-Луна) Луна приблизилась к Земле лишь на $10\,R_\oplus$. Поскольку гипотеза образования Луны в около-

земном рое предполагает образование Луны на расстоянии $10-20\ R_\oplus$ от Земли, можно считать такую малую диссипацию в Луне аргументом в пользу ее захвата.

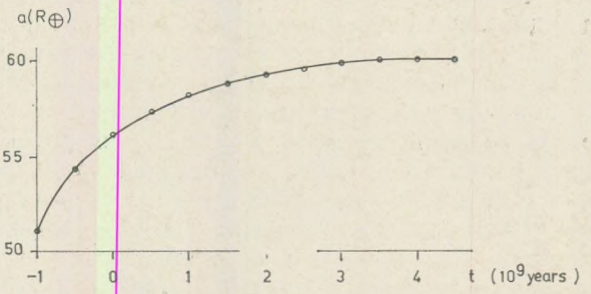

Рис. 5.а. Изменение расстояния Земля-Луна в прошлом при $\varphi_R = 1'$.
Fig. 5.a. The past variation of the earth-moon distance for $\varphi_R = 1'$.

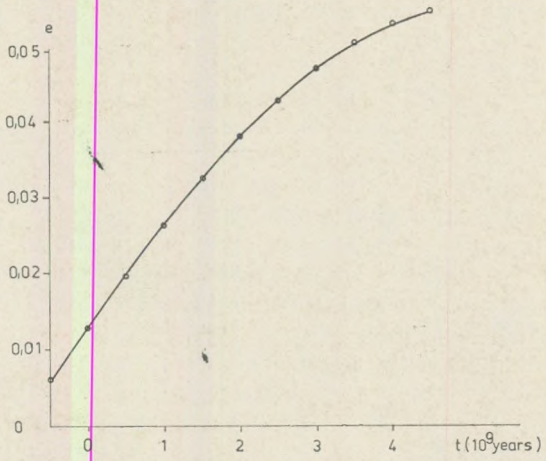

Рис. 5.b. Изменение эксцентриситета лунной орбиты в прошлом при $\varphi_R = 1'$.
Fig. 5.b. The past variation of the eccentricity of the moon's orbit for $\varphi_R = 1'$.

В заключение сделаем некоторые выводы из приведенных расчетов. Существование высоких гор и масконов при отсутствии полного изостатического выравнивания предполагает высокую степень твердости по крайней мере внешних частей Луны. Если вся Луна однородна по плотности или по крайней мере плотность ее меняется только с изменением расстояния от центра, то ее глубокие недра должны обладать значительной твердостью, так как форма Луны не является равновесной, то есть обусловленной ее собственным гравитационным потенциалом, гравитационным потенциалом Земли и центробежной силой, вызванной врашением Луны вокруг своей оси и по орбите. Наличие

концентраций масс под круглыми морями свидетельствует о том, что Луна уже была твердой в то время, когда они образовались на ранней стадии ее развития. При таких условиях недра Луны характеризуются, по-видимому, сравнительно низкими температурами, а время релаксации превосходит время существенного изменения лунной орбиты. Наиболее вероятная модель Луны в этом случае — эрто упругая почти однородная сфера, напряжения для которой мы расчитали в качестве исходной задачи. Если времена релаксации велики, то диссипация, скорее всего, низка. То есть более вероятны расчитанные нами малые углы запаздывания фаз деформаций. Если предположить, что преобладала одна и та же приливная характеристикаQ, то, интегрируя по времени назад, получаем, что Луна 4.5 млрд. лет назад находилась лишь на 10 $R_\oplus$ ближе к Земле, чем сейчас. Это заставляет нас либо принять гипотезу захвата, либо предположить, что в прошлом приливная диссипация была значительно больше, чем в настоящее время.

Таблица 3.

Зависимость угла запаздывания приливов на Луне от параметра Q.

Table 3.

The dependence of the moon tide phase lag on the parameter Q.

Q	100	1000	10 000
φ_H	3°·16	19'·00	1'·76
φ_T	23°·65	1°·82	14'·19
φ_R	9°·44	56'·64	3'·45

ЛИТЕРАТУРА

Arkani-Hamed, The Moon, 6 (1973).
Bodri, B., Ann. Univ. Sci. Bp., Sec. Geol., XVI (1973).
Bodri, B., Phys. Earth Planet. Inter., 9, 141–146 (1974).
Bodri, B., Nature, Vol. 254, March 27, 1975.
Farrell, W. E., Rev. Geophys. Space Phys., 10, 761–797 (1972).
Harrison, I. C., Journ. Geophys. Res., Vol. 68, N. 14 (1963).
Kaula, W. M., Revs. Geophys., Vol. 2 (1964).
Molodensky, M. S., Tr. Geofizicheskogo In-ta AN. SSSR, N. 19 (146), (1953).
Zharkov, V., N., Tr. Inst. Fiz. Zemil, 11, 36–60 (1960).

VARIATIONS OF THE WATER STOCK OF SOIL IN A BARE GROUND PROFILE

L. ERDŐS

Department of Meteorology, Eötvös University, Budapest
Received: 25 Juli 1974

SUMMARY

On the basis of a twenty years (1951 – 70) series of soil moisture measurements made at Erdőhát (Hungary) average and extreme variations of the water stock of soil (w) are dealt with, such as: yearly variation, changes with depth as well as variability of the annual values.

It is sometimes practical to compare the variations of the water stock and certain hydrophysical constants. The average water stock variations show the following characteristic features: the water content decreases with depth throughout the whole year and the moisture profile is not a linear one; the yearly variation is asymmetrical and it consists of a longer period of drying out and of a shorter interval of moistening; a phase shift is experienced with depth, in the yearly average the upper layer of the soil (down to 70 cm) is relatively more saturated, while in the lower layers a relative dryness is experienced; the extremes of the moisture profile at depth develop in J u n e, respectively in D e c e m b e r. In a more or less empirical way depth functions of the yearly average soil moisture depth-profile as well as that of the average yearly amplitude have been derived. Matching of the empirical and computed values is very good.

A simple model of extreme water content changes is presented and a lot of new characteristics defined, such as: the absolute yearly oscillation of the water stock (D_I), amplitudes of the extreme-functions (d_1, d_2) and their sum (D), the wideness characteristics (d_3, d_4), the distortion index (Δ), the passive, respectively fossil water stock etc. The yearly variation of $w_{max}(z)$ (maximum water stock as a function of depth) as well as the distribution of the fossil water stock with depth is shown. The empirical depth-functions of the extreme amplitudes (d_1, d_2) have been determined and the depth-function of the sum of the amplitudes is represented by a differential equation. Some other characteristics show similar features as the extreme amplitudes. The relative distortion index (Δ/D_I) is in connection with the relative water saturation state of the soil. The ratio of the extreme oscillation to the average water-stock is expressed by the function: $p(z,t)$, the yearly variation of which shows three types. The connection between average and extreme water stocks is represented by means of the expression: $D/\overline{w}$ and $D_I/\overline{w}$. The depth function of the absolute yearly oscillation has also been derived.

Introduction

Our knowledge about the characteristic features and rules of the variations of the water stock of soil is still rather scanty. The water content of the bare soil depends on the weather and on the hydrophysical features of the ground profile. Proved we have a sufficiently long and detailed moisture observation series from a given for the soil profile we are able to separate the role of the weather and soil in the variations of

the water stock of the soil. The soil moisture observation series of Erdőhát of twenty years (1951 – 1970) seems to be suitable for such analyses. As a first approximation we restrict ourselves here to a detailed descriptive discussion of variations in time and space of the water stock of the soil. We will study the average and extreme variations of the water content of the soil, especially with regards the drying out and moistening processes. Only studies made with the use of monthly averages of the layers will be shown.

Hydrophysical contants of the soil determine the frames of the possible variations in time and space of the moisture of soil, thus they serve as an important basis for the considerations (Table 1.)

Table 1.

Values of the most important hydrophysical constants (mm) Erdőhát

Layer cm	W'_k	H'_p	hW'_k	mkW'_k	tW'_k
0 – 25	74	27	47	103	106
25 – 50	61	23	38	102	120
0 – 50	135	50	85	205	226
50 – 100	109	40	69	204	242
100 – 150	81	25	56	213	233
150 – 200	75	16	59	209	217
0 – 100	245	90	154	409	468
0 – 200	400	131	269	831	918

In the soil of Erdőhát the following values of the hydrophysical parameters: field water capacity (W_k), wilting point (H_p), and the useful water capacity (hW_k) are diminishing with the depth, while the maximum capillary water capacity (mkW_k) and the total water capacity (tW_k) remain practically constant. So the depth distribution of soil moisture can not be considered a simple function of the weather. It is more practical to make more comparisons – and these in various ways – between variations of the soil moisture and the various hydrophysical parameters.

The climatic factors influencing for the most part the water balance of the soil at Erdőhát are: yearly average of rainfall: 555 mm, in the summer half year: 328 mm, yearly total of evaporation on bare ground: 388 mm, in the summer half year: 281 mm, etc. (E r d ő s, 1975). The observations parcels are surrounded by soil wall, thus a surface runoff is not possible.

1. Average variations of the water stock of the soil

The variations of the average water stock of the soil layers are shown in Table 2. In the course of analyses layers with dm thickness

are also used, but they will not be shown owing to their extent. On the basis of the Table some general features can be seen and a few important conclusions can be drawn.

Table 2.

Mean water stocks of various soil layers (mm)
Erdőhát, 1951 – 70

Layer (cm)	I	II	III	IV	V	VI	VII	VIII	IX	X	XI	XII
0 – 25	78	79	71	62	59	57	53	50	51	56	67	74
25 – 50	59	60	60	55	53	50	49	46	46	45	52	57
0 – 50	137	139	131	117	112	107	103	96	96	102	119	130
50 – 100	90	93	97	89	86	83	79	73	73	71	78	86
100 – 150	68	73	76	68	67	67	65	58	58	56	61	62
150 – 200	66	70	65	67	65	61	63	57	56	54	56	59
0 – 100	227	232	228	206	198	190	182	169	169	173	199	216
0 – 200	365	376	369	339	330	317	310	286	284	285	316	337

The water stocks of the layers are diminishing with depth throughout the whole year, except for the 0 – 10 cm layer, in which (and only in this) the layering of moisture in summer is reversed, but this does not disturb the order of distribution of the average values of the 0 – 25, cm respectively the 0 – 50 cm layers any more. At the same time we see that the depth profile of the moisture content is not linear.

For the average yearly variation of the water stock of the soil is characteristic a typical maximum at the and of the winter, as well as a minimum at the end of the summer, respectively in autumn. Thus, the yearly variation divides into a longer drying-out section and a shorter moistening period. We can observe a phase shift of the extremes with increasing depth. Based on a more detailed data (dm layers) it can be shown that the maximum occurs in February in the the upper layers, and it oscillates between February and March: in the deeper layers the minimum in the layer between 0 and 30 cm falls to August, between 30 and 50 cm to September, between 50 – 180 cm to October and between 180 and 200 cm to November. On more hard grounds, e. g. at Karcag the minimum of soil moisture will be shifted to December already at a depth of 100 cm. (Erdős – Morvay, 1961). Since the phase shift of the minimums with depth is greater than that of the maximums, the ratio of drying-out and moistening intervals is also shifting with depth: the moistening section becomes shorter and the drying-out interval seems to lengthen with depth.

In reality, also the intensive drying out section becomes shorter at greater depth, because in the first half of the year a rather long equillibrium interval of nearly constant moisture is inserted. Thus in the autumn in the whole layer (0 – 200 cm) drying out and moistening pro-

cesses take place simultaneously, and in the upper layers the moistening action is predominating already, when in the lower parts the drying out is still very active.

The winter end saturation of the profile of the soil reaches the free ground water capacity only in the 0 – 50 cm layer, while in the entire layer it only approximates it. On the other hand, during drying out the water stock does not decrease in either layer down to the Hp (except for the layer at 0 – 10 cm depth), i. e. the bare soil stores a significant amount of utilizable water during the whole year.

The average yearly water stocks of the soil layers can be represented by a depth function independent of the time, this function is denoted by $\overline{w}(z)$. We have seen that the depth distribution of the moisture of the soil is always decreasing and non-linear (Table 2.). This is valid of course for the $\overline{w}(z)$ function too. The relative depth distribution of the yearly average soil moisture can be characterized in connection with the water capacity.

The depth function of the relative differences of the two variables shows a very interesting connection (Fig. 1.) In a yearly average the relative water saturation of the soil is increasing down to a certain depth, then it starts decreasing. The whole layer can be separated into a relatively more saturated zone extending down to 70 – 80 cm (where the relative differences are below 20%), and a relatively less saturated one (downwards from 70 cm), where the relative differences surpass 20% and the "saturation deficit" increases with depth. The relative saturation of the soil is highest around 40 – 50 cm and lowest at the greatest depth (around 200 cm).

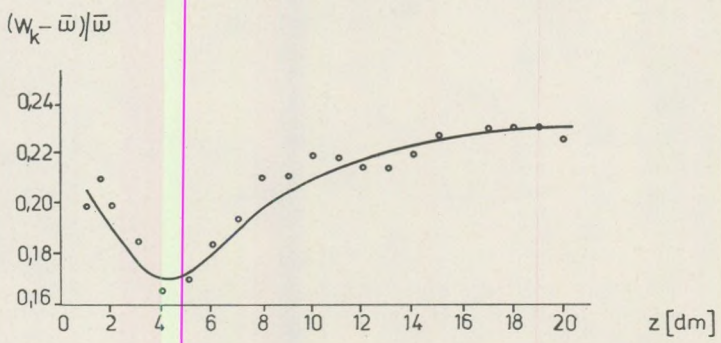

Fig. 1. Yearly mean relative water saturation of the soil, Erdőhát, 1951 – 70.

Of course, this relative saturation follows different depth distributions according to the seasons. E.g. in the winter half year the depth function of the relative differences is increasing monotonously in the whole layer, while in the summer half year it is very definitely decreasing down to 60 cm and it remains constant at greater depth. Considering these facts we could explain the curve of Fig. 1. in a somewhat para-

doxical manner as follows it represents the summer type on its upper section (where the saturation deficit is smaller) and the winter type appears on its lower part (where the saturation deficit turns to be greater).

The mean yearly oscillation ($\overline{w}_{max} - \overline{w}_{min}$) of the water stock of the soil is decreasing with depth. If we take a series of doubled (and intertwined) soil layers, e. g. layers of depth limits such as: 0 – 25, 0 – 50, 0 – 100, 0 – 200 cm, then the average values of the yearly oscillation (amplitudes) become one after another: 29, 43, 63 and 92 mm (Table 2.). We can detect a regularity on sight, if the thickness of the soil layer to be considered is doubled, the average yearly oscillation of the water stock within the layer increases only by factor of 1.5.

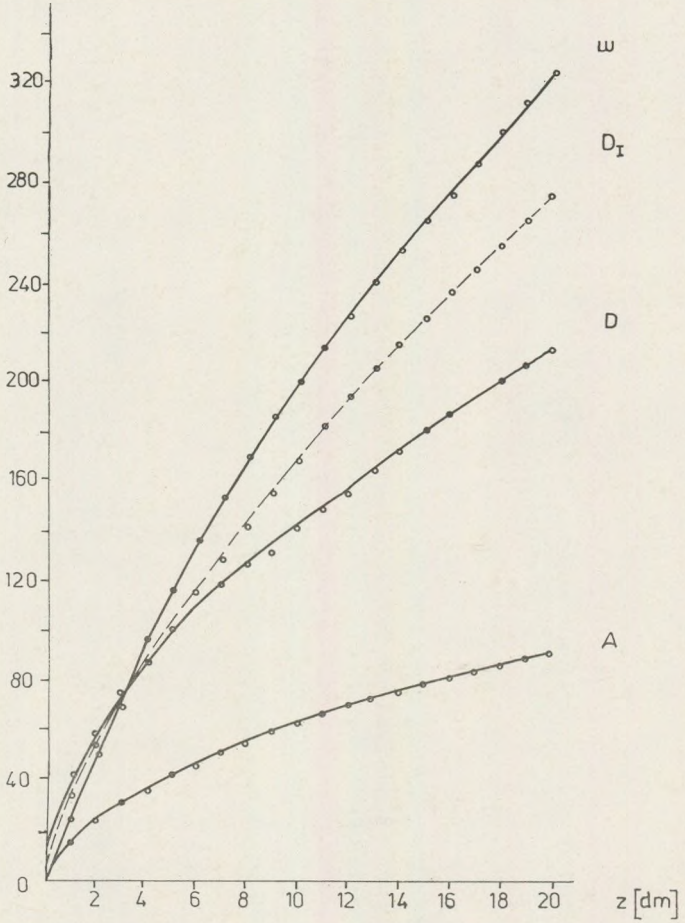

Fig. 2. Empirical cumulative depth- curves of important water stock characteristics Erdőhát, 1951 – 1970.
D_I – absolute yearly oscillation, D – sum of the extreme amplitudes, A – mean yearly amplitude, w – yearly mean water stock

By summing data of a fine 10 cm subdivision we can easily construct the empirical cumulative curve of the average yearly amplitude, which can be seen in Fig. 2.

Strating from the empirical connection above we have derived the depth function of the average amplitude total (E r d ő s, 1975) in the following form:

$$A(z) = A_1 \frac{B^{\lg z}}{z}, \tag{1}$$

where A_1 denotes the average amplitude in a starting layer chosen arbitrarily, B is a general constant, z is a linear dimensionless depth variable. The true amplitude – depth function – by means of which the amplitudes can be computed at any depth – can be obtained by differentiating equation (1):

$$A'(z) = A_1 B_1 \frac{B^{\lg z}}{z^2}, \tag{2}$$

where $B_1 = \ln B \lg e - 1$. The curve computed from equation (2) together with the empirical amplitude values is shown in Fig. 3. Computed and observed amplitude values fit very closely (except for a few cases).

From the empirical amplitude and from the data of the yearly average water stock we have constructed an empirical quotient-depth –

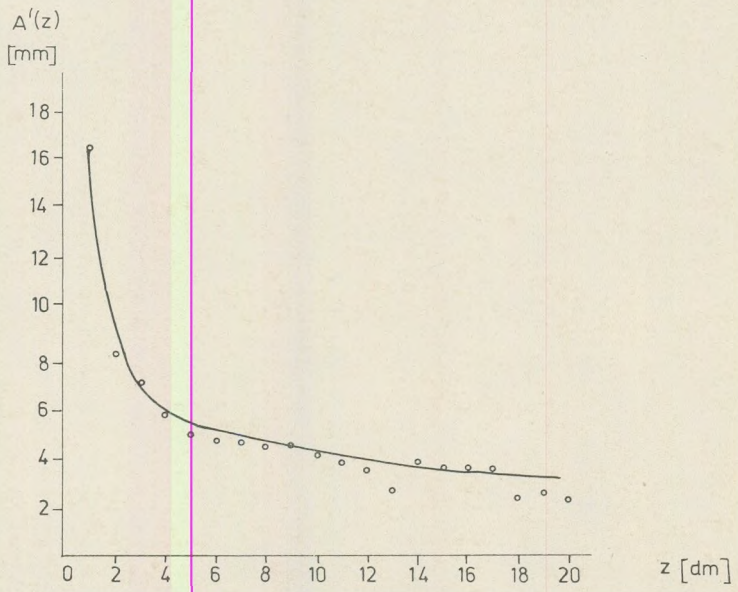

Fig. 3. The curve of the real amplitude-depth function together with the empirical values. Erdőhát, 1951 – 70.

function. Due to the linear transformation of the curve this function can be only a hyperbola, as follows:

$$\frac{A(z)}{\overline{w}(z)} = a + \frac{b}{z}. \tag{3}$$

It is justified to suppose that the depth function of the average water stocks is in a close and simple connection with that of the average yearly amplitude. From (1) and (3) we can obtain the depth function of the yearly average waterstock-total (Fig. 2.), as follows:

$$\overline{w}(z) = A_1 \frac{B^{\lg z}}{az+b}, \tag{4}$$

where a and b are empirical constants obtained by the use of least squares method. By derivation of the equation (4) we get the depth-profile function of the yearly average soil moisture in the following form:

$$\overline{w}'(z) = A_1 \frac{B^{\lg z}}{az+b}\left(\frac{M}{z} - \frac{1}{z+m}\right), \tag{5}$$

where: $M = \ln B \lg e$, $m = b/a$. The computed curve (using equation 5.) of the depth-profile of the yearly mean soil moisture – together with the observed empirical values – can be seen in Fig. 4. Except for the starting layer matching is surprisingly good. Thus the reality of the connection between the yearly mean soil water stocks and the yearly average amplitude can not be doubted.

In the yearly variation the absolute stocks of the complete layer are subjected to variations; they are decreasing within the drying out period and increasing during the moistening interval. In the course of these

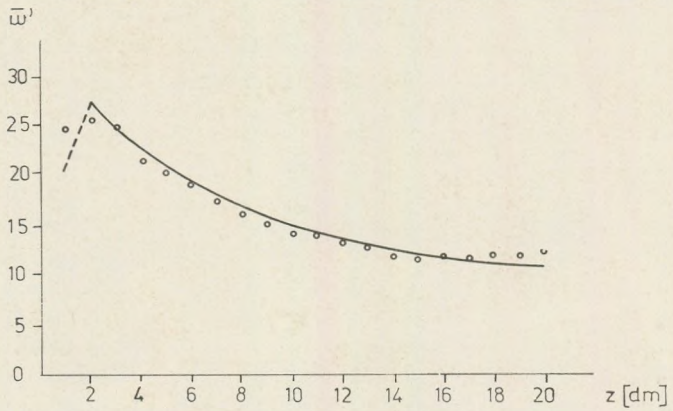

Fig. 4. The depth-profile function of the yearly mean soil moisture together with the empirical values. Erdőhát, 1951 – 70.

processes also the relative water stocks of the individual soil layers must change, because in both processes the upper surface is the active one, respectively the layers nearest to the surface are the most active.

The curve of the depth moisture profile becomes "straighter" during the drying out period, while in the moistening interval it becomes more "curved". This process has also its yearly variation and extreme positions. From Table 2. we can compute the relative water stock of the main soil layers for every month, but we will show here only the extreme positions (Table 3.). The following obvious statements can be made:

Table 3.

Relative water stocks of different soil layers (%)
Erdőhát, 1951 – 70

Layer (cm)	$\bar{w}'_{\max\ II}$	$\bar{w}'_{\min\ IX}$	$\bar{w}'_{VII}$	$\bar{w}'_{XII}$	W'_k	H'_p
0 – 50	37.1	33.9	33.3	38.6	33.7	38.2
50 – 100	24.8	25.8	25.4	25.5	27.2	30.5
100 – 150	19.4	20.5	21.0	18.4	20.3	19.1
150 – 200	18.7	19.8	20.3	17.5	18.8	12.2

In the whole layer the distribution of the water stock is the most balanced in July and the most irregular in December. In July we find one third part of the whole water stock in the highest of the four main layers (0 – 50 cm), which is much more than its proper proportion; in the layer between 50 and 100 cm we get the proper ratio of 1/4, while the two lower layers each have 1/5 -th part, i. e. less than their proper share would be. Similarly, in December the upper layer contains nearly 40% of the whole water stock, in the layer between 50 and 100 cm we can find also about the proper part, while the lower layers have much less than 1/5 th part of the stock. This extreme positions of the profile do not coincide in time with the extreme values of the water stock of the soil, but they develop in the middle of the drying out, respectively of the moistening period. The moisture profiles of yearly maxima and minima of the water stock of the soil (in February respectively September) are different one from another (no parallel shifting), neither do they agree with the profiles of the extreme positions.

The extreme profiles can be most practically compared one with another either using the computed moisture gradients, ore by a linear transformation of the profile curves. This latter method can be seen in Fig. 5. It is obvious that in Fig. 5. the homogeneous moisture profile would be represented by a straight line. The directional tangents of the July and December straight lines, respectively their difference could be a measure on the one hand for the deviation of the extreme profiles from the homogeneous one, and on the other hand they would indicate the limits, within which the actual variations of the moisture profile would

take place during the year. One can see in Fig. 5. that the "curvedness" of the moisture profile (its deviation from the homogeneous one) is during the whole year at least one and a half times or twice as big as the possible yearly change of the profile. Further, we can see that the W_k straight line intersects the straight line of the December profile from the left, that of the July profile from right, i. e. its tangent falls between those of these lines. That means that the real moisture profile agrees at least at two dates of the year with the most important hydrophysical moisture profile (i. e. it is parallel to the W_k line) independently of the circumstance that the average absolute water stock of the whole layer is always less than the free ground water capacity. We have to observe also that the more quick variations of the moisture profile take place in the second half of the year (from July to December 5/12 th part), while the more slow ones can be find during the first half of the year (from December to July, 7/12 th part.)

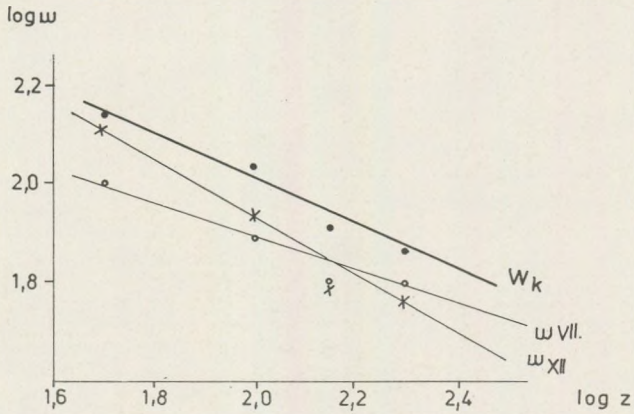

Fig. 5. Average yearly oscillation of the moisture profile at depth, Erdőhát, 1951 – 70.

The results of the analysis of the moisture profile depend also on the thickness of the soil layer considered. If thinner soil layers are under examination, the relative variations of the soil water stock are found more and more greater and also the moisture profiles are becoming more and more liable to changes. It is sufficient to point out that in the upper layers of 0 – 10 cm and 0 – 20 cm in the drying out period we can find a homogeneous moisture profile, resp. an inverse layering, and what is more, this is the characteristic in summer and in late summer.

2. Extreme variations of the soil water stock

The extreme variations of the soil water stock represent at least as important features of the water household of the soil as the average changes. When analysing the extreme soil water stock variations we take into account the following basic material. From the 20 years series of Erdőhát we have arranged the monthly means of the layers in an

order of size. The two highest, respectively the two lowest values have been averaged, these represent the extreme values of the soil moisture contet (w_{max}, w_{min}). By these extreme values we may represent the possible yearly oscillation of the water stock. Of course, we can investigate the yearly variation as well as its depth distribution. These variables are therefore empirical functions with two independent variables of the form $w_{max}(z,t)$, $w_{min}(z,t)$, where the depth, $z = 1, 2, \ldots, 200$ cm and the time $t = 1, 2, \ldots, 12$ in months. The depth functions are in most cases cumulative functions (cumultative curves) without any special signs, but the original functions are always denoted with a mark.

In what follows we will investigate in detail the characteristics of the functions $w_{max}(z,t)$ and $w_{min}(z,t)$ and we will describe the most important characteristics which can be derived with the help of the extremity functions. The scheme to be seen on Fig. 6. explains the definition of the new functions to be investigated. We need some special conceptual definitions. Let D be defined as: $D = D_I - D_{II} = d_1 + d_2$, where D_I is the absolute yearly oscillation of the water stock of the soil. It is obvious that we can have $D_{II} \leqq 0$, as well as $d_1 \leqq d_3$, respectively, corresponding to the former inequality. Characteristics d_1 and d_2 denote the yearly amplitudes of the extremity functions. Concerning the ratio of d_1 and d_2 we can not draw any conclusion in advance. The variables d_3 and d_4 are called the "wideness characteristics" of the extremity functions. The function $\delta(z,t) = w_{max}(z,t) - w_{min}(z,t)$ can not be defined unambiguously by means of the d(z) functions. What is cetrain is merely that during the year $\delta(t)$ assumes at least once the value of d_3, respectively d_4 in every layer. The yearly amplitude of the $\delta(z,t)$ function is a new depth function, $\Delta(z) = \delta(z,t_{max}) - \delta(z,t_{min})$, defined as "distortion index". In

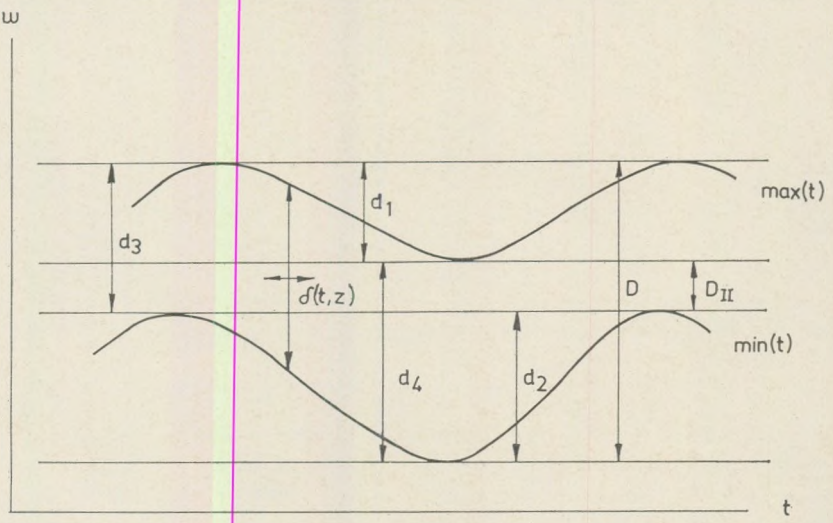

Fig. 6. Model of the empirical extremity functions and characteristics

the course of the detailed analysis we will have to introduce also some further new characteristics at a later stage.

For the $w_{min}(t)$ function a special interpretation is needed. As a matter of fact, this function represents that part of the water stock, which at the actual climatic conditions does not take part in the active water traffic of the soil. Let us call this water stock in what follows the passive water stock of the bare ground. The expression w_{min} (t_{min}) is the climatically determined minimal water stock, which never takes part in the water traffic of the bare soil. By using an approximate analogy let us call in what follows the water stock expressed by $w_{min}(t_{min})$ the fossil water stock of the bare soil. It is obvious that in case of the presence of a plant cover a part of the passive, respectively fossil water stock could be "activized" by the presence of the plant cover in the layers of the main root zone.

Let us consider at first the connection between the extreme water stocks and the hydrophysical constants. A few observations of general characters are as follows. All the changes of the extreme water stocks remain always between the values of the water stocks of the maximum capillary water capacity and that of the wilting point, (except for w_{min} at the depth of 0—10 cm, which is touching, respectively surpassing the limit of Hp in July—September). In the whole year we have: $Hp < w_{min} < w_k$, while we may have $w_{max} \leqq W_k$. For this later inequality we could have three types in time: 1., $w_{max} < W_k$ from November to March); 2., $w_{max} < W_k$ from July to October and 3., $w_{max} \leqq W_k$ from April to June, i. e. the cumultative curve of $w_{max}(z)$ intersect at some depth z_i the cumultative curve of $W_k(z)$. These intersection points can be found from April to June at the depth of 80, 100 and 120 cm one after another.

We can state also a score of such features in the connections with hydrophysical parameters and the w_{max} (z,t), respectively w_{min} (z,t) functions which do show more dissimilarity than similarity. Let us present here a few such features.

The profile changes of $w_{max}(z)$ (during the year) are showing regularities which are very similar to that of the average moisture profile. In the yearly variation the profile changes have a "straightening" and a "curving" section and the relative positions of these to the $W_k(z)$ profile are always well determined. The profiles of the extreme values of w_{max} (z,t) (March and October) are not identical with the extreme positions of the yearly profile changes. The extreme positions of the profile changes (in agreement with the profile changes of the mean moisture) fall to July, respectively to December. Fig. 7. shows the extremity profile together with the profile of water capacity. The water capacity profile is intersected by the two extremity profiles sumewhere within the whole layer under investigation, namely the extremity profile for July from below and the extremity profile for December from above. That means that the $w_{max}(z)$ profile agrees with the profile the water capacity, twice during the year and in that case also the absolute values of the $w_{max}(z)$ water stocks agree with the water capacity. The extreme positions of the

$w_{max}(z)$ profiles strongly deviate from those of a hypothetical homogeneous profile. The difference may equal sometimes the interval of the yearly changes of the profiles.

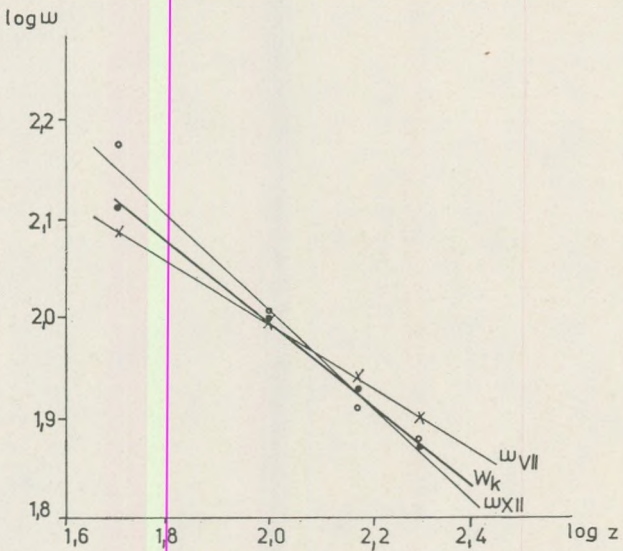

Fig. 7. Yearly oscillation of the depth profile of the maximum water stock. Erdőhát, 1951 – 70.

The $w_{min}(z)$ and Hp profiles show less similarity than the profiles $w_{max}(z)$ and $W_k(z)$. The relative distribution of $w_{min}(z)$ is in general more extreme than that of $w_{max}(z)$, but it is more uniform than that of $Hp(z)$. The $w_{min}(z)$ profiles are always more similar to the corresponding $w_{max}(z)$ profiles, than to the $Hp(z)$ profile. The yearly changes of the $w_{min}(z)$ profile are significant, its extreme positions fall into August, respectively December. The profile of August is about the same as that of July of $w_{max}(z)$ (parallel shifting), while in the December profile the average gradients are much greater than in the December profile of $w_{max}(z)$, but they are still much lower than in the $Hp(z)$ profile.

It is worthwhile to mention the relation of the passive and fossil water stock to the hydrophysical parameters. Part of these water stocks is not available for the plants, but some part of them is contained within the useful water capacity. This part as a relative quantity shall be expressed as follows: $u = \frac{(w_{min} - Hp)}{hw_k}$. The new variable $u(z,t)$ indicates, what part of the useful water capacity turns into passive water and when. It is obvious that the $u(z, t_{min})$ function gives always the corresponding part of the fossil moisture.

The features of the $u(z,t)$ function will not dealt with here in detail, only the depth distribution of the utilizable fossil waterstocks are shown

in Fig. 8. We can see a monotonously increasing function with a non-linear upper section because the effect of weather being strong here, but beginning with a certain depth it seems to become rigorously linear. Thus, in this depth zone the total of the fossil water stock above Hp increases by about the same constant value for every layer.

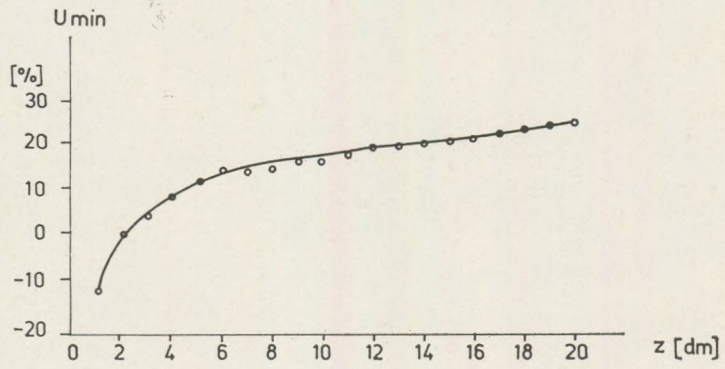

Fig. 8. Depth distribution of the utilizable fossil water stock. Erdőhát, 1951–70.

In the foregoing we defined several extremity characteristics which do not refer to time changes and they depend only on the depth. (Fig. 6.), e. g. D, D_{I}, D_{II}, Δ, d_1, d_2, d_3, d_4. In the course of detailed investigations one can find many interesting features, respectively regularity in the behaviour of these characteristics, and some of them will be shown here.

First of all we consider the domain of the whole water stock soil, of the expressed by the function $w_{\max}(z, t_{\max})$. According to the definition the absolute yearly oscillation of the water stock of the soil is

$$D_{\mathrm{I}} = w_{\max}(t_{\max}) - w_{\min}(t_{\min}) ,$$

and

$$\frac{D_{\mathrm{I}}}{w_{\min}(t_{\min})} = \frac{w_{\max}(t_{\max}) - w_{\min}(t_{\min})}{w_{\min}(t_{\min})} . \tag{7}$$

The expression (7) gives in reality the relative difference of extreme values of the extremity functions, which can characterize the internal structure of the whole domain of the water stock of the soil. The whole domain of the water stock of the soil can be assumed to consist of two partial domains. One of them is the domain of the fossil water stock $w_{\min}(t_{\min})$, which do not change with time, the other is the absolute yearly oscillation (D_{I}) domain, within which all the time changes occur. Both of them are of course functions of the depth.

Fig. 9. shows the depth function of the ratio of the two functions. The ratio decreases very quickly and non-linearly down to about 70–80 cm, then the curve becomes linear and what is more, the value of the

ratio becomes practically constant, i. e. does not depend on depth at all. The value of the ratio is in the whole layer always greater than the unity, i. e. the oscillation domain is always greater than that of constant moisture. In the uppermost layers the ratio turns to assume extreme values, it can surpass several times the unity, i. e. the extreme moisture oscillation extends to the most part of the whole domain. For sake of comparison we give the absolut values of the ratio components for the whole layer:

$$D_I(200) = 276{,}5 \text{ mm}, \qquad w_{\min}(200, t_{\min}) = 191{,}1 \text{ mm}.$$

The variables d_1, d_2, are the yearly amplitudes of the maximum, respectively the minimum functions, while d_3 and d_4 represent the "wideness" characteristics of the extremity functions. Let us consider the depth functions of their ratios.

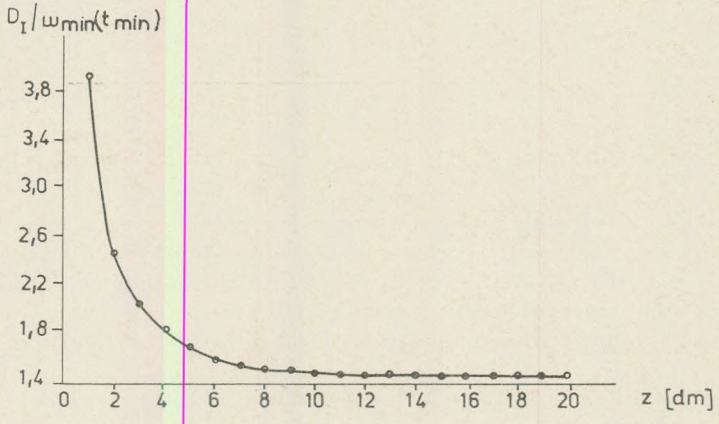

Fig. 9. Depth variation of the structure of the total water stock. Erdőhát, 1951 – 70.

When comparing the behaviour of the amplitudes and wideness characteristics against depth we find a very close similarity, so that itis sufficient to investigate only the depth function of the amplitude ratios. The depth function of the ratio d_1/d_2 presents an interesting regularity (Fig. 10.) at first it is decreasing down to abot 60 70 cm, then it is increasing troughout the whole layer, its value is always smaller than the unity and in the whole layer (0 – 200 cm) it is the same as in the uppermost layer (0 10 cm). The shape of the ratio-curve is surprisingly similar to that representing the relative water saturation of the soil.

In the relatively more saturated layer (down to 70 cm) the ratio-curve is falling, i. e. $d_2(z)$ is increasing more rapidly relatively, than $d_1(z)$, and what is more we can have $d_1' < d_2'$ also in the praxis. In the relatively less saturated layer (below 70 cm) the ratio-curve is rising, i. e. $d_1(z)$ is increasing more rapidly than $d_2(z)$, and what is more, there can also be found that $d_1' > d_2'$ in the praxis. This indicates that the behaviour of the two extremity functions is in close interrelation with the relative moisture state of the

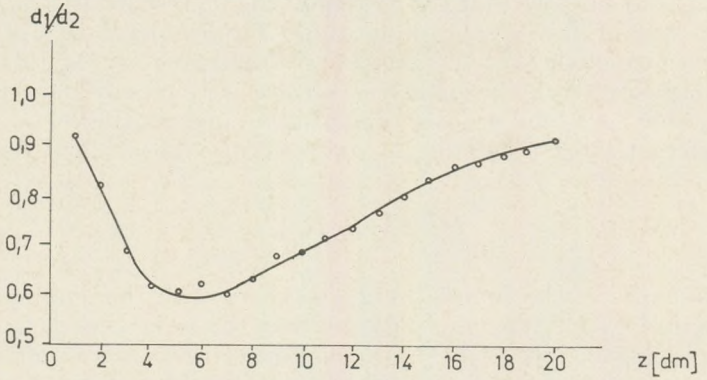

Fig. 10. Empirical depth function of the ratio of extreme amplitudes. Erdőhát, 1951 – 70.

soil and it is inversely reacting to it. Both amplitudes $d_1'(z)$ and d_2' are decreasing, but as long as $d_1'(z)$ changes relatively slowly and to a little extent, $d_2'(z)$ changes within the whole layer by an order of magnitude. Thus, for the relative moisture state of the soil it is the minimum function which is most indicative.

The depth functions of the amplitudes d_1 and d_2 could hardly be determined separately in a mathematical form. We have determined the depth function of the differences of the two amplitudes in a purely empirical manner as follows:

$$\frac{d_2 - d_1}{d_2} = a\, z^b\, e^{cz}\,, \tag{8}$$

from which we get

$$d_1 = d_2(1 - a\, z^b\, e^{cz})\,, \tag{9}$$

where a,b and c are empirical constants. The agreement between computed and empirical values is sufficiently good, so that an amplitude can be calculated approximately from the other one when necessary. On the other hand, the sum of the two extreme amplitudes

$$D - d_1 + d_2$$

represents also a depth function in the same manner as the mean amplitude. The function of the $D(z)$ characteristic analogue to (1) is (Fig. 2.):

$$D(z) = D_1 \frac{B^{\lg z}}{z}\,. \tag{11}$$

In (11) D_1 is the value of the characteristic in the starting layer, B is a general constant and z is a dimensionless depth variable.

The relative difference of the empirical values and of those computed from (11) is less than 4% (it surpasses this limit only at 20 and 30 cm)

It is proper to suppose that the equation (11) represents an exact function such as that of the average amplitude. From equations (10) and (11) we have to conclude that the extermity amplitudes $d_1(z)$ and $d_2(z)$ despite of their apparently deviating behaviour are very closely interrelated one with another and they are conditional upon one another.

Differentiating equation (11) we obtain the original depth function

$$D'(z) = B_1 D_1 \frac{B^{\lg z}}{z^2}. \tag{12}$$

The curve of the function (12) (together with the empirical values) appears in Fig. 11. We can easily see that the somewhat poor matching in a few cases can only be due to the random errors of the empirical values.

The position of the two extremity functions against each other — represented in some part by the wideness characteristics — is also typically changing with depth. The depth curve of the ratio d_3/d_4 is so similar to the curve of the Fig. 10. that it is not worth showing separately. The depth function of the relative differences of d_3 and d_4 is the same as (8), respectively (9), only the values of the parameter are different. The depth function of the sum of the wideness characteristics (d_3+d_4) can not be constructed in an analogous manner to the equation (12).

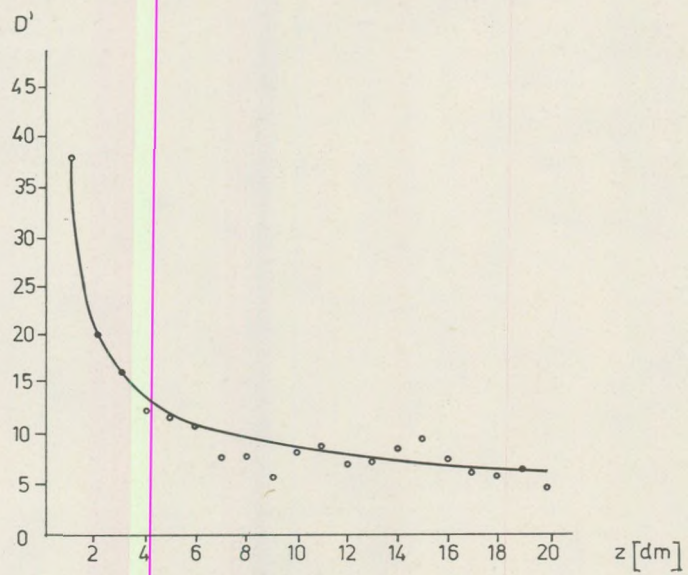

Fig. 11. Depth function constructed from the extreme amplitude sums. Erdőhát, 1951 – 70.

The depth function of the ratio Δ/D_1 is shown in Fig. 12. Out of the characteristics given above D_1 is the greatest, Δ the smallest (in absolute value). The function $\Delta/(z)$ can be interpreted as a certain "distortion"

index. One can imagine that $\Delta(z)$ figures in the absolute yearly oscillation as an additive term. If the distortion would be eliminated, i. e. the curve of any extremity function could be derived by a simple parallel shifting from the another, then the absolute yearly oscillation would diminish by $\Delta(z)$ or by a proportional part of it. Thus, the ratio Δ/D_I indicates the share of this distortion in the yearly oscillation.

The curve (Fig. 12.) is about the reflected image of the curves of ratios d_1/d_2, respectively d_3/d_4. Both component parts of the ratio are increasing, but in the upper layers $\Delta(z)$ is increasing steeper than $D_I(z)$, while it becomes reversed in the lower layers. Though $\Delta'(z)$ in the 0 – 10 cm layer assumes its highest value and it diminishes downwards, the relative distortion index $[\Delta(D_I)]$ is showing its maximum in the 0 – 60 cm layer (it surpasses 1/3) and it decreases quickly with the depth, and its value for the whole layer is only 17%. Thus, the distortion index is also connected to the relative (water) saturation state of the soil.

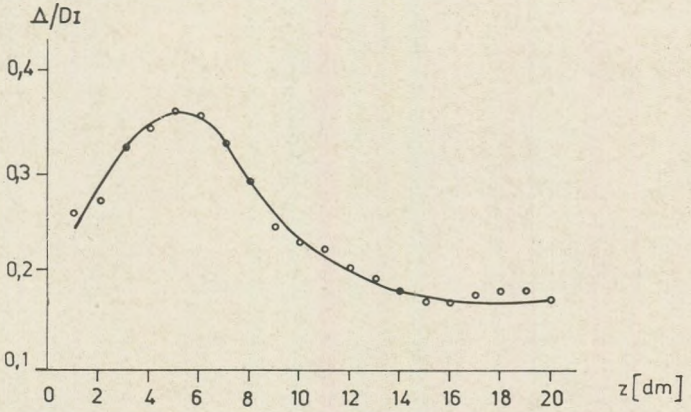

Fig. 12. Depth distribution of the relative distortion index. Erdőhát, 1951 – 70.

Finally we will introduce the function $p(z,t) = \delta(z,t)\ w(z,t)$ showing (in the seasonal variation) the ratio of the extrem eoscillation and of the average water stock. In the yearly variation of $p(z)$ we can separate three types, as shown on Fig. 13. Two of the types correspond to the extreme positions of the yearly variation and the third one is the dominating one. The first type (January curve) is characterised by the circumstance that in the upper layers (down to 60 – 70) cm $p(z)$ remains practically constant, then it is rising. With the second end of the summer type (August curve) the picture is principially reversed: the upper section is (not linearly) decreasing and the curve becomes constant in the lower section. The third dominant type (May curve) is a combination of the two extremity types: in the upper section it is showing the summer type, while in the lower one it is like the winter type. In the major part of the year (in seven months altogether) the third type prevails.

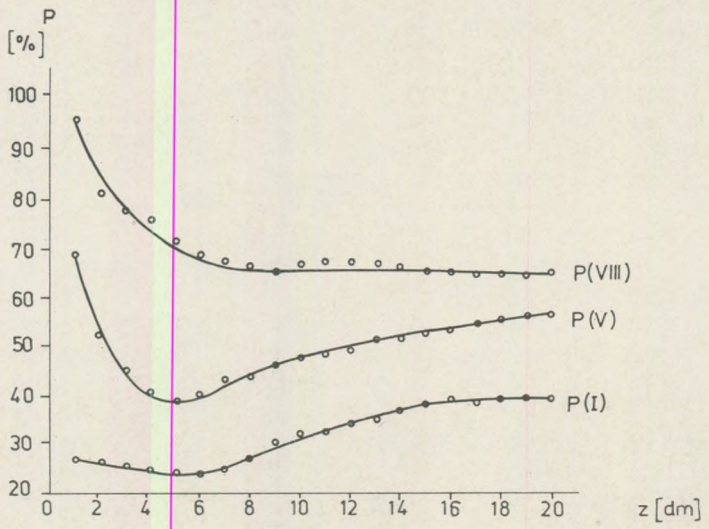

Fig. 13. Three basic types of the empirical $p(z,t)$ function. Erdőhát, 1951 – 70.

This is clearly supporting our earlier conclusion that the yearly variability of the soil moisture is closely, but inversely correlated with the relative (water) saturation of the soil. This is truly reflected in the seasonal variation and depth distribution too.

3. Connections of the average and extreme water stocks

Up to now we have investigated the average or extreme water stock changes and looked for regularities which showed themselves valid independently from one another. Our further aim is to detect the connections between mean and extreme variations which can indicate also the most general regularities of the moisture variations. From the numerous possibilities we will treat in detail here only two relations, the connection between the extremity characteristics and the yearly mean moisture content as well as some connections of the mean yearly amplitude.

We are showing on a common figure (Fig. 14.) the depth curves of the ratios $D/\overline{w}$ and $D_I/\overline{w}$. Both ratios have a common denominator and the numerators are also very close one to another with regards both their physical content and absolute values, as well as their depth variations. The features of the ratio-depth functions partly agree, partly deviate. Both functions surpass the unity in the uppermost section (down to about 30 cm), while in the other layers their value is less than 1. That means that the absolute yearly amplitude of the soil water stock may be greater than the average yearly stock. And that is true so much the more for the D-characteristic, since in the uppermost layers we have $D > D_I$. At the depth of 40 cm the two curves intersect, i. e. here we must have $D = D_I$ and $D_{II} = 0$. The depth curves of both

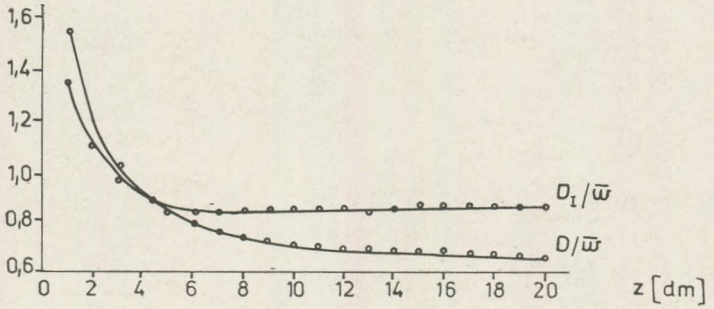

Fig. 14. Depth profiles of important characteristic ratios. Erdőhát, 1951 – 70.

ratios represent a non-linearly decreasing function. The ratio $D/\overline{w}$ is a monotonously decreasing function in the whole layer, while the curve of $D_I/\overline{w}$ is much more complicated. This one is also decreasing down to 70 cm (it has a local minimum hardly distinguishable there), then it increases somewhat, after it remains strictly constant in the layers between 100 and 200 cm. The similarity with the corresponding $p(z)$ functions is apparent (Fig. 13.).

Characteristic connections can be established also by using the mean yearly amplitude. An example for this can be seen on Fig. 15. The connection between mean and absolute yearly amplitude is surprisingly close and the ratio depth function is strictly linear. The ratio

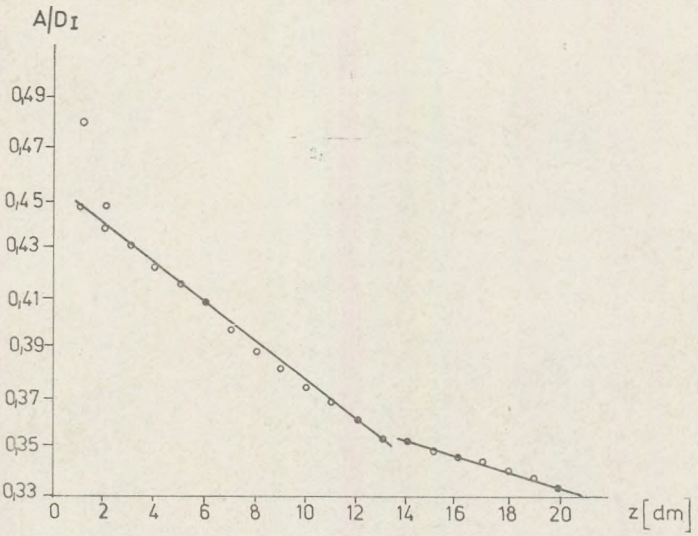

Fig. 15. Empirical depth functions of the ratio of the mean amplitude and absolute yearly oscillation. Erdőhát, 1951 – 70.

values do not deviate from the adjusted straight line except in the uppermost layer between 0—20 cm and a striking deviation is shown only by the 0—10 cm layer. In the whole layer two straight lines can be adjusted to the empirical values. The first one is valid for the 0—130 cm layer, the second one for the 130—200 cm one. The physical cause respectively the exact explanation of the deviation of the two domains is still lacking.

The ratio-depth-function of A/D_1 can be described by a linear regression equation as follows:

$$\varphi(z) = \beta - \alpha z_z . \tag{13}$$

since for the two domains two equations are valid, the values of the corresponding empirical parameters are different too. From the equations (1) and (13) we are able to express the depth function of the absolute yearly amplitude total (Fig. 2.) as follows:

$$D_1(z) = A_1 \frac{B^{\lg z}}{\beta z - \alpha z^2} . \tag{14}$$

The matching of the empirical and computed D_I values, obtained from equation (14) is very good. The relative differences fall within 0—3% and, in spite of the linear interpolation, even in the layer between 0 and 10 cm does not surpass 6,8%, which is still aceptable.

Differentiating equation (14) we get the original depth function of the absolute yearly oscillation

$$D_1'(z) = A_1 \frac{B^{\lg z}}{\beta z - \alpha z^2} \left(\frac{B_1}{z} + \frac{1}{p - z} \right), \tag{15}$$

where $p = \beta/\alpha$. We have to mention that (15) can be written by using equations (1) and (2) in the following form:

$$D_1'(z) = A(z) \frac{\alpha}{(\beta - \alpha z)^2} + A'(z) \frac{1}{(\beta - \alpha z)} . \tag{16}$$

Finally we will show the connection between the average yearly amplitude and the amplitudes of the extremity-functions (Fig. 16.). By this we get an additional proof of the fact that certain features of the two extremity-functions are significantly different. It is obvious that the yearly distribution function of the average water stock must be located between the extremity-functions, but the average amplitude does not necessarily fall between the extreme amplitudes. In reality we have $d_1(z) \leqq A(z) < d_2(z)$, as it can be checked by means of the values of the ratios. The ratio A/d_2 is a function of the same type as d_1/d_2 (Fig. 10.), while A/d_1 is a reflexted image of the previous one. Thus it follows that the depth function of the mean amplitude concerning its absolut values and other features (relative increments etc.) is very close to the amplitude of the maximum function and at the same time it differs significantly from the amplitude of the minimum function.

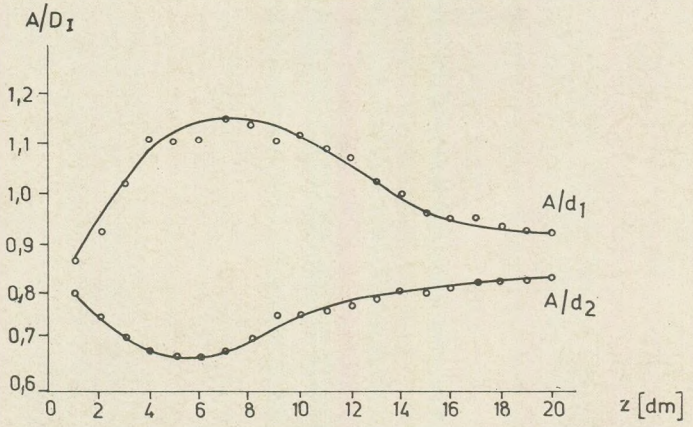

Fig. 16. Depth function curve of the absolute yearly oscillation. Erdőhát, 1951 – 70.

By the analyses above we have demonstrated though not exhausted the rich content of this domain of problems or its possibilities. A more detailed meteorological analysis of the connections and regularities detected here as well as their interpretation will be the subject of further studies.

REFERENCES

E r d ő s, L. – M o r v a y, A. (1961): Moisture march of a few soil types of our land. Időjárás, 65 (1): p. 47 – 55. (in Hungarian)

E r d ő s, L. (1975): Evaporation of bare and covered soil surface. Időjárás, (in print) (in Hungarian)

E r d ő s, L. (1975): Water stock variations of the bare soil. Időjárás (in print) (in Hungarian)

APPLICATION OF INVERSE FILTERING IN THE INTERPRETATION OF GRAVITY AND MAGNETIC ANOMALIES

by

K. KIS

Department of Geophysics, L. Eötvös University, Budapest
Received 15 March 1975

РЕЗЮМЕ

Аномалия моделей, применяемых в гравитационной и магнитной интерпретации может быть представлена в виде конволюции двух функций. Одна из них описывает плотность или намагниченность, а вторая – геометрию. Описание аномалий в конволюционной форме дает возможность применять аппарат линейной оптимальной фильтрации. Планирование обратных фильтров может быть доведено до конца только в случае определенной модели. Параметры обратного фильтра получаются как решения уравнения Вейнера с использованием в качестве автокорреляционной функции той функции, которая описывает геометрию. Параметры интерпретации получаются как результат конволюции измеренных данных и параметров обратного фильтра. Работа знакомит с планированием обратных фильтров и на синтетических примерах показывает определение параметров возмущающих тел.

SUMMARY

The anomalies of the models applied in gravity and magnetic interpretation can be obtained as a convolution of two functions. One of these describes the geometry (depth, shape) the second is connected to density distribution of magnetization. The description of anomalies by convolution makes possible the application of linear optimum filters. Inverse filters can be designed if the model is given. The coefficients of the inverse filters are obtained from the Wiener equation which contains the samples of the autocorrelation of the function describing the geometry of the models.

The parameters are supplied by the convolution of the inverse filter with measured data. Design procedure of the inverse filter is given and its application for determination of the parameters of the magnetic bodies is demonstrated by a synthetic example.

Introduction

The anomalies belonging to a class of models which are often applied in the interpretation of gravity and magnetic anomalies can be written as a convolution of two functions. One of these, denoted by $h(x)$, describes the density or magnetization (depending on the nature of the anomaly) the other one, denoted by $k(x)$, describes the geometry of the applied model. The anomaly in a point then becomes

$$a(x) = \int_{-\infty}^{+\infty} h(x)\, k\big((x'-x), Z_1, Z_2, \alpha, \beta\big)\, dx', \tag{1}$$

where the actual values of the parameters Z_1, Z_2, α and β can be determined by choosing an appropriate model; Z_1 and Z_2 denote the depths of the upper and lower boundaries of the causative body, α and β denote the direction of the Earth's magnetic field, and that of the magnetization of the body. (The two latter parameters obviously do not appear in the case of gravity anomalies). Formula (1) refers to two-dimensional causative bodies, but could be easily generalized to the three-dimensional case.

In a class of interpretational problems the function $h(x)$ is to be determined when $a(x)$ and $k(x)$ are known. Bott, M. H. P. (1967 and 1973) suggested two procedures for the solution of such problems but solutions can also be obtained by inverse filtering (Robinson and Treitel, 1967).

The inverse filter should output the $h(x)$, when the anomaly $a(x)$ is the input to the filter. The impulse response $w(x)$ can be determined by minimalization of the mean square deviation between actual and desired outputs, i. e. between $a(x) * w(x)$ and $h(x)$. In digital form the criterion can be written as

$$\mathcal{E}\left\{\left(h_i - \sum_j w_j a_{i-j}\right)^2\right\} = \min, \tag{2}$$

when E denotes the computation of the expected value.

Computing the deviatives of (2) with respect to the w_j filter coefficients the well-known Wiener equations, a set of linear simultaneous equations

$$\sum_j w_j \varphi_{aa}(k-j) = \varphi_{ha}(k) \qquad k = 0, 1, \ldots, K \tag{3}$$

is obtained and the solution of the equations supply the w_j coefficients. (In the equation φ_{aa} denotes the autocorrelation of the input, φ_{ha} denotes the cross-correlation of the desired output and the input).

The inverse filtering is but a special case of linear optimum filtering and the interpretation is based on the estimation of the φ_{aa} and φ_{ha} correlation functions.

The inverse filtering will be illustrated in the followings by syntetic examples in the interpretation of total magnetic fields due to two-dimensional prisms.

Total magnetic field due to two-dimensional prisms

The total magnetic field due to a two-dimensional magnetized prisms can be easily evaluated by the logarithmic potential (Grant F. S., West G. F., 1965). In the two-dimensional coordinate system (x,z), shown in Fig. 1., the total-field in an arbitrary point with coordinates x and z can be expressed as follows

$$t(x,z) = -2\frac{\partial^2}{\partial\alpha\,\partial\beta}\int_{z_1}^{z_2}\int_{x_1}^{x_2} m(x',z')\ln\left((x-x')^2+(z-z')^2\right)^{\frac{1}{2}} dx'\,dz', \tag{4}$$

where α denotes the direction of the Earth's magnetic field and β that of the magnetization, $m(x,z')$ is the magnetization of the prism. After some elementary manipulations the expression for the total-field in the point $P(x,o)$, shown in Fig. 1. becomes

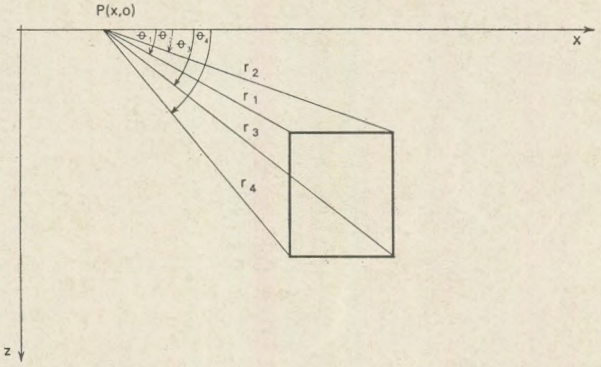

Fig. 1. The two-dimensional prism in the xz coordinate system

$$t(x,0) = -2m\left[(\Theta_1-\Theta_2-\Theta_4+\Theta_3)\cos\tau\cos I+\ln\frac{r_1 r_3}{r_2 r_4}\cos\tau\sin I+\right.$$

$$\left.+\ln\frac{r_1 r_3}{r_2 r_4}\sin\tau\cos I+(\Theta_2-\Theta_1-\Theta_3+\Theta_4)\sin\tau\sin I\right] \tag{5}$$

assuming homogeneous magnetization within the prism (m is the magnetization with direction τ, while I denotes the inclination of the Earth's magnetic field).

For the sake of simplicity let us assume that the magnetic anomaly is computed at the level $z = 0$, the inclination of the Earth's magnetic field is 90°, and the direction of the magnetization of the prism is either 90° or 270°. (It can be shown, that the assumptions simplify the computations but do not modify the general validity of the suggested computational procedure).

By using the assumptions again in equ. (4) after elementary computations we obtain for the total field the relation

$$t(x,0) = 2\sin\tau\int_{x_1}^{x_2} m(x')\left(\frac{z_1}{(x-x')^2+z_1^2}-\frac{z_2}{(x-x')^2+z_2^2}\right)dx' \tag{6}$$

if the magnetization m does not depend on z. Let us introduce the function

$$g(x) = \frac{z_1}{x^2+x_1^2}-\frac{z_2}{x^2+z_2^2}. \tag{7}$$

The function defined by (7) depends on the geometry of the prism, only and it is independent of the magnetization. Therefore the anomaly can be written as

$$t(x, 0) = 2 \sin \tau \int_{-\infty}^{+\infty} m(x')\, g(x - x')\, dx' \tag{8}$$

i. e. the total-field anomaly is indeed obtained as a convolution of a function $m(x)$ describing the magnetization and a function $g(x)$ describing the geometrical configuration. Equ. (8) is equivalent to equ. (6) only in those cases when the magnetization outside the prism is zero.

Determination of the inverse filter

In the previous part it was shown that the total-field anomaly can be written as the convolution

$$t(x) = m(x) * g(x) . \tag{9}$$

Let us assume that the $t(x)$ anomaly is due to a random distribution of the magnetization $m(x)$. It can also be assumed that the expected value of the magnetization is zero and the magnetizations of the prisms are uncorrelated, i. e.

$$\mathcal{E}\{m_k\} = 0 \tag{10}$$

and

$$\mathcal{E}\{m_k\, m_{k+l}\} = 0 . \tag{11}$$

A further assumption is that the anomaly $t(x)$ is a composite field due to prisms with different magnetization but identical shape.

The total-field in the i-th point of the magnetic profile within a stationary interval can be given by the general expression

$$t_i = m_i * g_i + n_i , \tag{12}$$

where n_i denote the random noise component.

The inverse filter tries to reconstitute the series m_i from the data t_i describing the profile. The length of the deconvolution operator (i. e. the length of the inverse filter) be L. Then the desired output

$$r_i = m_{i+p} , \tag{13}$$

where

$$p = \frac{L-1}{2} . \tag{14}$$

The actual output of the deconvolution becomes

$$e_i = \sum_{k=0}^{L} w_k t_{i-k} . \tag{15}$$

The operator $\{w_k\}$ minimalizes the deviation between the desired and actual outputs in the mean square sense, i. t.

$$\mathcal{E}\left\{(r_i - \sum_{k=0}^{L} w_k t_{i-k})^2\right\} = \min . \tag{16}$$

By the computation of the derivatives with respect to the filter coefficients w_k the Wiener equations are obtained:

$$\sum_{k=0}^{L} w_k \varphi_{tt}(l-k) = \varphi_{rt}(l) \qquad l = 0, 1, \ldots, L , \tag{17}$$

where φ_{tt} is the autocorrelation of the input, φ_{rt} the crosscorrelation of the desired output and the input.

First we estimate the autocorrelation φ_{tt} and cross-correlation φ_{rt}, then the solution of the set of linear simultaneous equations (17) yields the coefficient w_k. The definition of the autocorrelation φ_{tt} is

$$\varphi_{tt}(l) = \mathcal{E}\{(m_i * g_i - n_i)\,(m_{i+l} * g_{i+l} + n_{i+l})\} \tag{18}$$

and after taking the expected value of the product it yields

$$\varphi_{tt}(l) = S\,\varphi_{gg}(l) + \varphi_{nn}(l) , \tag{19}$$

where φ_{gg} and φ_{nn} are the autocorrelation of the function describing the geometry and that of the random noise component, respectively; while S denotes the autocorrelation of the magnetization for the argument zero. In deriving (19) we made use of the assumption that the noise and the data of the noise-free profile is uncorrelated. The definition of the cross correlation $\varphi_{rt}(l)$ is

$$\varphi_{rt}(l) = \mathcal{E}\left\{m_{i+p}\left(\sum_{k=0}^{L} g_k\, m_{i-l-k} + n_{i-l}\right)\right\} \tag{20}$$

which gives

$$\varphi_{rt}(l) = S\, g_{-l+p} . \tag{21}$$

Putting the correlations (19) and (21) into equation (17) we obtain

$$\sum_{k=0}^{L} w_k(\varphi_{gg}(l-k) + N^* \delta_{kl}) = g_{-l+p} \qquad l = 0, 1, \ldots, L, \tag{22}$$

where $N^* = N/S$ and δ_{kl} is the Kronecker delta symbol, i. e.

$$\varphi_{nn}(k) = \begin{cases} N & k = 0 \\ 0 & k \neq 0 . \end{cases} \tag{23}$$

Application of the inverse filters to synthetic models

For the solution of the equation (17) one has to know the function $g(x)$ and the autocorrelation $\varphi_{gg}(l)$. The latter can be computed from its definition

$$\varphi_{gg}(l) = \mathcal{E}\{g(x)\, g(x+l)\} \tag{24}$$

therefore

$$\varphi_{gg}(l) = \pi\left(\frac{2\,z_1}{\Delta_1}+\frac{2\,z_2}{\Delta_2}-\left(\frac{1}{\Delta_3^2+4\,l\,2z_1^2}\,(z_2\,\Delta_3+z_1\,\Delta_4)\right)-\right.$$

$$\left.-\left(\frac{1}{\Delta_4^2+4\,l^2\,z_2^2}\,(z_1\,\Delta_4+z_2\,\Delta_3)\right)\right), \tag{25}$$

where

$$\Delta_1 = l^2+4\,z_1^2; \qquad \Delta_2 = l_2+4\,z_2^2;$$

$$\Delta_3 = l^2+z_2^2-z_1^2; \qquad \Delta_4 = l_2+z_1^2-z_2^2\,. \tag{26}$$

Fig. 2. shown the normalized autocorrelation $\varphi_{gg}(l)/\varphi_{gg}(0)$.

In the model computions the effects of the random noise will be neglected. An efficient algorithm was developed by N. Levinson for the solution of the set of equations (17). (See e.g. in W i e n e r, 1947)

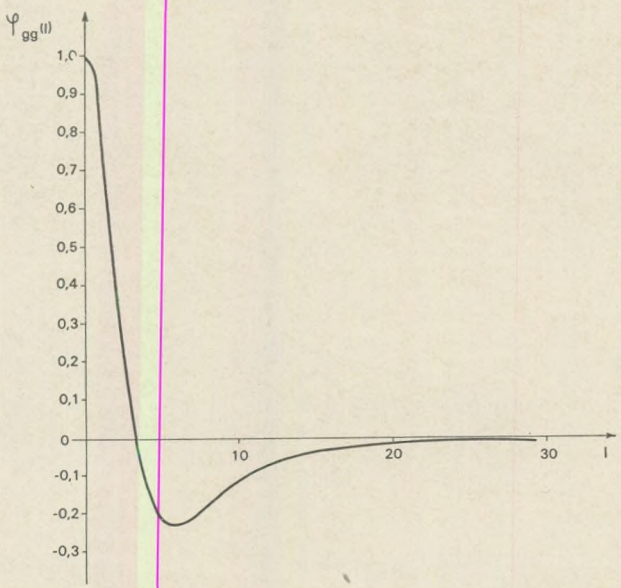

Fig. 2. The normalized autocorrelation of the function describing the geometry of the model

The first example shows the magnetic field of a two-dimensional prism with the parameters $h = 20$, $Z_1 = 2$, $Z_2 = 4$ (measured in the units of the sampling interval), $m = 0{,}02$ (in cgs units) $I = 90°$, $\tau = 90°$ and the result of the deconvolution. The prism and its magnetic field $t(x)$ is given in the upper part of Fig. 3, and the result obtained by a deconvolution filter with 101 coefficients is given in the lower part of Fig. 3. The output of the filter is a pulse, whose length is equal to the length of the prism and the amplitude is equal to magnetization of the prism. In the computation of the magnetization the constant multiplier (left out in the preceeding part) was also taken into consideration. The magnetization obtained by the inverse filter is denoted by $m_d(x)$. It is clearly seen that the relative error is less than 10%.

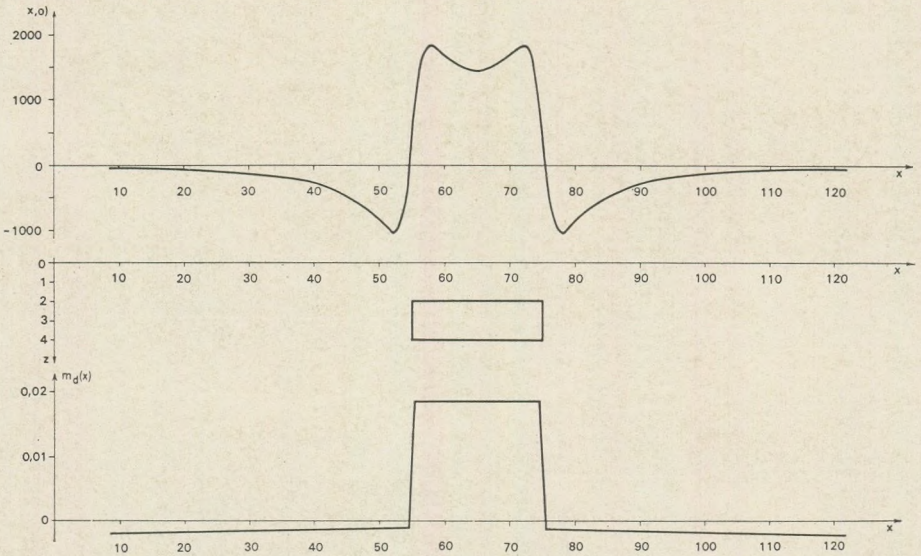

Fig. 3. Total magnetic field due to a vertically magnetized prism of length 20×sampling distance (in $\gamma - s$),
the position of the prism,
output of the deconvolution filter (the magnetization m_d is measured in cgs units)

The filter containing 101 coefficients has also been applied to the magnetic field due to a prism with the parameters 4 = 2 (length), $Z_1 = 2$, $Z_2 = 4$ and $m = 0{,}02$ (in cgs units), $I = 90°$, $\tau = 90°$. The prism, its field and the result of the deconvolution are shown in Fig. 4. The relalative error of m_d, obtained by the filter do not deviate more the 20% from the theoretical value 0.02.

The filter with 101 coefficients, which had been proved to be very efficient in the previous examples was applied to a magnetic profile

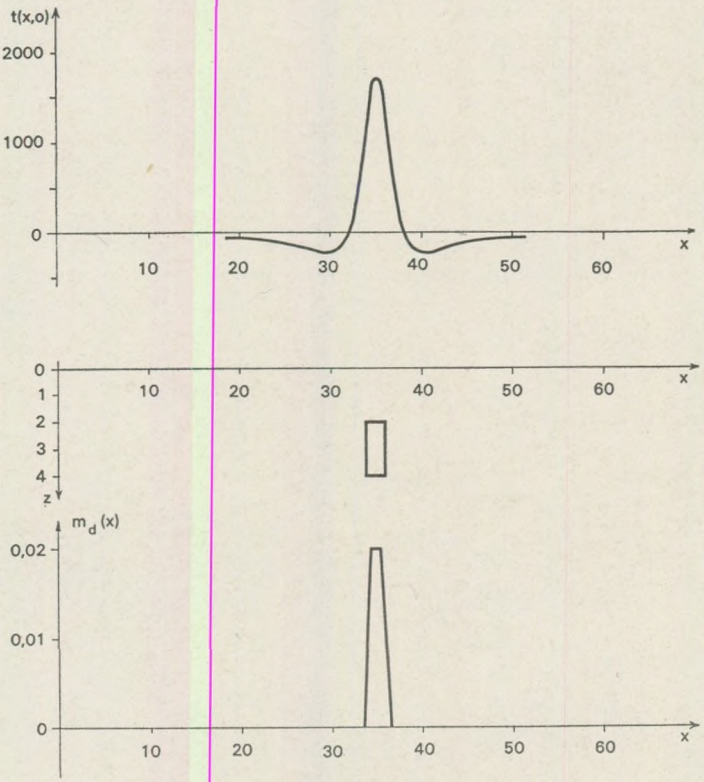

Fig. 4. Total magnetic field due to a vertically magnetized prism of length $2\times$ sampling distance (in $\gamma-$s)
the position of the prism
output of the deconvolution filter (the magnetization m_d is measured in cgs units)

obtained as the composite field due to 13 prisms with different parametets. These parameters are summarized in Table I. (h denotes the lengths of the prisms, Z_1 and Z_2 denote the depths of the top and the bottom, respectively, m gives the magnetization in cgs units, I is the inclination of the Earth's magnetic field and τ is the direction of magnetization of the prisms, both measured in degrees).

Normal and inverse magnetizations regularly follow in the sequence. The synthetic profile is symmetric with respect to the center. The magnetic field due to the sequence of prisms is shown in Fig. 5., together with the output of the deconvolution filter (in the upper and lower parts, respectively).

The filtered profile $m_d(x)$ correctly restores the original lenghts of the blocks, while the relative error in the magnetization amounts to $10-20\%$.

Table I

No	Z_1	Z_2	h	m [cgs]	I [°]	τ [°]
1	2	4	20	0.012	90	90
2	2	4	10	0,012	90	270
3	2	4	20	0.012	90	90
4	2	4	4	0.012	90	270
5	2	4	2	0.012	90	90
6	2	4	6	0.012	90	270
7	2	4	20	0.030	90	90
8	2	4	6	0.012	90	270
9	2	4	2	0.012	90	90
10	2	4	4	0.012	90	270
11	2	4	20	0.012	90	90
12	2	4	10	0.012	90	270
13	2	4	20	0.012	90	90

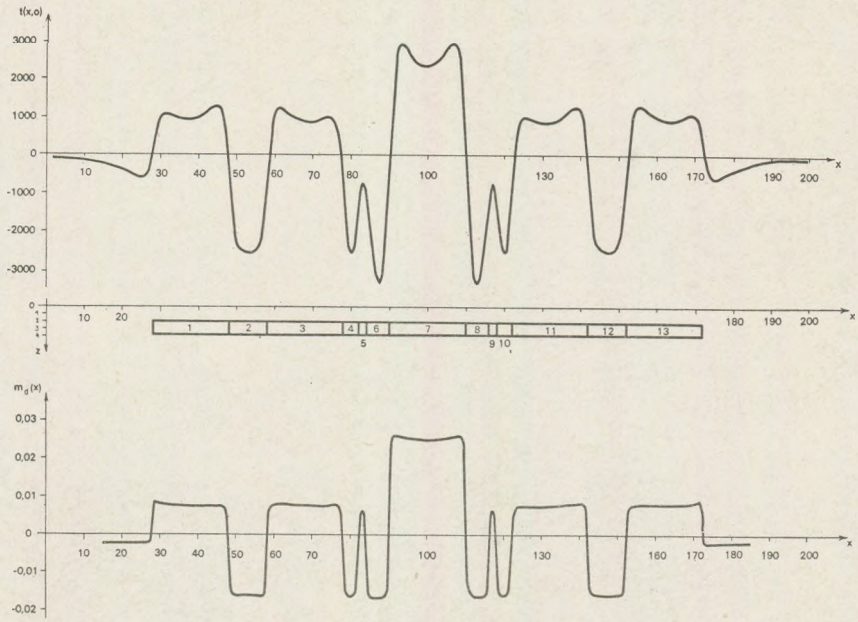

Fig. 5. Composite field of 13 prisms (in $\gamma-$s)
the position of the prisms,
the output of the deconvolution (m_d is measured in cgs units)

The author is greatly indebted to dr. A. Meskó for his help in the method of investigation.

Computations were made in the computer Center of the University by Razdan-3 and the provision of computing facilities is gratefully acknowledged.

REFERENCES

Bott, M. H. P., (1967): Solution of the linear inverse problem in magnetic interpretation with application to oceanic magnetic anomalies. Geophysical. J. R. Astr. Soc. Vol. 13, 313–323.

Bott, M. H. P., (1973): Inverse methods in the interpretation of magnetic and gravity anomalies. Methods in Computational Physics vol. 13, 133–162. Acad. Press New York and London.

Grant, F. S.–West, G. F., (1965): Interpretation theory in applied geophysics. Mc Graw Hill.

Meskó A., (1972): A digitalis szeizmikus feldolgozás alapjai. Tankönyvkiadó.

Numerikus szűrési módszerek alkalmazásai a geofizikai adatok feldolgozásában. (1973). Szerk.: Meskó A.

Remete L. (1973): Dekonvolúciós szűrők tervezése és alkalmazása. Magyar Geofizika XIV. évf. 3–4.

Robinson, E. A.–Treitel, S. (1967): Principles of digital Wiener filtering. Geophys. Prosp. vol. 15, 311–333.

Wiener, N. (1947): Extrapolation, interpolation and smoothing of stationary time series. The Technology Press of MIT.

A NEW ALGORITHM FOR THE COMPUTATION OF GRAVITATIONAL ATTRACTION DUE TO IRREGULARLY SHAPED BODIES

by

A. MESKÓ

Department, of Geophysics, L. Eötvös University, Budapest
Received: 1 March 1975

РЕЗЮМЕ

Тело неправильной формы разделяется на кубы, которые в свою очередь сужываются на точеные массы. Преобразование Фурье в двух переменных для вертикальной компоненты притяжения точечного источника известно в аналитической форме, влияние всех точечных масс, расположенных на одной и той же глубине, может быть задано посредством свёртки. Свёртка в области частот соответствует операции умножения, поэтому Фурье преобразование слоя, состоящего из кубов расположенииых на равных глубинах, легко может быть определено. Эти суммируются с целью получения Фурье преобразования функции, описывающей притяжение от всех точечных масс. Конечный результат получается посредством обратного фурье преобразования.

Скорость вышеупомянутой процедуры примерно на порядок больше чем у известных из литературы других методов. Точность при этом может быть как угодно повышена с увеличением числа точек, заменяюших тело.
Проледура сравнивается с методами Талвани и Евинг (1960) а также и Муфти (1975). Практическое применение проледуры иллюстоируется на двух примерах.

SUMMARY

The irregularly shaped body is divided into cubes and the cubes are concentrated in mass points. The-two-dimensional Fourier transform of the vertical component of the gravitational attraction due to a point source is given analytically, the contribution of all mass points at the same depth can be described by convolution. Convolution corresponds to multiplication in the frequency domain therefore the Fourier transform of each layer of cubes can be easily determined. These are su nmed to give the Fourier transform of the attraction due to all mass points. The result is obtained by inverse Fourier transformation.

The procedure is faster than the others known from the literature by about one order of magnitude. Accuracy can be made as high as necessary by applying properly dense spacing of points. The procedure is compared to those proposed by Talwani and Ewing (1960) and by Mufti (1975). Practical applications are illustrated by two examples.

Introduction

An algorithm is described for the rapid computation of the gravitational attraction due to irregularly shaped bodies. A number of methods with the same purpose have been proposed (e. g. Talwani and Ewing, 1960., Nagy, 1966, Botezatu et al., 1971, Mufti, 1975). The best of these methods is the latest one, published by Mufti but it is still not easy to implement and could be considerably improved.

The basic sources of improvement are the substitution of the body by a sufficiently large number of mass points and the utilization of the Fast Fourier Transform (in the followings FFT) algorithm. The first is an approximation which is justified when the spacing of the mass points is properly dense.

The starting point of the derivation is common with many previously developed methods known from the literature. The irregularly shaped body is divided into rectangular prisms. Most authors then compute the gravity fields of the prisms. Assuming that the prisms are small compared to the dimensions of the body the sum of their individual gravity fields gives a good approximation to the gravity field of the whole body. The gravity field due to a rectangular prism can be given analytically. Various formulas have been derived, none of them is easy to handle. The repeated evaluation of one of these formulas involves time-consuming computations which practically prohibits its use when the number of prisms are large and the gravity field is to be computed at many points. The gravity field due to a cube, however, can be approximated by the gravity field due to a sphere or a mass point in its center assuming that certain requirements are satisfied. The requirements can always be met by choosing sufficiently small cubes.

The two dimensional Fourier transform of the vertical component of the gravitational attraction due to a point source is also known analytically. Consider now all those points which are at the same depth. The total effect of these points is described by a convolution which includes the masses and their coordinates on the one hand and the effect of a single point of unit mass on the other. The convolution can be computed very fast by using the analytical expression for the effect due to a mass point and the two-dimensional FFT algorithm.

A similar but restricted version have been described by the present author (M e s k ó, 1976) for sheet-like bodies, i. e. for those bodies which are relatively thin and horizontally large. The restrictions have now been removed. The single layer of prisms with various heights, used in the cited paper, have been substituted by the necessary (but arbitririly large) number of cubes.

The difference between the present procedure and Mufti's procedure is twofold. First, always the approximate formula is used for the dimensions of the cubes are chosen according to the requirements. The use of sufficiently small cubes makes superfluous the iterative procedure suggested by M u f t i (1975). The second deviation which results is considerable gian is that the convolution is computed via the FFT.

The procedure has many applications. It can be used e. g. in gravity modelling, in combined interpretation of seismic, gravity and magnetic data and in the solution of the inverse gravity problem.

The algorithm is described in Part I., while some examples including the investigation of the accuracy are given in Part II.

PART I.

The computational algorithm

Before embarking upon the detailed description of the algorithm the approximation of the gravity field due to a cube by the gravity field due to a mass point is discussed.

Let us consider a cube with its center located in the origin of a rectangular coordinate system (z, y, z) and with sides parallel to the coordinate axes. The z-component of the gravitational attraction due to the cube is considered in a point $P(x, y, z)$ outside the body. Let us introduce dimensionless distances by the definitions

$$z' = \frac{z}{a} \quad \text{(vertical distance)}$$

and

$$r'_h = \left[\left(\frac{x}{a}\right)^2 + \left(\frac{y}{a}\right)^2\right]^{1/2} \quad \text{(horizontal distance)},$$

where 2a denotes the sidelength of the edges of the cube.

M u f t i (1973) has shown that the approximation obtained by concentrating the mass of the cube in the origin has an error equal to or less than $\pm 0.1\%$ when

$$z' \geq 3 \quad \text{and} \quad r'_h \geq 6.25 - z' \tag{1a}$$

or

$$z' < 3 \quad \text{but} \quad r'_h \geq 3.25\,. \tag{1b}$$

The grid spacing in routine gravity measurements is usually 0.5 km or 1 km. The gravity field of an assumed irregularly shaped body is obtained in a form directly comparable to the measurements when 2a is equal to the grid spacing. Inequality (1a) is obviously satisfied for any horizontal distance if $z' > 6.25$ or $z > 6.25$ a. Then the depth of the upper boundary should be greater than 1.31 km (for 0.5 km spacing) or 2.62 km (for 1 km spacing). Taking into consideration the depths encountered in practical applications we might draw the conclusion that cubes with sidelengths of 0.5 km almost always but in some cases even cubes with sidelengths of 1 km assure proper approximation. In the few remaining cases a finer subdivision can be applied where

$$a \leq \frac{h}{5.25} \tag{2}$$

(h is the depth of the upper boundary).

Let us assume in the followings that the body has a flat base i. e. the lower boundary is a plane at depth H and the upper boundary is described by $U(I,K)$ · ($U(I,K)$ gives uniformly digitized depth data).

The procedure is similar when the upper boundary is a plane (flat top bodies) and the lower boundary is given by the depth data $U(I,K)$ It is also obvious that a body of completely irregular shape can be built by these two type of elements. Therefore the somewhat restricted version of a body with arbitrary upper surface and flat base will be discussed.

A cube is considered to belong to the building elements of the body if its mass center is located somewhere between the upper and lower boundaries. We start at the flat base. The mass centers of the deepest layer of cubes are at the depth

$$H-a\,,$$

the mass centers of the next layer of cubes are at the depth

$$H-3a\,,$$

in general, the mass centers of the n-th layer of cubes are at depth

$$H-(2n+1)\,a\,. \tag{3}$$

The depth of the uppermost layer is determined by the largest $n_{\max}$ satisfying the inequality

$$H-(2n_{\max}+1)\,a \geq \min U(I,K)\,. \tag{4}$$

Assuming a homogeneous density distribution for the body the mass points in the n-th layer can be described by

$$M_n(I,K) = \varrho(2a)^3\,\vartheta_n(I,K)\,, \tag{5}$$

where $\vartheta_n(I,K) = 0$, if the center of cube is not in tie body,
$= 1$, if the center of cube is within the body.

The depth of the upper boundary of the body at the point (I,K) is considered the average of the depths in four points of the closest neighbourhood, i.e.

$$\overline{U}(I,K =$$

$$= \frac{1}{4}[U(I+a,K+a)+U(I+a,K-a)+U(I-a,K+a)+U(I-a,K-a)]\,.$$

The value of $\vartheta_n(I,K)$ is determined according to the following inequality

$$\vartheta_n(I,K) = 1\,, \quad \text{for} \quad \overline{U}(I,K) < H-(2n+1)\,a\,, \tag{6a}$$

$$= 0\,, \quad \text{for} \quad \overline{U}(I,K) \geq H-(2n+1)\,a\,. \tag{6b}$$

Other, more sophisticated criteria could have been used to decide whether a cube belongs to the body or not but the simple criteria (6a), (6b) proved to be satisfactory.

The vertical component of the gravity field at the point (J,L) of the surface due to a point mass $M_n(I,K)$ in the n-th layer is given by

$$g_{n,\,I,\,K}(J,L) = \frac{G\,\varrho(2a)^3\,H'}{\{(2a)^2[J-I)^2+(L-K)^2]+(H')^2\}^{3/2}}$$

where $H' = H-(2n+1)$a. If ϱ is given in gcm^{-3}, the distances in kms, and g is to be obtained in milligals

$$g_{n,\,I,\,K}(J,L) = 6.67\,\varrho(2a)^3\frac{H'}{\{(2a)^2[(J-I)^2+(L-K^2)]+(H')^2\}^{3/2}}. \quad (7)$$

The contribution of the n-th layer to the vertical component of the gravity field is obviously given by the convolution

$$g_n(J,L) = \sum_I\sum_k g_{n,\,I,\,K} = M_n(I,K) * S_n(I,K)\,, \quad (8)$$

where

$$S_n(I,K) = \frac{H'}{\{(2a)^2[I^2+K^2]+(H')^2\}^{3/2}}. \quad (9)$$

The Fourier transform of (9) is

$$F\{S_n(I,K)\} = e^{-2\pi H'(fx^2+fy^2)^{1/2}},$$

therefore the Fourier transform of the contribution from the n-th layer by the convolution theorem yields as

$$6.67\cdot F\{M_n(I,K)\}\,e^{-2\pi H'(fx^2+fy^2)^{1/2}}, \quad (10)$$

(where f_x and f_j denote spatial frequencies).

The Fourier transform of the sum of the contributions due to all layers is the sum of the Fourier transforms given by (10). The vertical component of the gravitational attraction is obtained at last by taking the inverse Fourier transform of the sum as follows

$$g(J,L) = 6.67\,F^{-1}\left\{\sum_{n=0}^{n_{\max}} F\{M_n(I,K)\}\,e^{-2\pi H'(fx^2+fy^2)^{1/2}}\right\}. \quad (11)$$

The two transformations can be computed very fast by the *FFT*, the determination of the $M_n(I,K)$ by (6a) and (6b) and the computation of the exponential expression in (11) do not require much computer time. As a result the whole procedure is much faster than those known from the literature. One order or two orders of magnitudes are fair estimates (depending on the dimensions of the body).

PART II.

Investigation of the accuracy, practical examples

The suggested procedure has been compared to those described in the literature. Because Mufti's method is the latest and best method known to the present author this has been chosen as a reference.

Mufti (1975) computed the gravitational attraction due to a sphere with a radius of 3000 feet and with its center at 4000 feet for a density 0.25 gcm^{-3}. The vertical component of the gravitational attraction has been determined as the sum of the lower and upper halves. Results obtained by the present method are shown in Figures 1. and 2. The gravity field due to a homogeneous sphere can be given analytically as

$$g(r_h) = MG\frac{H}{(r_h^2+H^2)^{3/2}}.$$

Deviations between the numerically computed values and those obtained from the evaluation of the simple analytical expression can be used to check the accuracy of various numerical methods.

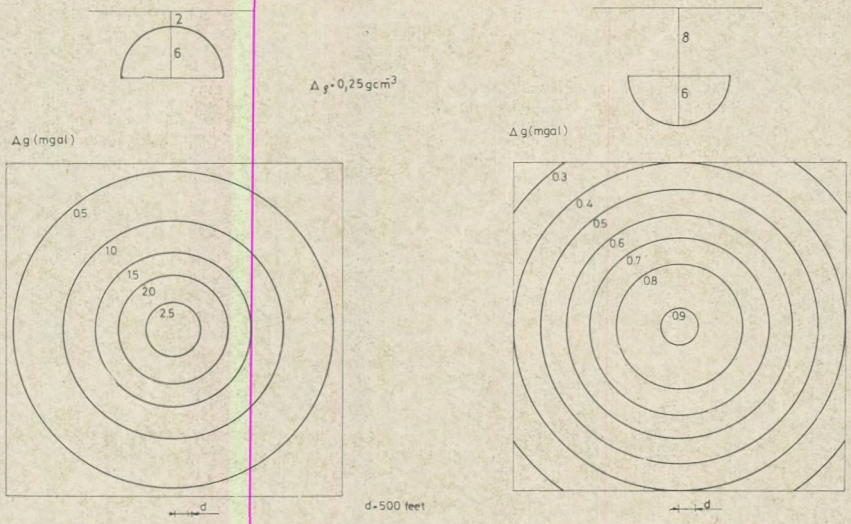

Fig. 1. Vertical component of the gravitational attraction due to half spheres. Distances indicated on the upper models are given in 500 feet units

Figure 3. shows the deviations for 4 methods. The cross section where analytical and numerical values are compared goes through the maximum of the anomaly. Both in the Talwani-Ewing's method and in the author's method 24 slices or 24 layers of cubes have been assumed to obtain a better comparison. It may be mentioned, however, that a subdivision with 48 layers of cubes have also been computed by the present method for the whole grid (32×32 points) in less time that the Talwani-Ewing method requires for a single point. Figure 3. clearly shows that the author's method is generally more accurate even in the pictured version (24 layers) than the others. There are two exceptions, the origin and the point at the distance of 1000 feet from the origin.

Errors of a 48 layer subdivision on the other hand, are always less than 1 μgal therefore could not be pictured in Figure 3.

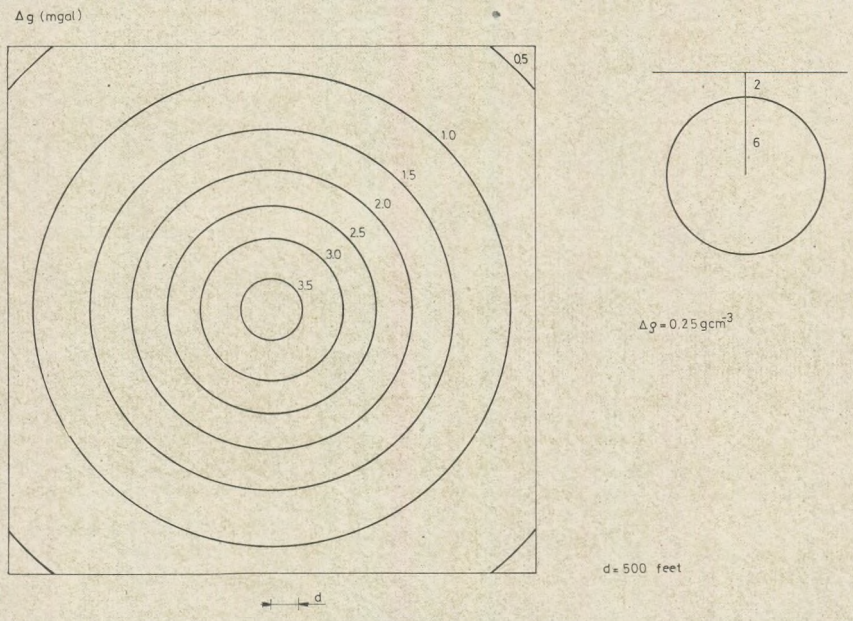

Fig. 2. Vertical component of the gravitational attraction due to a sphere as computed by the present algorithm. Distances indicated on the model are given in 500 feet units

Table 1. summarizes the numerical values.

Table 1.

Comparison of the vertical component of the gravity field computed by various methods
Model: sphere, radius: 1000 feet, depth of center: 3000 feet, density 0.25 cgs unit
Section: through the center of the anomaly

Distance from the origin measured along the x-axis in kilofeet	Analytical results (in mgals)	Talwani–Ewing method		Mufti, (1975) method		Meskó method	
		result (mgal)	error (μgal)	result mgal	error (μgal)	result mgal	error μgal
0	3.5926	3.6023	9.7	3.5947	2.0	3.6061	+13.5
1	3.2803	3.3099	29.6	3.2761	− 4,2	3.2845	+ 4.2
2	2.5707	2.6066	35.9	2.5530	−17.7	2.5696	− 1.1
3	1.8394	1.8702	30.8	1.8272	−12.2	1.8375	− 1.9
4	1.2702	1.2940	23.8	1.2627	− 7.5	1.2676	− 2.6
5	0.8758	0.8929	17.1	0.8710	− 4.8	0.8734	− 2.4
6	0.6132	1.6260	12.8	0.6098	− 3.4	0.6113	− 1.9
7	0.4388	0.4477	8.9	0.4363	− 2.5	0.4374	− 1.4
8	0.3213	0.3279	6.6	0.3196	− 1.7	0.3204	− 0.9
9	0.2407	0.2456	4.9	0.2395	− 1.4	0.2400	− 0.7
10	0.1840	0.1877	3.7	0.1830	− 1.0	0.1835	− 0.5

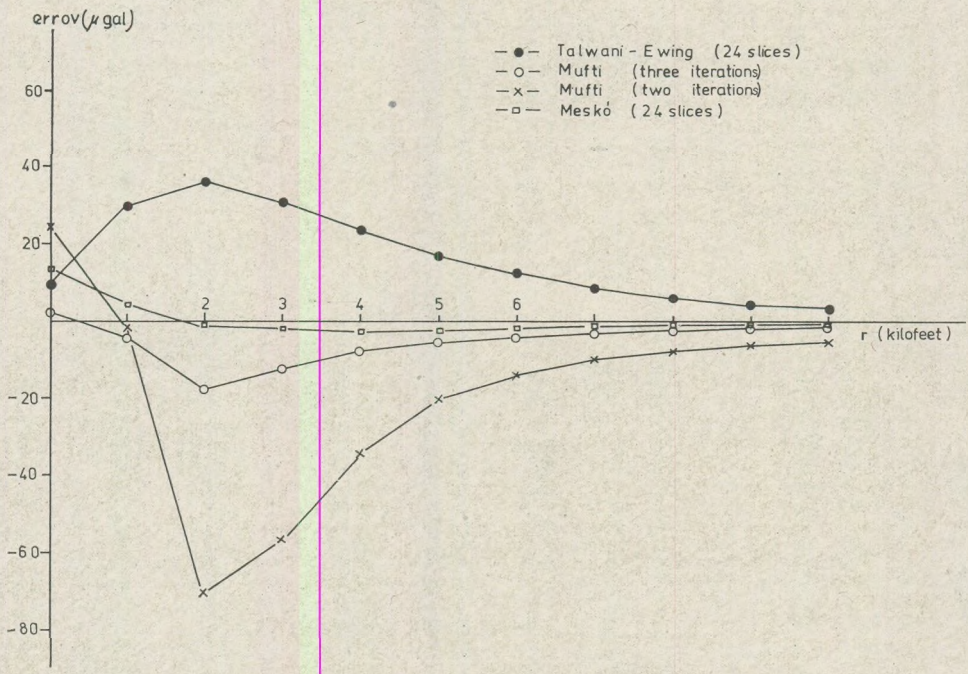

Fig. 3. Comparison the accuracy of various methods. Deviations between the analytical formula and various methods are plotted against the distance from the top of the anomaly

Figure 4. shows a model structure and its gravity field. The flat base is at the depth of 2 kms. The contours of the structure (height of the upper boundary above the flat base) are shown in the left hand side

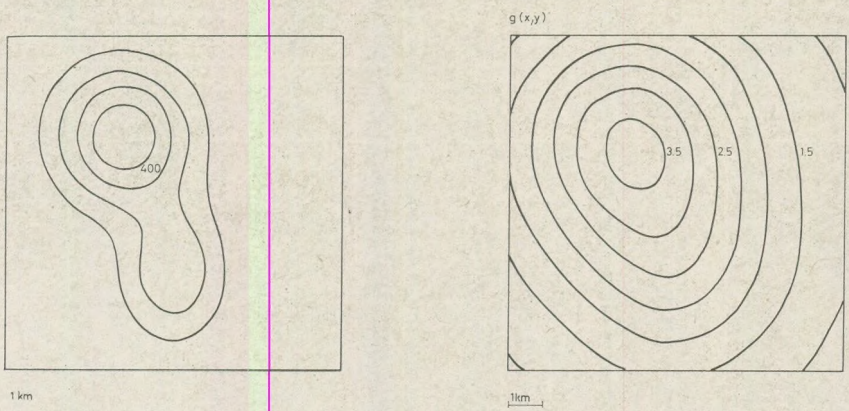

Fig. 4. A model structure and its gravitational attraction

of Figure 4. The density is 0.2 gcm^{-3}, which corresponds to the density contrast between a realistic volcanic body and its sedimentary surroundings.

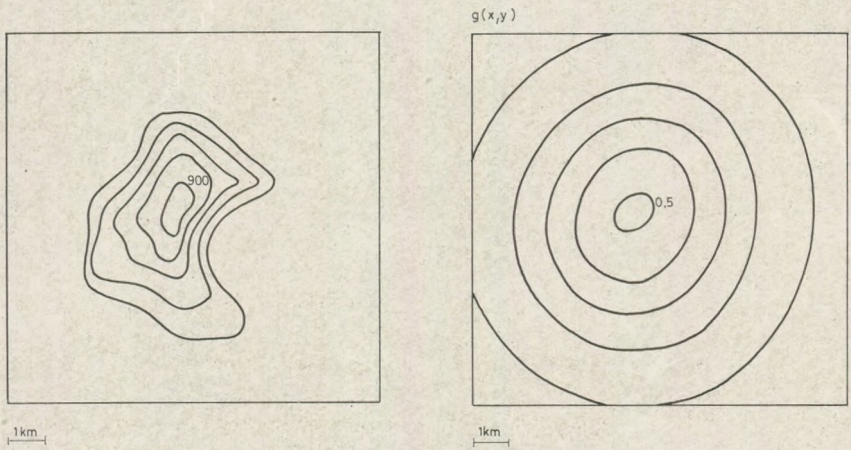

Fig. 5. A real geological structure determined by seismic reflections and its gravity field

Figure 5. shows a real geological structure determined by the reflection seismic method. The flat base is now at 3100 ms and the contours of the upper boundary (100, 300, 500, 700 and 900 meters above the plane) are given on the left hand side. A density contrast of 0.1 gcm^{-3} has been assumed. The computed gravity field (in mgal units) is shown on the right hand side.

The speed of the proposed method makes possible the experimentation with a large number of geological models. It is the hope of the author that the easy computability of gravity anomalies due to various models will influence advantageously the gravity interpretation as well as the combined interpretation of gravity, magnetic and seismic data.

REFERENCES

B o t e z a t u et al. (1971): Approximation of the gravitational attraction of geological bodies Geophys. Prosp. Vol 19., pp. 218–227.

M e s k ó A. (1976): An iterative solution of the inverse gravity problem for constrained models Annales, Vol XIX., pp. 83–113.

M u f t i, I. R. (1973): Rapid determination of the cube's gravity field. Geophys. Prosp. Vol 21., pp. 724–736.

M u f t i, I. R. (1975): Iterative gravity modeling by using cubical blocks Geophys. Prosp. Vol 23., pp. 163–199.

N a g y, D. (1966): The gravitational attraction of a right rectangular prism Geophysics, Vol 31., pp. 362–371.

T a l w a n i, M. and E w i n g, M. (1960): Rapid computation of gravitational attraction of three–dimensional bodies of arbitrary shape Geophysics, Vol 25., pp. 203–225.

OSTRACODE FAUNA FROM THE EOCENE OF GÁNT (TRANSDANUBIAN CENTRAL MOUNTAINS, HUNGARY)

by

M. MONOSTORI

Department of Paleontology, L. Eötvös University, Budapest
Received: 1 March 1975

РЕЗЮМЕ

В работе приведены результаты исследования фауны остракода слоев среднего эоцена бокситовпй шахты Багойхедь, расопложенной в местности Гант (Задунайское среднегорье, Венгрия). Новые виды и подвиды: *Cytherella (Cytherelloidea) gantensis, Novocypris gantensis, Clythrocytheridea faboides gantesis, Cytheridella gantnsis, Bradleya validornata hungarcia, Hermanites acuticosta gantensis, Xestoleberis gantensis.* Из известных вид в нами были найдены следую; *Bairdoppilata gliberi Keij, Pterygocythere jonesi (Méhes), Monsmirabilia triebeli Keil, Neocyprideis Williamsoniana (Bosquet) Krite bartonensis (Jones), Paracytheridea gradata (Bosquet), Caudites monsmirabiliensis Apostolescu, Schizocythere depressa (Méhes), Echinocythereis dadayana (Méhes), Hermanites haidingeri paijenborchiana Keij, Qudracythere augustcostata (Bosquet), Quadracythere vahrenkampi Moos.*

Известные виды соответствуют периоду среднего эоцена, определенного на основе другой фауны. Область образования глины была мелководная маргинальная территория с часто меняющейся концентрацией соли.

Introduction

The Eocene sequence around Gánt is known by its rich mollusc fauna, which was treated monographically by S z ő t s, E. (1953). The author of this present work collected a mollusc material from the overlying Eocene strata of the former bauxite mine of Bagolyhegy-hill and this collection resulted a well-preserved microfauna too. The author published previously the method (M o n o s t o r i 1973) and the preliminary report (M o n o s t o r i 1972) of the faunal investigations, the present work is the detailed description and evaluation of the fauna.

Method

The descriptions of the certain forms are presented here systematically. The systematic order and the scheme of the descriptions follow – with some modifications – those applied in the text-book of V a n M o r k h o v e n (1963.) The descriptions of outlines and ornamental elements were based on meshed ocular studies. The interpretation of the length, height and width is as usual, but measured on the periphery and not on the outer margin as in the cited Glossary (Treatise 1961, pp. 050, 51 – 52, 56). The horizontal component of the matrix is the length, its vertical component is the maximal height (Fig. 1). In some highly arched or specially shaped forms this latter does not mean actual height measured on the valve, but refers to the vertical distance between the

dorsal and ventral valve tangents parrallel to the length. Applying zoom-optic microscope the mesh can be set to give the positions of the certain characteristic peripheral and ornamentation points directly in the frac-

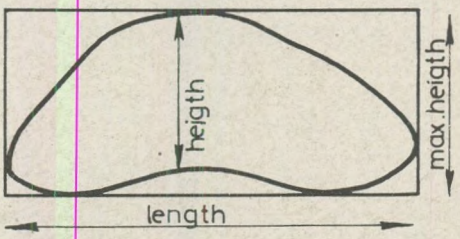

Fig. 1.

tions of the length and height. In lack of that kind of optics the valves can be photographed, and in standard-sized prints the dimensions can be measured with a mesh applied on tracing-paper. The angles (if characteristic) can be measured suitably on photographs. The co-ordinate method suggested by F a r k a s H. (1974) to fresh-water ostracodes can be applied at best to some groups of the marine forms. Related studies, regarding also the co-ordinate method of N e g a d a e v (1970), will be carried out in the future.

Paleontological descriptions

Subclassis Ostracoda Latreille, 1806

Ordo Podocopida Müller, 1894

Subordo Platicopina Sars, 1866

Familia Cytherellidae Sars, 1866

Genus Cytherella Jones, 1849

Cytherella (Cytherelloidea) gantensis n. sp. Pl. I. Fig. 1.

Derivatio nominis: After the name of the locality.
Holotypus: left valve; reposited in the type collection of the Hungarian Geological Survey.
Locus typicus: Bauxite-pit of Bagolyhegy-hill, Gánt, Transdanubian Central Mountains, Hungary.
Stratum typicum: Lutetian Stage, mollusc-bearing marl.
Diagnosis: Weakly ornamented Cytherelloidea, marginal ridge absent on the greater part of the dorsal margin and posteriorly.

D e s c r i p t i o n :

1. *Shape.* In o u t e r l a t e r a l v i e w anterior outline of l e f t v a l v e rounded symmetrically, gradually rounds into ventral

outline, which bears a symmterical sinus between one-third and two-third of length. Ventral outline acutely rounds into the nearly symmetrical posterior outline bearing an extremely shallow, slightly asymmetrical sinus between one-third and three-fifth of length, which is deepest somewhat before half-length of valve. Height posterior.

R i g h t v a l v e outline is similar. In d o r s a l v i e w surface rises with 15° angle to one-fifth of length, with about 10° angle to two-fifth of length and with 5° angle to five-sixth of length, and from there slopes with small radius, then perpendicularly.

2. *Ornamentation:* Surface of l e f t v a l v e smooth, finely pitted in the best-preserved specimens. Marginal ridge visible on the ventral nine-tenth to the dorsal two-fifth of length, most pronounced along the anterior margin. In dorsal side a slightly asymmetrical triangular depression appears between one-fifth and seven-tenth of length and the muscle-scar area. In ventral side there is an upwardly attenuating depression between the nine-tenth and two-fifth of length and the two-fifth of maximal height, which produces a sack-like swelling on the posteroventral surface. (In a few specimens the posterior tubercle and the depression absent.)
Ornamentation of r i g h t v a l v e is similar.

3. *Measurements* (on millimetres):

	Length	Height
left valve	0.64	0.35
right valve	0.63	0.32
right valve	0.56	0.29

4. *Inner lamella:* Very narrow.
5. *Marginal pore-canals:* Simple, visible only in some places.
6. *Hinge:* In left valve an edge, which fits into the groove of right valve around the entire margin.
7. *Normal pores:* Numerous, small, open.
8. Central *muscle scar* area with 11 scars arrenged in feather-shaped pattern.
9. *Eye-spot:* Absent.
10. *Overlap:* Right valve slightly overlaps left around the entire margin.
11. Forms without posterior tubercle and depression are probably the males.

C o m p a r i s o n. This species resembles C. (Cytherelloidea) jonesi Bosquet, 1852, but this latter shows stronger ornamentation, marginal ridge developed posteriorly and stronger anteriorly, and in this way the shape of valves exhibits sharp breaks in dorsal view.
Material: 3 left valves and 3 right valves.

Subordo Podocopina Sars, 1866
Superfamilia Bairdiacea Sars, 1888
Familia Bairdiidae Sars, 1888
Genus Bairdoppilata Coryell, Sample et Jennings, 1935
Bairdoppilata gliberti Keij, 1957
Plate I, Figs. 2–4.

1955. Bairdia subdeltoidea (Münster, 1830) – Apostolescu, pp. 245–246, pl. I figs. 9–10.
1957. Bairdoppilata gliberti Keij, 1957 – Keij, p. 53, pl. I, figs. 18–21.
1958. Bairdoppilata gliberti Keij, 1957 – Marliere, p. 18, pl. II, figs. 5–6.
?1959. Bairdoppilata gliberti Keij, 1957 – Ducasse, pp. 13–14, pl. X, figs. 2a–b.
?1964. Bairdoppilata gliberti Keij, 1957 – Sönmez – Göcken, p. 51, pl. I, fig. 1.
?1968. Bairdoppilata gliberti Keij, 1957 – Haskins, p. 3, pl. II, figs. 29–30.
1969. Bairdoppilata gliberti Keij, 1957 – Seremeta, pp. 57–58., pl. II, 15–16.
1969. Bairdia gliberti (Keij, 1957) – Pietrzeniuk, p. 15, pl. II figs. 9–10, pl. XVI, figs. 1–2.
1969. Bairdoppilata gliberti Keij, 1957 – Ducasse, p. 24, pl. II, fig. 29.
1971. Bairdoppilata gliberti Keij, 1957 – Blondeau, p. 25, pl. III, figs. 3–4.
?1972. Bairdia gliberti (Keij, 1957) – Khosla, p. 483, pl. I, fig. 9.

Description:

1. *Shape:* in outer lateral view anterior outline of left valve rounded asymmetrically, below two-third of maximal height breaks into dorsal outline, which forms a wide arch. Both the anterior and posterior lines of this arch are nearly straight, their directions make 90–120° angle, with weak concavity at about one-fifth of length. Posterior line slopes abruptly, with gradual transition into the posterior outline, which breaks by 80–100° at about one-third of maximal height, then gradually rounds into the ventral outline. The ventral outline straight, (slightly convex), between one-third and two-third of length, then gradually rounds into anterior outline. Height at half-length.
Dorsal outline of right valve is trapezoidally angular, the breaks are situated about two-fifth and three-quarter of length, with 140° angle. The middle, straight portion towards the ventral outline is convergent posteriorly. Posterior outline bears a small sinus between two- and three-fifth of maximal height, which results in acute posterior end. Ventral outline shows a sinus between the three- and six-eighth of the length. Height somewhat anterior.

In inner lateral view the outer margin of the left valve markedly deviates from the outline, it runs similarly as the right valve outline.

In dorsal view the surface rises anteriorly by 30° angle, and near to the middle rounds into a 30° slope, which slightly flattens out caudally. (Individual differences in the shape of the outlines may occur.)

2. *Ornamentation:* Surface of the valves finely, densely punctate.
3. *Measurements:*

	L	H
left valve	0.93	0.57
left valve	0.97	0.60
left valve	1.00	0.63
right valve	0.93	0.48
right valve	0.94	0.48

4. *Inner lamella:* Rather wide anteriorly and posteriorly, line of concrescence deviates from inner margin at the prominent anterior and posterior vestibula, more or less parallel to the outer margin. Selvage near to the outer margin.
5. *Marginal pore-canals:* Very numerous anteriorly and posteriorly, straight, simple.
6. *Hinge:* Dorsal edge of right valve fits into groove of left valve. Within the anterodorsal and posterodorsal angles of the valve, right valve bears crenulate tooth-like, left valve groove-like structure.
7. *Normal pores:* Numerous, small, open.
8. Central *muscle scars:* 10 in number, arranged on opaque area.
9. *Eye-spot:* Absent.
10. *Overlap:* Left valve conspicuously larger than right, especially dorsally and ventrally.

Remarks.

The Gánt form can be ranged into the species Baridoppilata gliberti Keij from the French Lutetian. It differs somewhat from the type, which shows a weak dorsal concavity in the left valve outline, near the posterior end, thus it is slightly acute. The outline shows a similar variability in the material, and the figures and descriptions mentioned in the synonymy suggest also some variations. Thus separation of a distinct subspecies cannot be justified.

Geological and geographical distribution:

Upper Ypresian – Ledian: France
Paleocene: Belgium
Upper Eocene: England
Upper Eocene – Lower Oligocene: GDR
Paleocene – Eocene: USSR
? Lower Eocene: India

Material: 5 left valves, 3 right valves.

Superfamilia Cypridacea Baird, 1845
Familia Cyprididae Baird, 1845
Genus Novocypris Ducasse, 1967
Novocypris ? gantensis n. sp.
Pl. I, Figs. 5–9.

Derivatio nominis: After the name of the locality.
Holotypus: Left valve; reposited in the type collection of the Hungarian Geological Survey.
Locus typicus: Bauxite-pit of Bagolyhegy-hill, Gánt, Transdanubian Central Mountains, Hungary.
Stratum typicum: Lutetian Stage, mollusc-bearing marl.
Diagnosis: Hinge conspicuously crenulate anteriorly and posteriorly, smooth medianly.

Description:

1. *Shape:* In outer lateral view anterior outline of left valve rounded symmetrically by rather small radius, and gradually curves into the dorsal outline, which is arched by greater radius. The outline breaks at four-fifth of length and near posterior end. Posterior outline with rather small radius and weakly breaks beneath the one-third of maximal height. Ventral outline nearly straight, gradually rounds into the anterior outline from about the one-fifth of length. Height at about half-lenght.
   The radius of the right valve anterior outline is somewhat smaller. Anterior portion of dorsal outline straighter. The break of the posterior outline stronger, near to the level of the ventral outline, thus the right valve is more acute posteriorly. Ventral outline bears a conspicious sinus, somewhat before half-length. (The breaks of the posterodorsal side absent in several specimens.)
   In inner lateral view outer outline of left valve markedly differs ventrally from the outer margin, which convergent to the outline of the right valve. In dorsal view the surface rises with 45° angle to one-tenth of length, abruptly in the beginning, then flattening out, the slope is 0–10° to four-fifth length, 10–40° between four-fifth and nine-tenth length and 45–60° to the valve end.
2. *Ornamentation:* Smooth valves without ornamentation.
3. *Measurements:*

	L	H
right valve	0.61	0.28
right valve	0.63	0.30
right valve	0.63	0.32
right valve	0.62	0.29
right valve	0.60	0.28
left valve	0.63	0.34
left valve	0.67	0.34
left valve	0.65	0.34

4. *Inner lamella:* Strongly wideneing anteriorly, somewhat weakly posteriorly. Large anterior and posterior vestibula, which are anteriorly especially larger near the ventral side.
5. *Marginal pore-canals:* Moderate in number, straight, simple, partially false.
6. *Hinge:* Strongly crenulate, fitting elements anteriorly and posteriorly in both valves, median elements smooth, groove in the right, bar in the left valve.
7. *Normal pores:* Few, scattered, small.
8. *Muscle scars:* 11 in number, of which 7 are arranged into a close group.
9. *Eye-spot:* Absent.
10. Left valve definitely *overlaps* right.

Comparison:

The hinge described by Ducasse (1967) as characteristic to this genus appear in modified form in this species, therefore the generic arrangement is conditional.

This Gánt species differs from the type species in outline, having anterior outline with smaller radius, dorsal outline with less pronounced breaks and with less acute posterior end.

Material: About 100 left valves and about 100 right valves.

Superfamilia Cytheracea Baird, 1850

Familia Brachycytheridae Puri, 1954

Genus Pterygocythere Hill, 1954

Pterygocythere jonesi (Méhes, 1936)

Pl. I, Figs. 10–12.

1936. Cytheropteron jonesi Méhes, 1936 – Méhes, pp. 22–25, pl. III, figs. 1–3, text-fig. 4.

Description:

1. *Shape:* In outer lateral view anterior margin of left valve rounded symmetrically. Radius of dorsal two-third part is larger than that of ventral two-third. Anterior outline and dorsal outline encloses an about 140° angle at one -fifth of length, the arch of the dorsal outline is of rather large radius. The junction with the posterior outline shows a hardly visible break, the ventral and dorsal lines of the posterior outline meet with about 90° angle at the two-third of the maximal height. Ventral line rounds with a weakly convex arch into the ventral outline, which is formed by a wing-like ventral extension at three-quarter of length. This gradually grows out from the anterior outline, straight between one-fifth and three-quarter of length, then breaks at about one-sixth of the maximal height and meets the posterior outline. Anterior outline – mainly

anteroventrally – with coarse denticulation, ventral line of posterior outline bears 5 to 6 denticles. Height near half-length.

In r i g h t v a l v e the roundness of anterior outline is more symmetric. Anterodorsal angle 150°, dorsal outline nearly straight, encloses 140° angle with the posterior outline at about eight-tenth of length. The wing-like extension overlaps only pertially the ventral outline, ends between two-third and three-quarter of valve-length. In i n n e r l a t e r a l v i e w of the l e f t v a l v e the straight running of the dorsal margin deviates from the outline. Ventral margin deviates from outline in both valves, forming weak sinus, and encloses posteriorly about 30° angle with the hinge margin.

In d o r s a l v i e w ventral ridge rises by 45° angle, and except its posterior, spinuous end, it slopes with 70–80° angle toward the posteriorly sloping, 10–15° posterior surface.

2. *Ornamentation:* Valve surface smooth. The wing-like extensions of both valves grade into anteromarginal rims, which reach the eye-tubercle.

3. *Measurements:*

	L	H
left valve	0.71	0.42
right valve	0.70	0.39

4. *Inner lamella:* Wide anteriorly, somewhat narrower posteriorly. Line of concrescence and inner margin coincide. Selvage subperipheral in left valve, removed from outer margin in right valve.
5. *Marginal pore-canals:* 20 to 25 in number anteriorly, 10 to 12 posteriorly. Simple, straight, with ampullae in the outer thirds.
6. *Hinge:* In l e f t v a l v e there are large anterior socket, small anteromedian tooth, crenulate posteromedian bar and elongate, crenulate posterior socket. Accomodation groove well-developed.
In r i g h t v a l v e the anterior tooth slightly elongated (bordering the eye-socket), its anterior part lower than the posterior. Anteromedian element is tooth-socket, which continues as crenulate posteromedian groove. Posterior tooth elongate, crenulate.
7. *Normal pores:* Few, open.
8. *Muscle scars:* "V"-shaped frontal scar in front of the row of four elongate adductor scars.
9. *Eye-spots:* Prominent, small in both valves.
10. The larger left valve especially dorsally *overlaps* the right.
11. The break of the dorsal outline is smaller in valves of more elongate specimens, probably these are the males.

Remarks:

On the basis of its morphological features, this Gánt form can be well identified with the species Cytheropteron jonesi described by Méhes (1936) from the Eocene of the vicinity of Budapest.

In the type figures of Pterygocythere hilli Keij, 1957 the antero-

dorsal angle is less prominent and is removed posteriorly, the running of the ventrolateral extension is different, the median hinge-element is acrenulate, and these may suggest at least subspecific difference.

Geological and geographical distribution:

Middle? Eocene: Budapest vicinity, Hungary.
Material: 3 left valves, 1 right valve.

Familia Bythocytheridae Sars, 1926

Genus Monoceratina Roth, 1928

Monoceratina sp.

Pl. II, Fig. 1.

Description:

1. *Shape:* In outer lateral view the outline of the left valve is damaged anteriorly and posteriorly. Dorsal outline completely straight, ventral outline slightly convex, which results from the convex running of the wing-like extension.
2. *Ornamentation:* The surface of the left valve is heavily ornamented. Along dorsal margin coarse ridge-like costa, near the ventral margin strong wing-like extension, which rises from about one-third of maximal height on anterior half, then overhangs the ventral margin and ends recurving posteriorly above that. Subcentrally deep sulcus rund downward in upper one-quarter of maximal height, bordered anteriorly by arched costa, which sharpens toward the end of the wing-like extension. The surface is steep posteriorly from the wing-like extension, the part along the posteroventral margin is wide and flat. Despite of the damage, it is visible, that the anterior valve-part is similarly flat. Height somewhat anterior.

4–5., 7–10: Inner features and the relation of the valves cannot be studied.

6 *Hinge:* Somewhat damaged terminally, hinge-elements on the preserved parts are not visible.

Remarks:

The ornamentation markedly differs from the described and figured Tertiary Monoceratina species, however, this single fragmentary specimen is incomplete for designation of a new species.
Material: One single damaged left valve.

Familia Cytherideidae Sars, 1925

Genus: Clithrocytheridea Stephenson, 1936

Clithrocytheridea faboides gantensis n. ssp.

Pl. II, Figs. 2–4.

Derivatio nominis: After the name of the locality.
Holotypus: Left valve; reposited in the type collection of the Hungarian

Geological Survey.

Locus typicus: Bauxite-pit of Bagolyhegy-hill, Gánt, Transdanubian Central Mountains, Hungary.

Stratum typicum: Lutetian Stage, mollusc-bearing marl.

Diagnosis: A form bearing deep anterior vestibulum, especially near the margins with concentrically arranged strong pits, with poster;orly narrowing left valve of nearly straight ventral and dorsal margins.

Description:

Stratum typicum: Lutetian Stage, mollusc-bearing marl.

Diagnosis: A form bearing deep anterior vestibulum, especially near the margins with concentrically arranged strong pits, with posteriorly narrowing left valve of nearly straight ventral and dorsal margins.

Description:

1. *Shape:* In outer lateral view the anterior outline of the left valve is markedly asymmetric, arching with large radius from about the one-third of the maximal height toward the dorsal outline, with which it encloses about 140° angle at the one-third of the length. Dorsal outline straight (except a weak sinus behind the protruding cardinal angle) to three-quarter of length, where grades with a weak break into the posterior outline, which is rounded by small radius. Posterior outline gradually rounds into the hardly convex ventral outline, of which direction with that of dorsal outline encloses a posteriorly convergent 10 to 15° angle. The ventral outline arches into the anterior outline with a very short radius, before the arch somewhat depressed. The lower part of the anterior outline may bear slight denticulation. Height at anterior cardinal angle.
   The anterior outline of right valve is rounded asymmetrically, from the half of maximal height, arching with a long radius into the dorsal outline, which breaks slightly about the half of the length, then straight to four-fifth of length, and grade with an other break into the posterior outline, which arches with a very small radius into the nearly straight ventral outline. Behind the one-fifth of the length the ventral outline shows weak sinus. Lower third of anterior outline somewhat denticulated. Height slightly anterior.
   In inner lateral view outer margin and outline are nearly coincidental.
   In dorsal view the maximal width is situated somewhat before the middle of the length. Anterior part more compressed, posterior more inflated.
2. *Ornamentation:* Valves markedly pitted, the dense, relatively coarse pots appear in concentric arrangement (similarity to reticulation). In anterior part of the left valve the portion between the pits becomes stronger, just like concentric costa. Ornamentation absent around the cardinal angle of left valve.

3. *Measurements:*

	L	H	Width
left valve	0.42	0.23	
left valve	0.46	0.24	
right valve	0.42	0.22	
carapace	0.41	0.22	0.18

4. *Inner lamella:* Moderately wide, widest anteriorly. Subtriangular vestibulum anteriorly, thus the inner margin markedly different here. Marginal zone widest anteriorly. Selvage subperipheral, in left valve slightly, in right valve strongly removed anteriorly inward.
5. *Marginal pore-canals:* Very numerous. Simple, straight, with ampullae near the half-length. Scattered in upper, and dense in lower part of anterior zone, common along ventral margin and dense in lower part of posterior zone.
6. *Hinge:* In l e f t v a l v e the two terminal elements are coarsely crenulate grooves, connected by crenulate bar.
   In r i g h t v a l v e the hinge-elements are corresponding terminally crenulate teeth, medianly crenulate groove.
7. *Normal pores:* Moderately numerous.
8. *Muscle scars:* In l e f t v a l v e the four adductor scars are arranged into a single row, in the level of the uppermost one there is an anteriorly open "V"-shaped frontal scar, in the level of the lowermost adductor scar is an elongate, obliquely, upward and aneriorly oriented scar.
9. *Eye-spot:* Absent.
10. *Overlap:* Left valve overlaps right at cardinal angle, at middle portion of ventral side and slightly anteriorly and posteriorly.
11. A part of the specimens shows more elongate, lower and narrower shape, probably these are males.

C o m p a r i s o n :

This form differs from the type species Clithrocytheridea faboides (Bosquet) revised by Keij (1957), in shape (stronger dorsal and ventral depressions and posteriorly higher left valve in the type subspecies), in ornamentation (somewaht denser and more regular pitting in the Gánt subspecies), and in the structure of the inner lamella (coarse subtriangular vestibulum in the Gánt subspecies). The present new subspecies also differs from the species Clithrocytheridea bipunctata Ducasse (1967) (which can be regarded rather as a subspecies) in the character of the vestibulum and in the absence of the separation of ornamentation.
Material: 6 left valves, 4 right valves.

Genus Neocyprideis Apostolescu, 1946

Neocyprideis williamsoniana (Bosquet, 1852)

Pl. II, Fig. 8.

1852. Cytheridea williamsoniana Bosquet, 1852 – Bosquet, pp. 43–44, pl. II, fig. 6.

1957. Cyprideis (Goelichia) williamsoniana (Bosquet, 1852) – Keij, p. 70, pl. VII, figs. 6–8, pl. XVIII, figs. 18–20.
1958. Neocyprideis williamsoniana (Bosquet, 1852) – Kollmann, p. 137, pl. 12, fig. 8, pl. 20, figs. 8–10, pl. 20, figs. 6–7.
1969. Cyprideis (Neocyprideis) williamsoniana (Bosquet, 1852) – Haskins, pp. 155–158, pl. 4, figs. 10–20.
1972. Neocyprideis williamsoniana (Bosquet, 1852) – Keen, p. 297, pl. 52, fig. 13.

Description:

1. *Shape:* In outer lateral view anterior outline of left valve, which is formed by the markedly strong flange, is somewhat rounded asymmetrically, radius of the arch of the upper part is larger than that of lower part, at the third of the length it gradually rounds into the hardly convex dorsal outline, which breaks in a 120° angle near the five-sixth of length, and curves into the asymmetrically rounded posterior outline. Ventral outline nearly straight, somewhat sinuous in its middle portion. Height posterior.
   In right valve the ventral sinus is somewhat deeper, dorsal outline with weak depression near the middle.
   In inner lateral view the outer margins are more sinuous than the outlines on both valves.
   In dorsal view the surface of the valve, after a flat peripheral portion, rises with about 30° angle to one-sixth of length, then the rise decreases from 20° to 0° angle at half-length, then the rise increases from 0° to 10° angle to five-sixth of length, and finally the slope increases abruptly to 90° to the posterior margin.
2. *Ornamentation:* In left valve the surface is densely pitted or smooth, hyaline and polished, with a weak, downwardly narrowing, triangular depression between one-third and half of length. At posterodorsal angle a small swelling appears, which is visible in outline too.
   In right valve the anterodorsal depression is deeper, with a small swelling before.
3. *Measurements:*

	L	H
left valve	0.72	0.41
right valve	0.67	0.39

4. *Inner lamella:* Rather narrow, inner margin and line of concrescence coincide. Selvage strong, subperipheral.
5. *Marginal pore-canals:* About 15 in number anteriorly, simple, straight, widely separated.
6. *Hinge:* In left valve anteriorly long, posteriorly shorter, curved, crenulate socket, with a crenulate bar which slightly arched in lateral and straight in dorsal view.
   Right valve shows the corresponding hinge-elelments.
   7.–8. *Normal pores* and *muscle scars* cannot be studied.

9. *Eye-spot:* Absent.
10. Left valve *overlaps* right, especially posterodorsally.
11. In the rarer, posteriorly less inflated male left valves the maximal height is removed at, or before the median line.

Remarks:

On the basis of the completely smooth valves and the slight curve of the hinge bar Keij (1957) ranged the Lutetian specimens into the N. apostolescui (Keij, 1957) species. In the Gánt material hyaline ans shiny, smooth and markedly densely-pitted forms are equally common within a single sample, consequently, the appearance or absence of the pitting is a phenotypic feature. The hinge bar is slightly curved in lateral view, thus it is an undiagnostic character. All in the Gánt specimens the ventral outline of the left valve is markedly concave before the anterior outline junction. This feature characterizes the species N. williamsoniana, while in the original description and figures of N. apostolescui the ventral margin of the left valve is straight or convex.

Geological and geographical distribution:

Sannoisian – Stampian. France
Upper Tongrian – Rupelian: Belgium
Tongrian: England
Material: One left valve and one right valve.

Genus Monsmirabilia Apostolescu, 1955

Monsmirabilia triebeli (Keij, 1957)

Pl. II, Figs. 5–7.

1957. Cuneocythere (Monsmirabilia) triebeli Keij, 1957 – Keij, p. 79., pl. IX, figs. 1–4.
1959. Cuneocythere (Monsmirabilia) triebeli Keij, 1957 – Ducasse, p. 23, 23, pl. XII, figs. 2a b.
1968. Cuneocythere (Monsmirabilia) triebeli Keij, 1957 – Haskins, pp. 174–175, pl. 3, figs. 26–34.
1969. Monsmirabilia triebeli (Keij, 1957) – Ducasse, p. 60, pl. IV, fig. 77.
1971. Monsmirabilia triebeli (Keij, 1957) – Blondeau, p. 79, pl. IX, fig. 4.
1973. Cuneocythere (Monsmirabilia) triebeli Keij, 1957 – Moos, pl. 7, figs. 2–3.

Description:

1. *Shape:* In outer lateral view anterior outline of left valve widely, asymmetricall rounded, gradually curves into dorsal outline, which slightly convex between three-eighth and five-eighth of length, somewhat broken at five-eighth, and after the three--quarter of length, with an other slight break, grades into posterior

outline, which bears a slight break above one-third of maximal height. Posterior outline rounds into convexely arched ventral outline with a rather small radius. Ventral outline gradually rounds into anterior outline. Height near to valve-median.

Anterior outline of r i g h t v a l v e rounds also gradually into dorsal outline, which bears slight breaks near the half and three--quarter of length. Posterior outline of small radius continuously grades into ventral outline, which shows slight asymmetrical sinus between one-quarter and half of length.

In i n n e r l a t e r a l v i e w the outer margin of l e f t v a l v e differs ventrally from the outline, having straight running with slight median sinus instead of convexity.

The outer margin of r i g h t v a l v e nearly coincides with the outline.

In v e n t r a l v i e w the rise of the valve surface is 25—0° near to the two-third of length (maximal width), and decreases continuously to nine-tenth of length, finally with 50° angle, and at the end of the valves, a depressive part, corresponding to about a quarter of maximal width may appear.

The r i g h t v a l v e is depressive in one-tenth of length along the anterior margin, here the slope has a smaller angle.

2. *Ornamentation:* Valves densely, finely pitted, on left valve with weak, on right valve with sharp, coarse anteromarginal rim. On both valves the anterodorsal margins show slight depression, which result in a prominent portion on the outer sutface, corresponding to the hinge margin.

3. *Measurements:*

	L	H
left valve	0.53	0.35
left valve	0.53	0.33
right valve	0.47	0.23
right valve	0.49	0.27

4. *Inner lamella:* Very wide anteriorly, inner margin and line of concrescence coincide. Selvage subperipheral, strong in right valve. In left valve at the outer third of the marginal zone a list, farther in striae are visible.
5. *Marginal pore-canals:* Very dense in anterior half, more than 40 in number, and about 20 posteriorly. Simple, slightly curved, with ampullae near the outer margin.
6. *Hinge:* In l e f t v a l v e , between about one-third and eight-ninth of valve-length runs a gradually narrowing groove, which is bordered inward by a narrow, anteriorly slightly thickening ridge. Above the groove weak accomodation groove occurs.

   In r i g h t v a l v e the bar fitting into the groove of left valve shows a small tooth-like thickening before three-eighth of length.
7. *Normal-pores:* Rather numerous.

8. *Muscle scars:* The four undivided adductor scars are arranged into a single row, in right valve a dorsally open „V"-shaped frontal scar and above a smaller scar are visible.
9. Distinct *eye-spot* absent (the prominent dorsal portions mentioned in the ornamentation cannot be regarded as definite eye-structures).
10. *Overlap:* Left valves much larger and overlaps right all around the periphery.
11. A smaller part of the specimens is more elongate, less inflated posteriorly, probably these are males.

Remarks:

The specimens from Gánt can be well identified with the type described and figured by K e i j (1957).

Geological and geographical distribution:

Eocene: France
Upper Ypresian – Bartonian: Belgium
Bartonian: the Netherlands
Ypresian – Bartonian: England
Material: Four left valves and four right valves.

Genus Krithe Brady, Crosskey, Robertson, 1874

Krithe bartonensis (Jones, 1857)

Pl. I, Figs. 9, 11, 13–14.

1857. Cytherideis bartonensis Jones, 1857 – Jones, p. 50, pl. V, figs. 2a–b, 3a–b.
?1894. Krithe bartonensis (Jones, 1857) – Lienenklaus, pp. 252–253. pl. XVII, fig. 9.
?1936. Krithe bartonensis (Jones, 1857), – Méhes, pp. 37–38, pl. III, figs. 26–29, text-fig. 30.
1957. Krithe bartonensis (Jones, 1857) – Keij, p. 85, pl. VIII, figs. 11–12, figs. 13–17.
1959. Krithe bartonensis (Jones, 1957) – Ducasse, pp. 49–50, pl. III, fig. 1, pl. XX, figs. 3a–b.
1969. Krithe bartonensis (Jones, 1857) – Scheremeta, pp. 88 89, pl. VII, figs. 1–2.
1969. Krithe bartonensis (Jones, 1857) – Pietrzeniuk, p. 21, pl. V, fig. 12, pl. XV, figs. 4–6, text-figs. 5–6.
1970. Krithe bartonensis (Jones, 1857) – Haskins, pp. 13–16, pl. 1, figs. 5–14.
1971. Krithe bartonensis (Jones, 1857) – Blondeau, pp. 82–83, pl. IX, fig. 6.
1972. Krithe bartonensis (Jones, 1857) – Khosla, p. 485, pl. 1, fig. 19.

Description:

1. *Shape:* In outer lateral view anterior outline of left valve symmetrically rounded, gradually rounds into dorsal outline,

which nearly straight between one-quarter and two-third of length, then widely arches into the posterior outline, of which radius of roundness decreases in its lower half. At the junction with ventral outline a break occurs, ventral outline nearly straight between eleven-twelfth and one-quarter, shows a weak undulation with concavity at two-fifth of length, weak convexity after three-fifth of valve and a slight concavity at four-fifth of length (regarding the respective symmetry axes). Transition towards anterior outline is continuous. Height posterior.

The lower part of the anterior outline in r i g h t v a l v e is weakly truncate, the nearly straight running of the dorsal outline is divided by a slight sinus before the one-third of the length. The gradual transition into the posterior outline starts slightly earlier, the radius of roundness decreases more slowly, thus the posterior end less obtuse, Anterior concavity on ventral outline strong, with maximum slightly before mid-valve, otherwise the outline is straight.

In l a t e r a l v i e w the outher margin somewhat deviates ventrally from the outline, anterior sinus stronger.

In d o r s a l v i e w the outline in left valve rises with 40° angle to one-tenth of length, then with $40-0°$ angle to half-length, then with $0-20°$ angle to nine-tenth of length and finally with 20 to 90° angle. In right valve the slope is more flattened, recessive at posterior end.

2. *Ornamentation:* Valve surface smooth.

3. *Measurements:*

	L	H	W
left valve	0.66	0.33	
left valve	0.66	0.30	
right valve	0.66	0.30	
right valve	0.63	0.29	
carapace	0.65	0.30	0,27

4. *Inner lamella:* Wide anteriorly and ventrally (except middle portion), narrower posteriorly. In lower half of anterior part is generally the characteristic vestibulum. Line of concrescence and inner margin are markedly separated anteriorly. Selvage subperipheral, posteriorly runs at a considerable distance from the outer margin, crossing straight caudal process.
5. *Marginal pore-canals:* Few, straight, simple, a number are false. About 12 at the anterior, 5 to 7 at the ventral and 4 to 6 at the posterior.
6. *Hinge:* In left valve groove, which is separated between one-quarter and two-third by an inner bar with edge-shaped posterior end.
The r i g h t v a l v e fits into the groove of left valve with an edge with slight curve before two-fifth of length.
7. *Normal pores:* Few, large.
8. *Muscle scars:* There are rows of four elongate adductor scar in both valves. The lowermost scars are smaller, the uppermost in left valve is curved upward. In front of the upper two scars the frontal scar

of two separated parts is situated. Its forwardly and somewhat upwardly curved part surrounds the smaller, circular part. Mandibular scar is situated more forward, before the lowermost adductor scar.

9. *Eye-spot:* Absent.
10. Left valve larger, *overlaps* right.
11. A smaller part of the forms is more elongate, probaly these are males.

Remarks:

In specimens from Gánt the parallelism of dorsal and ventral outlines is more pronounced as compared to that in specimens of Haskins (1970) from the type locality, and the posterior end is somewhat blunter. Taking the marked variability of this species into consideration, these slight differences cannot be regarded as of taxonomic value.

Geological and geographical distribution:

Lutetian – Stampian: France
? Bartonian: Belgium, the Netherlands
Ledian – Tongrian: England
Upper Eocene – Lower Oligocene: GDR
Upper Eocene: USSR
Lower Eocene: India
Material: About 30 left valves and about 30 right valves.

Familia Cytheruridae G. W. Müller, 1894

Genus Paracytheridea G. W. Müller, 1894

Paracytheridea gradata (Bosquet, 1852) n. ssp. ?

Pl. II, Fig. 12.

1852. Cythere gradata Bosquet, 1852 – Bosquet, pp. 127 – 128, pl. VI, fig. 11.
1955. Paracytheridea gradata (Bosquet, 1852) – Apostolescu, pp. 249 – 250, pl. II, fig. 25.
1957. Paracytheridea (Paracytheridea) gradata (Bosquet, 1852) – Keij, p. 159, pl. XXII, figs. 2 – 4.
?1959. Paracytheridea gradata (Bosquet, 1852) – Moyes, p. 12, pl. 3, fig. 6.
1961. Paracytheridea gradata (Bosquet, 1852) – Deltel, p. 126, pl. 9, fig. 138.
1966. Paracytheridea gradata (Bosquet, 1852) – Moussou, pp. 72 – 73, pl. 20, figs. 82a – c.
1969. Paracytheridea gradata (Bosquet, 1852) – Ducasse, p. 88, pl. VI, fig. 124.
1970. Paracytheridea gradata (Bosquet, 1852) – Haskins, p. 18, pl. 2, figs. 4 – 9.

Description:

1. *Shape:* In outher lateral view anterior outline of left valve angular, straight between one- and four-fifth of maximal height and roughly perpendicular to the dorsal outline, then braking with about 110° angle, runs to cardinal angle (about a quarter of length). Here an abrupt recess occurs (remarkably coarse cardinal angle), then the dorsal outline straight (except parts mentioned in ornamentaion) to slightly more than three-quarter of length, where grades into the convex line of posterior outline with an about 140° angle break. Posterior outline forms prominent caudal process, with a truncate end at one-sixth maximal height. Ventral line of posterior outline is parallel to dorsal outline. Ventral outline is formed by the ventrolateral wing-like extension, which ends perpendicularly to the dorsal line of posterior outline, slightly behind two-third of length. Half of the distance between this perpendicular end and caudal end is covered by the projected posteroventral spine. Ventral outline straight to one-sixth of length, and nearly parallel with dorsal outline. Here grades with an about 140° angle into anterior outline, which is broken with 110° angle at about one-fifth of maximal height. Height at anterodorsal angle.
   In inner lateral view dorsal outline completely straight, ventral outline slightly concave throughout.
   In dorsal view of left valve the outline rises with 45° angle to about one-third of length, horizontal to half-length, where a blunt, short, spiniform process occurs, then slopes with 90° angle to the half of maximal width. In the following portions slopes with 30° angle to seven-eighth of length, with an oblique, backwardly projected spine in the middle. Slope between seven-eighth length and caudal end is lower than 10° angle.
2. *Ornamentation:* The main ornamentation element is the ventral wing-like extension. It bears a sharp, ridge-like edge from the anterior margin throughout. From one-third of length to end of extension three anterodorsally directed processes run, with intervening depressions. The last forms the ridge running between the end of extension and valve-center, the anterior is a ventrally removed, bisected subcentral tubercle. In front of this, between the cardinal angle and ventral extension, runs a costa nearly parallel to the anterior margin. Behind the extension, a large, wide, posteroventrally directed spine is situated. The eye-tubercle is situated in the depressive surface between subcentral tubercle and half of dorsal outline. On dorsal side a prominent surface-part occurs between half and five-eighth of length, modifying the runing of dorsal outline. Posterior and anterior parts are smooth, middle part is weakly, irregularly reticulated.
3. *Measurements:*

	IL	H	W
left valve	0.46	0.20	0.17

4. *Inner lamella:* Rather wide anteriorly and posteriorly. Line of concrescence and inner margin coincide, caudally deviate from outer margin. Selvage subperipheral.
5. *Marginal pore-canals:* Few, simple, straight.
6. *Hinge:* In left valve there is incompletely closed socket anteriorly and posteriorly. On anterior part of median crenulate bar, tooth-like structure of three strong lobes occurs.
7. *Normal pores:* Few, rather large.
8. *Muscle scars:* Not seen.
9. *Eye-spot:* Prominent at caudal angle.

Comparison:

On the basis of the description and figure given by Keij (1957), the Gánt form resembles the type of Paracytheridea gradata (Bosquet, 1852) from France. However, the Gánt specimens differ in having a different running of the caudal process and protrusions dominating the ornamentation, which suggest new subspecies. Only a single left valve is known so far, thus an adequate designation of a new subspecies requires additional specimens.

Geological and geographical distribution:

Middle Eocene – ? Burdigalian: France
Ypresian – Bartonian: Belgium, the Netherlands
Ypresian – Tongrian: England
Material: One left valve.

Familia Hemicytheridae Puri, 1953

Genus Caudites Coryell, Fields, 1937

Caudites monsmirabiliensis Apostolescu, 1955

Pl. II, Fig. 10.

1955. Caudites monsmirabiliensis Apostolescu, 1955 – Apostolescu, p. 251, pl. II, figs. 33–34.
?1959. Caudites minsmirabiliensis Apostolescu, 1955 – Ducasse, p. 57, pl. XXI, fig. 4.

Description:

1. *Shape:* In outer lateral view anterior outline of left valve strongly rounded asymmetrically, upper part truncate. It encloses with the straight dorsal outline an about 140° angle at the one-quarter of the length (at the caudal angle). Cardinal angle projected. The straight dorsal outline runs to five-sixth of length, between five-eighth and three-quarter of length it is disrupted by the projected dorsal ridge. Upper half of posterior outline deeply concave, perpendicular to dorsal outline at the start, but finally encloses an angle smaller than 10°. Caudal part acute, lower and upper lines of posterior

outline enclose an about 55° angle at the start. This angle decreases to about 25° later, at six-seventh of length, where the posterior outline rounds into ventral outline. Ventral outline deviates from dorsal, strongly asymmetric between half and quarter of length, where a sinus occurs. Anterior outline with weak denticulation, lower line of posterior ouline shows 5 to 6 stronger denticles, the middle of the upper line bears a single denticle. Height at anterodorsal angle.

In inner lateral view outer margin completely straight dorsally, its ventral depression is somewhat deeper than that of outline.

In dorsal view shape of side is nearly parallel to about the half of maximal width to one-quarter of length, then rises to three-eighth of length with about 30° angle, slightly depressive between the subcentral tubercle and ventral ridge, and slopes from ventral ridge with 40 – 50° angle, finally parallel to about one-third of maximal width. Dorsal ridge ends nearly perpendicularly to dorsal margin.

2. *Ornamentation:* Wide and coarse marginal ridge runs anteriorly throughout the valve, except dorsal margin. Before half of valve-length, prominent subcentral tubercle occurs. Between half and three-quarter of length runs the dorsal ridge, which encloses a small angle with dorsal outline, finally modifying the latter. At the end it breaks perpendicularly to the dorsal outline, and with an another break encloses a 45° angle with its main line, and fade into the valve surface at one-quarter of height. Ventral ridge prominent only between half and two-third of length, with strongly upwardly curved end. Side-surface depressive anteriorly, and between the cardinal angle and subcentral tubercle. From the line between the ends of ventral and dorsal ridges, the surface slopes abruptly towards the depressive caudal part. Anterior and caudal parts are smooth. The prominent side-surface and the dorsal depression slightly, irregularly reticulated. The subcentral tubercle is smooth.

3. *Measurements:*

	L	H
right valve	0.54	0.25

4. *Inner lamella:* Widest anteriorly, where the line of concrescence deviates from inner margin. Prominent vestibulum. Selvage subperipheral.
5. *Marginal pore-canals:* about 30 anteriorly, about 12 posteroventrally. Generally simple, straight.
6. *Hinge:* In right valve the anterior element is a "two-stepped" tooth, anteromedian is a closed socket, the posteromedian is a groove, and the posterior is a "two-stepped", acute tooth.
7. *Normal pores:* Scattered, large.
8. *Muscle scars:* Not seen.
9. *Eye-spot:* Strong in cardinal angle.

Remarks:

The Gánt form is somewhat less acute caudally, more concave ventrally and slightly more asymmetric anteriorly than the type. With these features it resembles Caudites sp. 1. described by Deltel (1961), however, its ornamentation is closer to thet of the type. On the basis of the available single right valve, these small differences cannot be interpreted even as of subspecific.

Geological and geographical distribution:

Lower Eocene – Upper Eocene + Stampian: France
Material: One right valve.

Familia Linocytheridae Klie, 1938

Genus Cytheridella Daday, 1905

Cytheridella? gántensis n. sp.

Pl. II, Figs. 15–17.

Derivatio nominis: After the name of the locality.
Holotypus: Right valve; reposited in the type collection of the Hungarian Geological Survey.
Locus typicus: Bauxite-pit of Bagolyhegy-hill, Gánt, Transdanubian Central Mountains, Hungary.
Stratum typicum: Lutetian Stage, mollusc-bearing marl.
Diagnosis: Anteriorly strongly, posteriorly less asymmetrically rounded form, with prominent anteromedian sulcus and weakly, densely pitted surface.

Description:

1 *Shape:* In outer lateral view anterior outline of right valve asymmetrically rounded, its upper half truncate, and arches into dorsal outline with about 140° angle at one-quarter of length. Dorsal outline nearly straight, gradually curves into the nearly asymmetrically rounded posterior outline, which weakly truncate dorsally. Ventral outline slightly concave throughout, the sinus is symmetrical with a maximum at half-length. Height anterior.
Anterior outline of left valve more asymmetric, the arch into the dorsal outline is more gradual. Posterior angle on dorsal outline prominent, dorsal half of posterior outline distinctly truncate, very slightly concave, its ventral half is rounded with a rather small radius and gradually curves into the ventral outline, which runs similarly as that of right valve.
In inner lateral view outline coincides with outer margin. In dorsal view the shape of sides rises with about 20° angle to one-sixth of length then arches convexely (with 45–10° angle) to five-twelfth of length, and rises with 20° angle to seven-twelfth of length. From this point it slopes with about 15° angle to after five-

sixth of length, then curves with 45 – 90° angle nearly to the valve-end, where grades into a very short margin of 45° slope. In a smaller part of the speciemens the slope from seven-twelfth of length is constant nearly throughout, with an angle of about 45°.

2. *Ornamentation:* Valve-surface finely pitted. Along anteromarginal rim weak ridge occurs, which especially prominent in right valve. In the upper part of the valve, the junction of the anterior and dorsal outline, the part of dorsal outline at half-length, as well as the area between dorsal outline and muscle-scars, show depressions. Ventral part of valves extended, abrupt towards ventral margin.

3. *Measurements:*

	L	H
right valve	0.76	0.35
right valve	0.77	0.37
left valve	0.80	0,39
left valve	0.78	0.35

4. *Inner lamella:* Rather wide anteriorly, but very thin, thus the prominent vestibulum is visible rarely and fragmentarily. Marginal zone rather narrow anteriorly and posteriorly too. Prominent selvage in both valves, in right valve near the line of concrescence: in left valve in somewhat outwardly removed position. In both valves its running posteriorly deviates from the outline and is removed inward. Posteroventrally strong flange is visible.
5. *Marginal pore-canals:* Rather numerous anteroventrally, simple, straight.
6. *Hinge:* In right valve hinge-elements are positive, hardly divided from selvage, anteriorly and posteriorly a hardly prominent, undivided tooth occurs, with intervening median bar. All these hinge-elements fit into the corresponding groove of left valve.

7 – 8. *Normal pores* and *muscle scars* not seen.

9. *Eye-spot:* Absent.
10. Left valve slightly *overlaps* right.
11. The few more elongate, low specimens are probably the males; these show the posteriorly less inflated valves mentioned in dorsal view's description.

Comparison:

Morphologically this form has no Tertiary allies. Its visible outer and inner features, as well as its sexual dimorphism suggest agreement with the Recent genus of Daday. The uncertain generic status is necessitated by the partially incomplete preservation.

Material: Eight right valves and three left valves.

Familia Loxoconchidae Sars, 1925

Genus Loxoconcha Sars, 1866

Loxoconcha sp.

Pl. II, Fig. 18.

Description:

1. *Shape:* In outher lateral view anterior outline of left valve asymmetrically rounded, its upper part truncate. It encloses with dorsal outline an about 140° angle behind the one-sixth of the length. Dorsal outline nearly straight (obscured by the coarse ornamentation) to six-seventh of length, where encloses also with posterior outline a nearly 140° angle. Upper line of posterior outline straight in the part corresponding to one-fifth of maximal length, lower line slightly convex, the two lines are perpendicular to each other. Ventral outline is formed by the ventral wing-like extension between one-fifth and two-third of length, its running is hardly convex. The transition of ventral and anterior outlines – because of the damage – cannot be studied. Height at eye-tubercle.
   In inner lateral view the one outer margin of left valve strongly deviates from the margin ventrally, and shows a deep sinus between one- and two-third of length.
   In dorsal view the side-surface rises with about 35° angle to one-quater of length, then with 10 to 8° angle to two-third of length, and slopes with about 50° angle to nine-tenth of length then with 10° angle to the end of the valve.
2. *Ornamentation:* Left valve surface coarsely, irregularly reticulate, with sharp riblets. Reticulation absent on the flattened caudal part. Near the anterior margin runs a fine anteromarginal ridge, from which anteriorly no reticulation is visible. Dorsal side shows a downwardly narrowing, very shallow triangular depression. The ridge-like costa running on the ventral extension breaks upwardly near the ventral outline, at about two-third of length and ends near three-quarter length acutely.
   In ventral view the ventral extension shows paired costa parallel to the outline, which ends perpendicularly towards the ventral margin. Valve -parts below these costae are depressive.
   Ornamentation becomes coarser posterodorsally and is similar to radial ribbing anteriorly.

3. *Measurements:*	L	H	W/2
left valve	0.37	0.19	0.10

4. *Inner lamella:* Wide anteriorly, inner margin and line of concrescence slightly deviate anteriorly, narrow vestibulum is present. Selvage subperipheral.

5. Anteriorly 8 straight, simple *marginal pore-canals* are visible.
6. *Hinge:* In left valve small socket anteriorly, which is surrounded by the anteromedian tooth. Posteriomedian element is a finely crenulate bar, posterior element cannot be seen.
7. *Normal pores:* Rather few, large.
8. *Muscle scars:* Not seen.
9. *Eye-spot:* Prominent before one-third of length, near to the dorsal outline (behind the cardinal angle).

Remarks:

The Gánt form resembles the species Loxoconcha curryi Keij, 1957 and Loxoconcha limbata Haskins, 1971 in shape and ornamentation. In the type figures of the former the shape is thicker, the dorsal outline more irregular and the end of the ventral costa is different. The latter form seems to be closer in shape, however, in the Gánt specimen the outline – because of the overhang of the ventral extension – is somewhat different, and the anteromarginal ridge is weaker, the ventral ridge is less projected and its anterior and posterior running and ending are also different. Because of the single, incompletely preserved valve, the precise identification is impossible.
Material: One single left valve.

Familia Schizocytheridae Howe, 1961

Genus Schizocythere Triebel, 1950

Schizocythere depressa (Méhes, 1936)

Pl. III, Figs. 1–4.

1936. Eucytherura depressa Méhes, 1936 – Méhes, pp. 25–26, pl. III, figs. 5–8.

Description:

1. *Shape:* In outher lateral view anterior outline of left valve rounded asymmetrically, its upper part truncate, encloses with the nearly straight dorsal outline a 120–130° angle, somewhat before one-quarter of length. The straight running of dorsal outline is disturbed by the prominent cardinal angle, and the strong, obliquely projected spiniform element. At five-sixth of length the dorsal outline rounds into the posterior outline, of which upper line is markedly concave and encloses with its lower line a 90° angle at about one-third of length. This lower line rounds from slightly concave into convex and bears a strong posteroventral spine behind five-sixth length. The caudal process arising from the junction of the two lines is rounded or truncate. The slightly curved ventral outline is formed by the ventral ridge betwen one- and two-third of length. Because of the processes of the ornamentation elements, the lower part of the anterior outline shows 3 to 4 projections. Height anterior, near to the cardinal angle.

Anterior outline of r i g h t v a l v e more truncate above, encloses with dorsal outline an about 140° angle near one-third of length. Dorsal outline slightly convex, without strong cardinal angle and posterior spine, but the strong break at the junction with posterior outline is present.

In inn e r l a t e r a l vi e w ventral outline of l e f t v a l v e shows a shallow sinus between about one-quarter and one-third of length, with maximal concavity behind one-third of length.

In d o r s a l v i e w anterior side-surface rises with 45° angle to one-quarter of length, with about 20° to five-ninth of length, then slopes with about 40° angle to nine-tenth of length, finally with about 30° angle to the posterior end.

2. *Ornamentation:* L e f t v a l v e surface irregularly reticulate. On ventral side a prominent, arched ventral ridge occurs, which is formed by the strenghtening of two costae. The lower runs from lower part of anterior margin towards ventral margin, then forms the ventral outline with a convex arch, and ends abruptly in front of posterior spine. The upper costa arises near the lower third of the maximal height, from anterior margin, to one-third is convergent, then parallel to the lower costa, and at the ending of this latter, fades into the reticulation. Behind lower costa, with a separating interspace, a strong, obliquely backward-oriented spine occurs. Valve surface under lower costa is concave and reticulate. Along the dorsal margin the strengthening of the reticulation forms a weak dorsal ridge, which most prominent posterodorsally and near the cardinal angle; intervening valve surface depressive. Along anterior margin especially in its lower part – reticulation is weak or absent in wide zones. Above the two costae of ventral margin, an other, weaker and shorter costa runs to the anterior margin. One or two weak longitudinal costae may run onto caudal process. Reticulation weaker anterodorsally and centrally. Reticulation becomes sharper posteriorly.

Ornamentation of r i g h t v a l v e is similar.

3. *Measurements:*

	L	H	W
left valve	0.44	0.27	
left valve	0.40	0.27	
left valve	0.42	0.28	
left valve	0.41	0.27	
left valve	0.40	0.26	
right valve	0.44	0.26	
right valve	0.42	0.27	
right valve	0.40	0.26	
right valve	0.42	0.27	
right valve	0.40	0.25	
carapace	0.44	0.28	0.27
carapace	0.45	0.28	0.27

4. *Inner lamella:* Wide anteriorly and posteriorly. Line of concrescence coincides with inner margin. Flange strong, selvage runs centrally.
5. *Marginal pore-canals:* Few, straight, simple.
6. *Hinge:* In left valve strong anterior socket, bifid tooth, crenulate median bar and elongate crenulate posterior socket.
   In right valve anteriorly strong "two-stepped" bifid tooth, socket, median crenulate groove and posteriorly crenulate, elongate tooth.
7. *Normal pores:* Few, large, sieve-type, situated in interspaces of the reticulation.
8. *Muscle scars:* Hardly visible in detail.
9. *Eye-spot:* Prominent on cardinal angle in both valves.
10. Left valve *overlaps* right dorsally.
11. A part of the specimens is of more elongate, these are probably males.
12. In undeveloped forms the smaller size is associated with weaker ornamentation and less-developed hinge.

Remarks:

The studied specimens can be identified with the species described by Méhes (1936). Certain parts of the original description – especially the hinge – are inaccurate. It is caused by the unadequate equipments and the bad preservation
The Gánt specimens differ from Schizocythere appendicula Triebel, 1950 in having straighter ventral outline, more prominent cardinal and posterodorsal angles, more pronounced caudal process and different details in the ornamentation. From the French Lutetian Deltel (1961) figured forms, under the name Schizocythree appendicula, which seem to belong rather into the species of Méhes. The close relation of the two species seems to be obvious, however, because of the lostness of the holotype, the recognition of the degree of relation needs further studies on material from the type locality.

Geological and geographical distribution:

Middle? Eocene; Budapest- vicinity, Hungary.
Material: 100 right and left valves, three carapaces.

Familia Tracyleberididae Sylvester-Bradley, 1948

Genus Bradleya Hornibrook, 1952

Bradleya validornata hungarica n. ssp.

Pl. III, Figs. 5–8.

Derivatio nominis: After Hungary.
Holotypus: Left valve, reposited in the type collection of the Hungarian Geological Survey.
Locus typicus: Bauxite-pit of Bagolyhegy-hill, Gánt, Transdanubian Central Mountains, Hungary.

Stratum typicum: Lutetian Stage, mollusc-bearing marl.
Diagnosis: A form with denticulate anterior margin and strong ventral and dorsal costae.

Description:

1. *Shape:* In outer lateral view anterior outline of left valve rounded asymmetrically, with great radius in its upper two-third. Anterior outline encloses with dorsal outline a 120° angle at about one-fifth of length. The straight running of dorsal outline is modified by a slight protrusion at cardinal angle and the extension between one-third and three-quarter of length. Dorsal outline breaks upward by 150° angle threequarter of length and ends with a spiniform projection. The upper part of the joining posterior outline is concave in the start, nearly perpendicular to the main direction of the dorsal outline. Its lower portion slightly convex, somewhat angularly grades into the weakly convex ventral outline, which is formed between two-fifth and seven-tenth by the ventral ridge. Lower line of posterior margin bears 5 denticles, and its junction with the upper line an other, differently directed, smaller denticle occurs. Fine marginal denticulation appears posteriorly. Height near cardinal angle.
In right valve the anterior outline is more symmetrical, rounds into dorsal outline at about one-third of length, with a 140° angle, cardinal angle without protrusion, dorsal outline nearly straight, the short posterior portion of the dorsal outline markedly concave, which results a more pronounced spiniform projection between the dorsal outline and the concave line of posterior outline.
In inner lateral view the outer margin in left valve straight dorsally, deviates from outline. Both valves show ventral sinus on outer margin between one-sixth and two-third of length.
In dorsal view the valves are anteriorly parallel to about one-quarter of maximal width up to one-tenth of length, then rise with about 45° angle to one-third of length. From this to three-quarter length the outline of sides is uneven, nearly parallel, then slopes with about 45° angle to nine-tenth of length, finally parallel to about one-quarter of maximal width.
Ventral ridge in ventral view of carapace is slightly asymmetrical, rises with about 20° angle in left valve, with 30° angle in right valve. Ridges end perpendicularly to hinge-direction in both valves.
2. *Ornamentation:* Along anterior margin of left valve a ridge runs, which extends onto anterior third of the ventral part. Between half and three-quarter length a strong dorsal ridge appears, which breaks with 90° angle at its end, and fade into reticulation at upper one-third of local height. Ventral ridge similarly strong, it is formed by two slightly arched, posteriorly somewhat divergent costae. The upper costa ends at about one-sixth of local height, lower one ends below ventral margin. Valve-surface coarsely reticulate throughout,

the polygonal reticulation is formed by sharp, ridge-like riblets, which are arranged into two concentric rows anteriorly and more irregularly in other parts. The weakly developed subcentral tubercle appears slightly before half-length.
In r i g h t v a l v e the ridges – especially the dorsal one – developed more weakly.

3. *Measurements:*

	L	H
left valve	0.92	0.53
left valve	0.89	0.52
left valve	0.85	0.52
right valve	1.04	0.50
right valve	0.90	0.50
right valve	0.87	0.50

4. *Inner lamella:* Rather wide antero- and posteroventrally. Line of concrescence and inner margin coincide. Selvage distinct, subperipheral.
5. *Marginal pore-canals:* Numerous (higher than 20), about 10 posteriorly Espacially dense anteroventrally. Simple, straight, with ampullae in outer third.
6. *Hinge:* In l e f t v a l v e anterior socket, small anteromedian tooth, smooth posteromedian bar and relatively large posterior socket. In r i g h t v a l v e anterior element is a strong tooth, anteromedian element is a small socket, which continues in a smooth posteromedian groove. Posterior tooth elongate, arched.
7. *Normal pores:* Numerous, large, sieve-type.
8. *Muscle scars:* The four elongate adductor scars are arranged in a single row, with 2 frontal scars before.
9. *Eye-spot:* Pronounced, slightly behind and below cardinal angle.
10. Left valve *overlaps* right considerably at cardinal angle.
11. A part of the specimens are of more elongate, with weaker ridge; these probably are males.

C o m p a r i s o n :

In relation to the type subspecies of P i e t r z e n i u k (1969), this form shows pronounced ventral and dorsal ridges and finely denticulated anterior margin.
Material: Seven right valves and four left valves.

Genus Echinocythereis Puri, 1954

Echinocythereis dadayana (Méhes, 1941)

Pl. III, Figs. 9–11.

1936. Cythereis dadayi Méhes, 1936 – Méhes, pp. 40–42, pl. IV, figs. 12–13. (non Cythereis dadayi Zalányi, 1913).
1941. Cythereis dadayana Méhes, 1941, nom. nov. – Méhes, p. 43.

Description:

1. *Shape:* Anterior outline in outer lateral view of left valve rounded asymmetrically, radius of roundness is rather small in the lower part. Anterior outline at one-third of length curves into the nearly straight dorsal outline, of which straight running is diturbed by the protrusion of the cardinal angle. Dorsal outline angularly grades into posterior outline, with about 120° angle, slightly behind nine-tenth of length. Upper part of posterior outline slightly concave, lower part gradually curves – after a strong break – into ventral outline, which hardly concave in its running. Lower part of anterior outline finely denticulate, lower line of posterior outline bears 4 to 5 denticles. Height at cardinal angle.
Anterior outline of right valve is nearly symmetrical, dorsal outline uneven, with short, protruded portion near to two-fifth of length, and with inclined posterior portion. Upper line of posterior outline markedly concave, thus the valve is acute caudally. Ventral outline shows strong asymmetrical sinus between about one-quarter and three-fifth of length, with maximal concavity at two-fifth of length.
In inner lateral view outer margin deviates from the outline in both valves, straight dorsally and shows strong asymmetric sinus ventrally.
In dorsal view the surfaces are parallel to one-sixth of maximal width up to one-twelfth of length, rise with 30° angle to about five-twelfth of length, from this part are parallel to about two-third of length, then slopes with about 20° angle to five-sixth of length, and with about 40° angle to eleven-twelfth of length, and finally are parallel to the one-quarter of maximal width.

2. *Ornamentation:* Left valve surface bears dense longitudinal, irregularly branching and convergent costation, with transversal elements, which result a common ornamentetion network. Near ventral margin a strong ventral costa occurs, which runs from the maximum of ventral sinus to the four-fifth of length, and ends abruptly towards the surface. Surface below ventral costa nearly perpendicular to the plane between the valves. Starting from half-length, a short, slightly arched costa runs dorsally, which ends abruptly towards surface before the end of dorsal outline. Reticulation confines to certain parts of the surface, absent behind the connecting line between posterior ends of the two costae, and in anterior third of surface. Coarseness of ornamentation varies individually.
Ornamentation of right valve is similar.

3. *Measurements:*

	L	H
left valve	0.77	0.46
left valve	0.80	0.45
left valve	0.74	0.44
right valve	0.83	0.42
right valve	0.78	0.41
right valve	0.76	0.40

4. *Inner lamella:* Wide anteriorly and posteriorly, inner margin and line of concrescence coincide. Selvage stronger in right valve, situated in the outer third, with inner striae.
5. *Marginal pore-canals:* Dense, straight, some bifurcating.
6. *Hinge.* In right valve strong, "two-stepped" anterior tooth, smaller socket with associated smooth median groove and arched, lamellar, somewhat lobate posterior tooth.
   In left valve anterior socket is followed by a smaller, knob-like tooth, which continues into smooth median bar; posterior element is a narrow, arched, ventrally somewhat open socket.
7. *Normal pores:* Few, open.
8. *Muscle scars:* Anterior to the row of four elongate adductor scars two frontal scars are present. Partially constricted or subdivided adductor scars are obliquely oriented, their row is vertical.
9. *Eye-spot:* Clearly developed.
10. Left valve slightly *overlaps* right dorsally and ventrally
11. A part of the specimens are of much elongate, these are probably that males.

Remarks:

This studied form with its outer and inner features suggests a range into the genus Echinocythereis. However, it is unusual, that this genus, known previously as a deep-water form, occurs in a shallow-water, near-shore, even brackish-water environment. It is a common form in other localities in Hungary. (According to preliminary studies, in al cases in shallow-water, near-shore assemblages.)

Geological and geographical distribution:

Middle ? Eocene: Budapest-vicinity, Hungary.
Material: 30 right valves and left valves, 1 carapace.

Genus Hermanites Puri, 1955

Hermanites acuticosta gantensis n. ssp.

Pl. IV, Figs. 3–6.

Derivation nominis: After the name of the locality.
Holotypus: Left valve; reposited in the type collection of the Hungarian Geological Survey.

Locus typicus: Bauxite-pit of Bagolyhegy-hill, Gánt, Transdanubian Cantral Mountains, Hungary.
Stratum typicum: Lutetian Stage, mollusc-bearing marl.
Diagnosis: Posteriorly more acute valves, as compared to those of the nominate subspecies, with radial costae anteromarginally. In left valve the cardinal angle is spiniform, projected.

Description:

1. *Shape:* In outer lateral view anterior outline of left valve rounded asymmetrically, with truncate upper quarter. Anterior outline with fine denticulation, which is covered by the strong anteromarginal ridge in some places. It encloses with dorsal outline an about 135° angle behind one-quarter of length. Anterodorsal angle is projected highly above dorsal margin. From three-eighth of length the dorsal outline is formed by the two lamellar protrusions of the dorsal ridge, with an interspace near five-eighth of length. The small projected lamella in the posterodorsal angle makes the dorsal outline more uneven. Near five-sixth of length the dorsal outline grades – with a sharp break – into posterior outline, which is straight or somewhat concave in its upper two-third, bears a strong, overhanging spine in its middle portion, and after a break of about 90° angle in the lower third, it rounds gradually into ventral outline. This side shows four strong spines. Ventral outline has an asymmetric sinus between one- and three-quarter of lenght, which is slightly covered by the ventral ridge. Ventral outline rounds with a small radius into anterior.
   In right valve the posterodorsal outline is just projected, dorsal outline less broken at the junction with posterior outline. Upper line of posterior outline is markedly concave, thus the caudal part is more elongate. Upper line rounds into lower with an about 70° angle. The sinus of the ventral outline is more asymmetric.
   In inner lateral view outer margin considerably deviates from outline dorsally, where it is straight. The sinus of ventral outline is also more pronounced than that of outline, with maximal concavity before half-length.
   In dorsal view the surface is parallel to one-third of width to about one-eighth of length, rises with about 30° angle to three-eighth of length, nearly parallel to five-eighth of length, then slopes with about 30° angle to seven-eighth of length and finally parallel to one-quarter of width.
   In ventral view ventral ridge extends to three-quarter of length and rises with about 20° angle (the rise decreases toward its end).
2. *Ornamentation:* Left valve shows sharp, lamellar anteromargonal ridge. The strong, lamellar dorsal ridge forms the greater part of the dorsal outline. It is divided into two lamellae, the posterior one rounds toward valve-center and ends abruptly at three-quarter of

length, at the upper third of the local height. Ventral ridge starts near the ventral outline, from one-quarter of length, shows a weak arch towards ventral side, protrudes over ventral margin and ens in a spine before three-quarter of length, at one-sixth of local height. Strong spiniform elements are situated in posterodorsal angle, in the middle portion of upper line of posterior outline, beside the end of ventral ridge and in the middle of the space between posterior end and ends of the two ridges. Subcentral tubercle with numerous, smaller, protruding knobs. Four strong spines in the space between ridges behind, one strong spine above and 5 smaller spines before subcentral tubercle. From anteromarginal ridge 6 radial costae run to anterior spiniferous field. Weak, irregular reticulation visible throughout the spiny surface.

The ornamentation of the r i g h t v a l v e is similar.

3. *Measurements:*

	L	H
left valve	0.59	0.33
left valve	0.57	0.32
left valve	0.54	0.32
left valve	0.59	0.33
right valve	0.57	0.30
right valve	0.57	0.31
right valve	0.59	0.33

4. *Inner lamella:* Wide anteriorly and posteroventrally, line of concrescence and inner margin coincide. Selvage subperipheral.
5. *Marginal pore-canals:* 35 anteriorly, about 15 posteroventrally. Simple, straight, or slightly bent, with ampullae in their outer part.
6. *Hinge:* In l e f t v a l v e anterior socket, conical tooth and connecting crenulate median bar, the posterior element is a socket. In r i g h t v a l v e strong, "two-stepped" anterior tooth, socket and connecting crenulate median groove, the posterior element is an arched, lobate tooth.
7. *Normal pores:* Numerous, large, sieve-type.
8. *Muscle scars:* Four markedly elongate adductor scars in a ventral row, the lower three are obliquely, anteriorly oriented. In front of row of adductor scars, there are 2 close, circular frontal scars.
9. *Eye-spot:* Well-developed at anterodorsal angle.
10. Left valve *overlaps* right, especially at anterodorsal angle.
11. The somewhat more elongated specimens are presumably the males.

C o m p a r i s o n :

This form differs from the nominate subspecies (P i e t r z e n i u k, 1965) in having stronger caudal acuteness, and costae joining anteromarginal ridge. The reticulation between the ridges is weaker, but more extended. Different is the distribution and number of the spines, as well as the more acutely projected cardinal angle. An other difference is the presence of the "two-stepped" tooth.

The similarly close H. camelus turbidus Moos, 1968 has more numerous ornamental elements and different shape of caudal end.
Material: 300 right and left valves.

Hermanites haidingeri paijenborchiana Keij, 1957

Pl. IV, Figs. 1 – 2.

1852. Cythere haidingeri (Reuss, 1860) – Bosquet, pp. 125 – 126, pl. VI, fig. 10.
1955. Cythereis haidingeri (Reuss, 1850) – Apostolescu, pp. 269, pl. VII, figs. 114 – 115.
1957. Hermanites paijenborchiana Keij, 1957 – Keij, p. 110, pl. XVII, figs. 11 – 14, pl. XXI, figs. 10 – 11.
?1961. Hermanites paijenborchiana Keij, 1957 – Deltel, pp. 168 – 169, pl. 16, ifgs. 279 – 280.
1962. Hermanites paijenborchiana Keij, 1957 – Hinte, pp. 180 – 182, pl. I, fig. 5, pl. III, figs. 1 – 2,8,10.
1969. Hermanites paijenborchiana Keij, 1957 – Seremeta, pp. 199 – 200, pl. XVIII, figs. 15 – 16.
1969. Hermanites paijenborchiana Keij, 1957 – Ducasse, p. 115, pl. VIII, fig. 169.

Description:

1. *Shape:* In outer lateral view anterior outline of left valve somewhat asymmetrically rounded, its upper part truncate. The nearly straight dorsal outline, because of the coarse ornamentation, runs unevenly, and encloses a 130° angle with the anterior outline. Dorsal outline protruded above eye-spot. The dorsal ridge and a posterodorsal extension also modifies the dorsal outline. Dorsal line of posterior outline encloses 120 – 130° angle with dorsal outline, with spiniform, protruded angle at the junction. Its ventral line encloses 130 – 140° angle with the ventral outline. Dorsal line concave, ventral slightly convex. Ventral side of posterior outline shows 7 spines, and an additional one in its lowermost part. Ventral outline nearly straight, divergent anteriorly from dorsal, and arches into anterior outline with a small radius. Anterior outline finely denticulated, especially on its ventral part. Height at cardinal angle.
In inner lateral view outer margin of left valve deviates from outline by the coarse ornamentation. Dorsal outline straight, posterior outline concave dorsally, convex ventrally, ventral outline bears shallow sinus between three- and seven-tenth of length.
In dorsal view the posterior portions of dorsal ridges in left valve are somewhat more projected.
In ventral view the ventral ridge of left valve rises with 30° from one-tenth to about four fifth of length. Surface is parallel to about one-third of maximal width to one-tenth, then subcentral

tubercle forms a convexity to half-length, and the outline is formed by the above described ventral ridge. From that the outline slopes with 60—70° angle to five-sixth of legth, and finally parallel to one-third of maximal width.

2. *Ornamentation:* In left valve, near tot the anterior margin, runs a parallel anteromarginal ridge. Main ornamentation elements are the ventral ridge, the dorsal ridge and the subcentral tubercle. The slightly curved ventral ridge arises near the ventral margin, and later removes from that.
   Dorsal ridge arises at three-tenth of legth, somewhat arched below dorsal outline, and reaches dorsal outline at half-length. Dorsal outline is formed by the dorsal ridge to about four-fifth of length, and, breaking with a 70—80° angle at one-third of local height, it fades into the reticulation. Subcentral tubercle behind one-third of length. Secondary ornamentation is formed by network-reticulation, which is weak in central part of subcentral tubercle. Ornamentation is arranged in concetric rows along anterior margin, especially the three anterior spaces, where an additional, regular radial, arrangement, with 5 pronounced costae, appears. Around subcentral tubercle an annular arrangement of 12 spaces occurs. Reticulation is sponge-like.

3. *Measurements:*

	L	H
left valve	0.72	0.40
left valve	0.77	0.40

4. *Inner lamella:* Moderately wide, inner margin coincides with line of concrescence and runs parallel to outer margin. Selvage is near to outer margin in left valve.
5. *Marginal pore-canals:* Approximately 20 anteriorly, 10 posteriventrally, straight, simple, partially with ampullae.
6. *Hinge:* In left valve large, closed anterior socket, anteromedian element is a smaller tooth, which continues into the smooth posteromedian bar, posterior element is a socket, which is open towards valve-interior.
7. *Normal pores:* Large, their number corresponds to the spaces of the reticulation.
8. *Muscle scars:* In front of the ventral row of four adductor scars, a "V"-shaped frontal scar is situated.
9. *Eye-spot:* Well developed at anterodorsal angle.
10. The more elongate specimens are probably the males.
11. Beside smaller size and weaker calcification, the embrional valves are characterized by weakly-developed inner lamella and hinge.

Remarks:

The French Lutetian forms were described by Keij (1957) as new species H. paijenborchiana, who regarded its less regular anterior ornamentation and laterally more projected dorsal ridge as main distinguishing features

from the Miocene H. haidingeri. Hinte in 1962 described from the Eocene of Sonneberg Hermanites paijenborchiana specimens with a more regular anterior ornamentation, which is close to that of H. haidingeri. The regularity of the anterior ornamentation may be different in several subspecies of H. haidingeri.

On the basis of the literature, H. paijenborchiana and H. haidingeri can be distinguished only on subspecific level.

The specimens from Gánt are identical even in the fines ornamentation details with the left valve of H. haidingeri haidingeri figured by Moos (1965) from the Tortonian of Grusbach (Austria). The shape is slightly different, because in the Gánt specimens the height difference between posterior and anterior ends of dorsal outline is smaller, the anterior margin is more asymmetric, the posterodorsal spine is weaker, the dorsal line of posterior outline is smaller, less concave, and the center of the subcentral tubercle is smooth. Different is the laterally less protruding character of the dorsal ridge, too. As compared to the type of H. paijenborchiana, the Gánt specimens show maximal concavity of ventral outline in anterior third, and more protruded caudal angle. The ornamentation is similar as that of the holotype, but the type figure does not show marked regularity in the anterior ornamentation.

Geological and geographical distribution:

Eocene – Stampian ?: France
Ypresian – Lutetian: Belgium
Eocene: Austria
Lower Eocene: USSR
Material: Two left valves and one embryonal left valve.

Genus Quadracythere Hornibrook, 1952.

Quadracythere angusticostata (Bosquet, 1852)

Pl. IV, Figs. 7 – 10.

1852. Cythere angusticostata (Bosquet, 1852) – Bosquet, pp. 91 – 92, pl. IV, fig. 12.
1957. Quadracythere angusticostata (Bosquet, 1852) – Keij, p. 104, pl. XII, fig. 16, pl. XIX, fig. 12.
1959. Quadracythere angusticostata (Bosquet, 1852) – Ducasse, p. 66, pl. V, fig. 3, pl. XXIV. figs. 30a – b.
1969. Bradleya angusticostata (Bosquet, 1852) – Ducasse, p. 107, pl. VII, fig. 155.
1971. Bradleya angusticostata (Bosquet, 1852) – Blondeau, pp. 39 – 40, pl. IV, figs. 7 – 8.

Description:

1. *Shape:* In outher lateral view anterior outline of left valve asymmetrically rounded, its upper part truncate, and encloses with dorsal outline an about 130° angle at one-fifth of length.

The straight running of dorsal outline is divided by the markedly protruded cardinal angle, the projected part of the dorsal ridge with two smaller protrusions before, and the spiniform projection of the posterodorsal angle. Dorsal outline encloses with posterior outline an about 120° angle at nine-tenth of length, the upper line of posterior outline is somewhat concave, its lower line is slightly convex and these lines enclose an about 130° angle with each other. Lower line bears 5 strong denticles. Ventral outline nearly straight, somewhat concave, and rounds into anterior outline gradually. Height anterior. In r i g h t v a l v e the cardinal angle markedly deviates from the outer margin, which runs straight. Outer margin shows a strong, somewhat asymmetric ventral sinus between one- and two-third of length.

In d o r s a l v i e w the side-outline is parallel to about one-third of width to one-tenth of length, rises with 40° angle to four-tenth of length, then somewhat recessive, and then nearly parallel or rising with 10—15° angle to five-sixth of length, and from that, slopes with about 45° angle to eleven-twelfth of length, and finally parallel to one-fifth of length.

In v e n t r a l v i e w it is visible, that the angle of ventral ridge and plane of valve-closure is decreasing from 30° to 0° between one-sixth and three-fourth of length. Ventral ridges of the two valves are symmetric.

2. *Ornamentation:* Along anterior margin of l e f t v a l v e runs a strong anteromarginal costa. Between half and five-sixth of length an uneven dorsal ridge appears, which ends with a 90° break at one-quarter of local width and fades into the reticulation. Strong ventral ridge appears, which runs with a weak arch, nearly parallel to the ventral margin. It runs from about one-fifth to two-third of length, with a thickening at its abrupt end. Surface markedly reticulated throughout, the riblets are sharp. The 6 strong radial costae enclose large, elongate interspaces, anteriorly, the costa rising from the eye-spot is especially strong. Subcentral tubercle prominent, without reticulation on its central part. The reticulation of the other parts of the surface is irregular. On the surface between ventral ridge and ventral margin, strong riblets occur.

The ornamentation of the r i g h t v a l v e is similar.

3. *Measurement:*

	L	H
left valve	0.83	0.46
left valve	0.79	0.46
right valve	0.81	0.45
right valve	0.83	0.44
right valve	0.80	0.42

4. *Inner lamella:* Relatively wide anteriorly and posteriorly. Line of concrescence and inner margin coincide. Selvage strong, runs centrally.

5. *Marginal pore-canals:* Approximately 30 anteriorly, 10 posteriorly, simple, straight, with ampulla-like thickening in the middle.
6. *Hinge:* In left valve closed anterior socket, conical tooth and associated crenulate median bar, posterior socket. In right valve strong anterior tooth, socket with associated, crenulate (?) median groove, and lamellar, arched, dorsally curve posterior tooth.
7. *Normal pores:* Numerous, large, sieve-type.
8. *Muscle scars:* In front of the row of adductor scars, two well-visible frontal scars are situated.
9. *Eye-spot:* Well-developed, prominent in the cardinal angle.
10. Left valve *overlaps* right, especially at cardinal and posterodorsal angles.
11. A part of the specimens is of more elongate, these are probaly the males.
12. There are several larval valves in the material. In these specimens the ornamental subcentral tubercle, the dorsal, ventral, and anteromarginal ridges are well-developed, reticulation only on central surface. Antero- and posteromarginal denticultion is prominent, on dorsal and ventral ridges prominent spines are visible.
    The inner lamella and the hinge margin are undeveloped, hardly separated.
    In fornt of the row of four adductor scars, "V"-shaped frontal scar appears.
    The valves are thin and fragile, smaller than in adults.

Remarks:

The Gánt specimens are identical in detail with the description and figure of Keij (1957) revision; the difference is the simpler ornamentation of the subcentral tubercle.

Geological and geographical distribution:

Eocene: France
Material: 300 right and left valves.

Quadracythere vahrenkampi Moos, 1965

Plate IV, Figs. 11–13.

1965. Quadracythere (Hornibrookella) vahrenkampi Moos, 1965 – Moos, pp. 599–602, pl. 34, figs. 5 8.
1968. Quadracythere (Hornibrookella) vahrenkampi Moos, 1965 – Moos, pp. 6–7, pl. 1, figs. 5–11.
1969. Quadracythere (Hornibrookella) vahrenkampi Moos, 1965 – Pietrzeniuk, p. 72, pl. XIII, fig. 5, pl. XXVII, figs. 11–14, text-fig. 16.

Description:

1. *Shape:* In outer lateral view anterior outline of right valve rounded asymmetrically, its lower part with small: upper part with large radius. Anterior outline rounds with an about 150° angle into the nearly straight dorsal outline behind one-third of length, Cardinal angle at the junction is somewhat protruded. On dorsal outline, behind the end of dorsal ridge, after four-fifth of length, a small recession appears. Dorsal outline, somewhat before nine-tenth of length, rounds with 110 120° angle into posterior outline, of which upper line is nearly straight, and encloses with its nearly straight median portion a 130 – 140° angle. Its slightly convex lower line encloses with the median portion a less than 90° angle and grades with a small break into the ventral outline at nine-tenth of length. Ventral outline convex, with a concave sinus, maximal convexity at three-fifth, maximal concavity before two-fifth of legth. Lower line of posterior outline bears 5 denticles and the anterior outline, especially its lower part, is finely denticulated. Height at cardinal angle. In outer lateral view the outer margin straight dorsally. Ventral sinus of ventral margin is stronger as that of the outline. In ventral view the surface is parallel to about one-third of maximal width to one-sixth of length, then rises with about 30° angle to five-twelfth of length, and from this, after a short depression, attains this width again at three-quarter of length, then slopes with about 45° angle to five-sixth of length, and finally is parallel to about one-third of maximal width to the caudal end.
2. *Ornamentation:* In left valve prominent dorsal, anterimarginal and ventral ridges occur. Dorsal ridge forms the dorsal outline between three- and four-fifth of length, then with a 90° angle break in one-third of local height, fades into the reticulation. At the break it is spiniform, being perpendicular to the surface. Ventral ridge runs near the ventral outline, between one-quarter and two-third of length, and curves upward posteriorly. Encloses about 45° angle with the surface at its end. At two-fifth of length a protruded subcentral tubercle appears. Surface coarsely reticulated, concentric and radial arrangement anteriorly, the anteromarginal ridge is associated with 6 strongly elongate, radially arranged interspaces. Ventral ridge is formed by two parallel, strong costae. The reticulate interspaces between the subcentral tubercle and posterior ends of ridges are elongate. Marginal ridge persists on caudal part too.

3. *Measurements:*

	L	H
right valve	0.76	0.39

4. *Inner lamella:* Rather wide anteriorly and posteroventrally. Line of concrescence and inner margin coincide. Selvage runs parallelly and near to the outer margin.

5. *Marginal pore-canals:* Numerous anteriorly, straight, simple, with ampullae in the middle.
6. *Hinge:* In r i g h t v a l v e "two-stepped" conical anterior tooth, large, closed anteromedian socket and continuing crenulate median bar, and outwardly curved, wearkly lobate, flattened posterior tooth.

7–8. *Normal pores* and *muscle scars* cannot be studied sufficiently.

9. *Eye-spot:* Well-developed at cardinal angle.

12. The majority of the specimens is presumably larval valves, or individuals which were modified by the unfavourable ecological conditions. The right valves of these forms are different in having perpendicular prong of dorsal ridge with two spiniform divisions, in longer upper line and in an about 40–50° angle enclosed by lower and median line of posterior outline, thus a more acute caudal extension. Ventral ridge ends spiniformly at two-third of length, and shows two additional spines. Anteromarginal ridge and anterior and posterior valve-halves show a weaker ornamentation as compared to that of adult. Inner lamella less-developed. However, the hinge is specific.

Measurements:	L	H
left valve	0.58	0.33
left valve	0.59	0.34
right valve	0.59	0.31
right valve	0.58	0.31

Remarks:

As compared to the type, in Gánt specimens the cardinal angle is removed backwards, the posterior outline somewhat deeper upwards, angular, reticulation extends to subcentral tubercle too, and the reticulation not sponge-like. The small quantity of the available material does not enable to decide, whether these Hungarian specimens form a new subspecies. So much so, that even the author of this species demonstrated similar individual and spatial differences within the Lower Oligocene of Germany.

Geological and geographical distribution:

Lower Oligocene: Germany
Upper Eocene: GDR
Material: One left valve, 10 larval (?) right and left valves.

Familia Xestoleberididae Sars, 1928

Genus Xestoleberis Sars, 1866

Xestoleberis gantensis n. sp.

Pl. IV, Figs. 14 17.

Derivatio nominis: After the name of the locality.
Holotypus: Left valve; reposited in the type collection of the Hungarian Geological Survey.

Locus typicus: Bauxite-pit of Bagolyhegy-hill, Gánt, Transdanubian Central Mountains, Hungary.
Stratum typicum: Lutetian Stage, mollusc-bearing marl.
Diagnosis: A form with slightly convex ventral outline, moderately truncate anteriorly, dorsal outline broken medianly, its posterior part runs straighter than the anterior.

Description:

1. *Shape:* In outer lateral view anterior outline of left valve rounded asymmetrically. Its lower half curves with small, upper half with large radius, the upper half rounds gradually into the widely arched dorsal outline, which breaks at about half-length, and the somewhat straighter posterior part enclosses with the anterior part an about 150° angle. The junction with the posterior outline shows similar break, posterior outline runs somewhat asymmetrically, but rounds into ventral outline more gradually. Ventral outline slightly convex, with nearly straight anterior part. Height at five-eigth of length. Ventral outline of right valve still less convex, the break on dorsal outline is situated at two-fifth of length, the dorsal outline is nearly parallel to the straight portion of ventral outline behind.
   In inner lateral view outer margin shows a marked asymmetric ventral sinus at about two-fifth of length.
   In dorsal view the slope of the surface decreases from 40° to 0° at two-third of length, i. e. at maximal width, slopes slightly to three-quarter of length, from this its angle increases abruptly, and ends with a 60° angle.
2. *Ornamentation:* Valve-surface smooth, shiny.
3. *Measurements:*

	L	H
left valve	0.59	0.40
left valve	0.55	0.37
right valve	0.55	0.33
right valve	0.55	0.35

4. *Inner lamella.* Rather narrow, widest anteriorly, and posteroventrally. Prominent vestibulum anteriorly.
5. *Marginal pore-canals:* Dense anteriorly and anteroventrally, simple, straight, short.
6. *Hinge.* Anteriorly and posteriorly elongate, strongly crenulate teeth, with median groove between them.
7. *Normal pores:* Relatively few, scattered, large.
8. *Muscle scars:* Four undivided, elongate adductor scars in ventral row. In front of the second adductor scar from above, a „V"-shaped frontal scar, and further down two mandibular scars are situated.
9. *Eye-spot:* Absent. The characteristic "Xestoleberis spot" is visible.
10. Left valve *overlaps* right, especially ventrally and dorsally.

12. Greater part of the available specimens are larval valves. These are generally more elongate than the adults, and their ventral outline is straight or partially concave. Valves are thin, fragile, markedly smaller.

Comparison:

This spesies is close to X. subglobosa (B o s q u e t, 1852), but less inflated and its dorsal outline shows a stronger break. The other similar species, X. muelleriana (Lienenklaus, 1900) has a more truncate dorsal outline anteriorly, just as in X. obtusa (Lienenklaus, 1900).

Material: Two left and two right valves, 22 larval valves and 5 larval carapaces.

Stratigraphic evaluation

From the 19 specifically identified form of the ostracode fauna of Gánt, 4 are new species, 3 are new subspecies and 3 are forms which were described previously only from Hungary, from stratigraphically uncertain samples. Thus merely 9 species can be evaluated stratigraphically. The majority of these latter forms – except two – are represented by small specimen number.

This fauna is unquestionably of Eocene in age, but for a closer age-determination within the Eocene, these 9 species are unsuitable, because there are no species, which confines – according to all authors – to a special part of the Eocene. This can also be due to the fact, that the stratigraphic range of some species is widely interpreted by the authors, on the other hand a more extensive use of subspecies is much to be wished.

The Middle Eocene age of the locality is proved previously by its extremely rich macrofauna (S z ő t s 1953, 1956), and the majority of the stratigraphically evaluable ostracode species are forms common in Middle Eocene. Two forms are known so far from beds not older than Middle Eocene. In the case of Neocyprideis williamsonia it is probably caused by determination problems (see description), while in Quadracythere vahrenkampi the single valve unables the detailed evaluation of the differences.

Paleoecological evaluations

The environmental conditions which ruled during the depostion of te Middle Eocene mollusc-bearing marl in the Gánt area are treated in a previously published study (Monostori 1972).

The detailed studies show that the washing separates, which came from infillings of different gastropods, may be remarkably different, and this fact made possible to work out the varied environmental conditions of the area and the different ecological requirements of the gastropods as well.

The ecological characteristics of the separate elements of the fauna are as foll lows:

1. *Salinity*

The majority of the species of Cytherella, Bairdia, Krithe, Schizocythere, Bradleya, Hermanites and Quadracythere live under normal saline, marine conditions.
Characteristic brackish-water elements are the Neocyprideis and Cytheridella (living even is fresh-water), and a remarkable part of the Xestoleberis species.
The species ranged into Novocypris genus presumably characterizes areas of markedly unstable (seasonally changing) salinity. According to previous studies, this latter species commonly forms monospecific assemblages, or associations with a Cytheromorpha species, under unfavourable circumstances (probably characterized by strong seasonal salinity-changes). These associations are usually the ostracodes appearing first after the coal formations, in the beginning of the Eocene transgression.

2. *Water depth*

a) Euryhaline forms;

The heavily calcified, coarsely ornamented Bradleya, Hermanites and Quadracythere species characterize coastal, shallow-water (litoral – upper sublitoral) environments (B e n s o n 1959).

The Recent species of the genus Schizocythere are somewhat deeper sublitoral forms (Schornikov 1974), and previous studies on Hungarian Eocene sequences show, that these are commonly associated with Krithe species of great specimen number, and this also suggest deeper water.

The majority of the Recent Krithe species are distinctly of deep-water forms (Morkhoven 1963), while the genera Cytherella and Bairdia live in varied water depth.

b) Brackish-water forms commonly inhabit extremely shallow estuaries and tide-pools (Benson 1959).

c) On the basis of the previously evaluated occurences of the genus Novocypris, a litoral – upper sublitoral, open habitat is suggested.
In the evaluation of the following subdivision of the ostracode genera with great specimen number is given:

- Litoral – upper sublitoral forms living in normal salinity: Bradleya + Hermanites + Quadracythere;
- Especially normal salinity forms living in varied water depth: Cytherella + Bairdia + Krithe;
- Deeper sublitoral form living in normal salinity: Schizocythere;
- Litoral – upper sublitoral form living in changing salinity: Novocypris;
- Estuarine forms living in brackish water: Neocyprideis + Cytheridella;
- Form living in tide-pools: Xestoleberis.

The distributions in the certain washing separates are as follows:

1. Washing separate of Cerithium subcorvinum Opph. infilling:
   Bradleya + Hermanites + Quadracythere: more than 50%,
   Cytherella + Bairdia + Krithe: 10%,
   Schizocythere: 10 to 20%,
   Novocypris: 10 to 20%,
   Neocyprideis + Cytheridella: scattered,
   Xestoleberis: scattered.
2. Washing separate of Cantharus brongniarti (d'Orb.) infilling:
   Bradleya + Hermanites + Quadracythere: 40%,
   Cytherella + Bairdia + Krithe: 10%,
   Schizocythere: 10%,
   Novocypris: 30 to 40%,
   Neocyprideis + Cytherodella: more than 5%,
   Xestoleberis: fewer than 10%.
3. Washing separate of Ampullina perusta (Defr.) infilling:
   Bradleya + Hermanites + Quadracythere: 30%.
   Cytherella + Bairdia + Krithe: fewer than 5%,
   Schizocythere: scattered,
   Novocypris: 50 to 60%,
   Neocyprideis + Cytheridella: 10%,
   Xestoleberis: fewer than 5%.
4. Washing separates from other Naticidae infillings:
   Bradleya + Hermanites + Quadracythere: 40%,
   Cytherella + Bairdia + Krithe: 20%,
   Schizocythere: 5%,
   Novocypris: 20 to 30%,
   Neocyprideis + Cytheridella: fewer than 5%,
   Xestoleberis: 5%.
5. Washing separates from Tympanotonus calcaratus (Bongf.) ingnilling:
   Bradleya + Hermanites + Quadracythere: more than 30%,
   Cytherella + Bairdia + Krithe: scattered,
   Schizocythere: scattered,
   Novocypris: 50%,
   Neocyprideis + Cytheridella: 10%,
   Xestoleberis: 5%.
6. Washing separates from Tympanotonus hungaricus (Zitt.) infilling:
   Bradleya + Hermanites + Quadracythere: 40 to 50%,
   Cytherella + Bairidia + Krithe: scattered,
   Schizocythere: fewer than 10%,
   Novocypris: 30 to 40%,
   Neocyprideis + Cytheridella: 5 to 10%,
   Xestoleberis: fewer than 10%.

7. Washing separates from Tympanotonus rozlozsniki Szőts infilling:

Bradleya + Hermanites + Quadracythere: 30%,
Cytherella + Bairdia + Krithe: scattered,
Novocypris: 60%.
Neocyprideis + Cytheridella: 10%,
Xestoleberis: scattered.

8. Washing separates from Faunus fornensis (Zitt.) infilling

Bradleya + Hermanites + Quadracythere: 10%,
Cytherella + Bairdia + Krithe: scattered,
Schizocythere: scattered,
Novocypris: 30 to 40%,
Neocyprideis + Cytheridella: 10%,
Xestoleberis: 40 to 50%.

On the basis of these studies:

1. The fauna came from the infillings of Cerithium subcorvinum, Cantharus brongniarti and Naticidae – except Ampullina perusta – probably lived in near-shore, litoral-shallow sublitoral waters in basically normal, temporally changing salinity.
2. The fauna yielded by infillings of Tympanotonus calcaratus, T. rozlozsniki and Ampullina perusta shells suggests presumably stronger changes in salinity.
3. In the case of the fauna from Faunus fornensis infilling, beside strong salinity changes, litoral environment is suggested.
4. The occurence of estuarine forms increases together with the strenght of salinity changes (approaching coast-line), however, characteristic estuarine fauna is unknown.

The genus Novocypris commonly occurs in all samples, because the salinity changes were characteristic, repeated phenomena. The faunal mixture – naturally – was an important factor. It is well-known from studies on modern sediments, that the data of recent shells in the sediments are divergent from those of distribution of living specimens. It is true especially in the case of fossil sediments, where the washed samples may result populations, which are different temporally as compared to the individual life-spans of the respective animals. In the case of gastropod infillings this latter unfavourable condition can be avoided (M o n o s t o r i 1973).

According to these considerations, it is possible to trace the formerly existed different environments, which were favourable to the ostracodes. Naturally, these faunas can hardly regarded as clear populations, because temporally different forms are represented.

On the basis of the ostracodes, about the formation of the Middle Eocene mollusc-bearing marl of Gánt, the following picture can be drawn.

This region was a near-shore, shallow-water marine area in some extent separated from the open sea. On greater parts the salinity was

near to normal, but great temporal (firstly seasonal) differences may have been occur. On the basis of the fauna, it is suggested the presence of smaller lagoons and tide-pools for certain parts of the region, or for its vicinity. The degree of the salinity changes, as well as the appearance of the lagoonal character was presumably variable in time.

The character of the ostracode fauna suggests that the complete lack of certain faunal groups, e. g. nummulites, cannot be due to a stable low salinity (about 25 0/00 by S t r a u s z 1962), but rather to the frequently changing salinity. This latter is indicated by recently described coral finds, too (Mihály 1975). In this way, the comparison to the Hungarian Sarmatian depositional conditions (S t r a u s z 1962) is unjustified. On the other hand, the Sarmatian rocks contain a completely different ostracode fauna, characterized by distinctly brackish-water forms.

Conclusions

Washing separates from the Middle Eocene mollusc-bearing marl of Gánt yielded an extremely rich ostracode fauna. This fauna contains 19 species and subspecies, from which 7 species and subspecies proved to be as new. On the basis of the several endemic element of the mollusc fauna, a certain endemism of the ostracode fauna was similarly to be expected. To determine the degree of this endemism, it is necessary to study other Eocene faunas of localities in Hungary and in the neighbouring countries.

The previously known species are in accordance with the Middle Eocene age determined by other fossil groups, however, these are inadequate for more detailed stratigraphic determinations at the present.

The marl deposited in shallow-water, near-shore marine region, where marked salinity changes (mainly of seasonal) occured, with associated estuaries.

REFERENCES

A p o s t o l e s c u, V. (1955): Description de quelques ostracodes du Lutétien du Bassin de Paris. Cahires Gél, 28/29, pp. 241 – 279, pls. 1 – 8.

B e n s o n, (1959): Ecology of Recent ostracodes of the Todos Santos Bay region, Baja California, Mexico. Kansas Univ. Paleont. Contrib., 23, 1., pp. 1 – 90.

B l o n d e a u, M. A. (1971): Contribution a l'etude des ostracodes eocenes des Bassins de Campbon et de Saffre (Loire – Atlantique). Thes de l'Univ. Nantes, pp. 1 – 157, pls. 1 – 17.

B o s q u e t, J. (1852): Déscription des Entomostracés fossiles des terrains tertiaires de la France et de la Belgique. Mem. sav. étrang. Acad. Roy. Sci. Belgique, 24. pp. 1 – 142, pls. 1 – 6.

D e l t e l, B. (1961): Les Ostracodes du Paléogene moyen et supérieur d'Aquitaine méridionale. These Troisieme Cycle, Univ. de Bordeaux, No. 95. pp. 1 – 215, pls. 1 – 19.

D u c a s s e, O. (1959): Les Ostracodes de l'Eocene du sous-sol Bordelais: répartition, intéret stratigraphique et paléogéographique. These Troisieme Cycle, Univ. de Bordeaux, No, 40, pp. 1 – 132, pls. 1 – 28.

D u c a s s e, O. (1967): Nouveaux Ostracodes de l'Eocene nord aquitain. Proc. – Verb. Soc. Sc. Phys. Natur. Bordeaux, 7/2, pp. 1 – 89, pls. 1 – 5.

D u c a s s e, O. (1969): Etude micropaléontologique (Ostracodes) de l'Eocene Nord-Aquitain. These Univ. Bordeaux, pp. 1 – 381, pls. 1 – 20.

Farkas, H. (1974): Morphological analysis of Ostracods (Crustacea). I. The problem of Cypridopsis vidua and Cypridopsis obesa. Acta Zool. Hung., 20, pp. 33–46.
Haskins, C. W. (1968, 1969, 1970, 1971): Tertiary Ostracoda from the Isle of Wight and Barton, Hampshire, England. Parts II–VI. Revue de Micropaléont., 11, pp. 3–12, pl. 1–2; 11, pp. 161–175, pls. 1–3; 12, pp. 149–170, pls. 1–4; 13, pp. 13–29, pls. 1–3; 13, pp. 207–221, pls. 1–3.
Hinte, J. E. (1962): Ostracoden aus dem Alttertiär des Sonneberges, Kärnten, Österreich. Proc. Kon. Nederl. Akad. Wetensch., (B), 65, pp. 166–179.
Jones, T. R. (1857): A monograph of the Tertiary Entomostracoda of England. Paleontogr. Soc. London, pp. 1–68, pls. 1–5.
Keen, M. C. (1972): The Sannoisian and some other Upper Paleogene ostracoda from North–West Europe. Palaeontology, 15, pp. 267–325, pls. 45–56.
Keij, A. J. (1957): Eocene and Oligocene Ostracoda of Belgium. Mém. Inst. Roy. Sci. Nat. Belgique, 136, pp. 1–120p, pls. 1–26.
Khosla, S. C. (1972): Ostracodes from the Eocene beds of Rajasthan, India. Micropalaeontology, 18, pp. 476–507, pls. 1–5.
Kollmann, K. (1958): Cytherideinae und Schulerideinae n. subfam. aus dem Neogen des östlichen Österrreich. Mitt. Geol. Ges. Wien, 51, pp. 89–195, pls. 1–21.
Lienenklaus, E. (1894): Monographie der Ostracoden des nordwestdeutschen Tertiärs. Zeitschr. Deutsch. Geol. Ges., 46, pp. 158–268, pls. 13–18.
Lienenklaus, E. (1900): Die Tertiär-Ostracoden des mittleren Nord-Deutschlands. Zeitschr. deutsch. geol. Ges., Bd. 52, pp. 497–550, pls. 1–4.
Marliere, R. (1958): Ostracodes du Montien de Mons et résultats de leur étude. Mém. in 8^{e} Soc. Belge Géol. Paléontol. Hydrol., 5, pp. 1–5., pls. 1–6.
Méhes, Gy. (1936): Budapest vidékének eocén Ostracodái (Die Eocänen Ostracoden der Umgebung von Budapest). Geol. Hung., Ser. Pal., 12. pp. 1–57, pls. 1–4.
Méhes, Gy. (1941): Budapest környékének felsőoligocén Ostracodái (Die Ostracoden des Oberoligozäns der Umgebung von Budapest). Geol. Hung., Ser. Pal., 16, pp. 1–95, pls. 1–7.
Mihály, S. (1975): Paleoökológiai megfigyelés a gánti középsőeocénből (Paleoecological observations in the Middle Eocene of Gánt, Hungary). Földt. Közl., 105, pp. 75–811 pl. 1.
Monostori, M. (1972): A gánti eocén Ostracodák fácies értékelése (Ecological evaluation of Eocene ostracods from Gánt, Transdanubia, Hungary). Őslénytani Viták, 20, pp. 55–61.
Monostori, M. (1972): Beitrag zur Methodik der Aufsammlung von Mikrofossilen: Mikrofauna aus Gastropoden. Ann. Univ. Sci. Budapest., Sect. Geol., 16, pp. 137–142.
Moore, R. C. (Edit) (1961): Treatise of Invertebrate Paleontology. Part Q. Univ. Press, Kansas, pp. 1–442.
Moos, B. (1965): Die Ostracoden-Fauna des Unteroligozäns von Bünde (Bl. Herford-West, 3817) und einige verwandte jüngere Arten (Ostr., Crust.) I. Quadracythere (Hornibrookella) n. subg., Pokornyella, Hemicythere, Hermanites. Geol. Jahrb., 82. pp. 593–630, 917. pls. 34–39.
Moos, B. (1968): Zur Ostracoden-Fauna (Crust.) des Unteroligozäns von Latdorf. Geol. Jahrb., 87, pp. 1–40, pls. 1–4.
Moussou, A. (1966): Contribution a l'étude des Ostracodes de l'Oligocene girondin. These Troisieme Cycle, Univ. de Bordeaux, No. 374, pp. 1–218, pls. 1–33.
Moyes, J. (1959): Répartition et valeur des Ostracodes dans l'interprétation du Miocen nord-aquitain. These Troisieme Cycle, Univ. de Bordeaux, No. 41, pp. 1–117, pls. 1–16.
Pietrzeniuk, E. (1965): Zwei neue Bradleya-Arten (Ostracoda) aus dem deutschen Obereozän. Geologie, 14. 7., pp. 878–891, pls. 1–3.
Pietrzeniuk, E. (1969): Taxonomische und biostratigraphische Untersuchungen an Ostracoden des Eozäns 5 im Norden der Deutschen Demokratischen Republik. Paläont. Abh., Abt. A., 4. pp. 1–162, pls. 1–28.
Seremeta, V. G. (1969): The Paleogene ostracods of the Ukraine. Izd. Univ. Lvov., pp. 1–274, pls. 1–21. (in russian).

Schornikov, E. I. (1974): To study of ostracods (Crustacea) from the intertidal zone of the Kurile Islands. Sborn. rab. Inst. Biol. Mor., Dalnevost. Nauchn. Centr. An. SSSR., 1. pp. 137–214, pls. 1–4.

Sönmetz – Gökcen, N. (1964): Notice sur le nouvel age détérminé par les ostracodes de la série a Congeria du Néogene des environs de Catalca (Thace). Bull-Mineral Res. and Explor. Inst. Turkey.
Foreign Ed. No. 63, pp. 47–59, pls. 1–2.

Strausz, L. (1962): A gánti eocén fauna ökológiai viszonyai (Über die paläoökologischen Verhältnisse der Eozänfauna von Gánt). Földt. Közl., 92, pp. 308–318.

Szőts, E. (1953): Magyarország eocén puhatestűi I. Gántkörnyéki eocén puhatestűek (Mollusques Eocenes de la Hongrie I. Les Mollusques Eocénes des environs de Gánt). Geol. Hung., Ser. Pal., 22. pp. 1–270, pls. 1–20.

Szőts, E. (1956): Magyarország eocén (paleogén) képződményei (L'Eocene (Paleogene) de la Hongrie). Geol. Hung., Ser. Geol., 9, pp. 1–320.

Triebel, E. (1950): Homöomorphe Ostracoden-Gattungen. Senckenbergiana, 31, pp. 313–330.

van Morkhoven, E. P. C. M. (1963): Post-Paleozoic Ostracoda, I–II. Elsevier, pp. 1–204; 1–478.

PLATE I.

Fig. 1. Cytherella (Cytherelloidea) gantensis n.sp. Left valve; Holotype.

Figs. 2 – 4. Bairdoppilata gliberti Keij.

Figs. 2 – 3.: Left valve

Fig. 4: Right valve

Figs. 5 – 9. Novocypris ? gantensis n.sp.

Figs. 5, 7, 9: Left valve

Figs. 6, 8: Right valve

Fig. 9: Holotype

Figs. 10 – 12. Pterygocythere jonesi (Méhes)

Figs. 10 – 11: Left valve

Fig. 12: Right valve

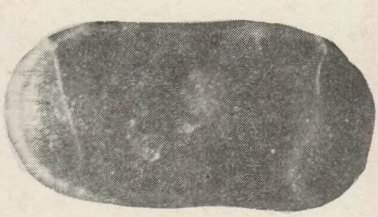

1

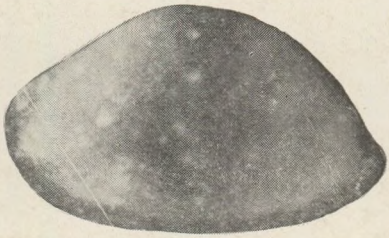

2

3

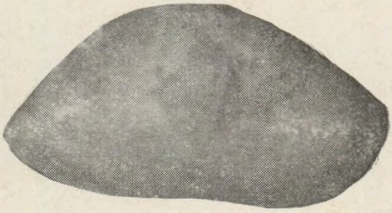

4

5

6

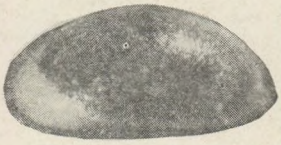

7

8

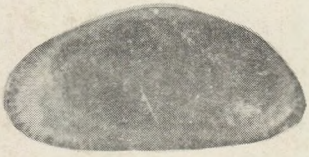

9

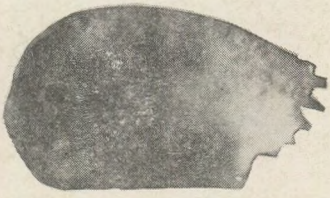

10

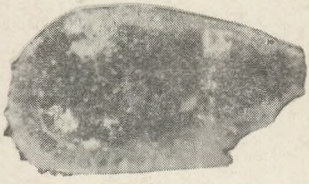

11

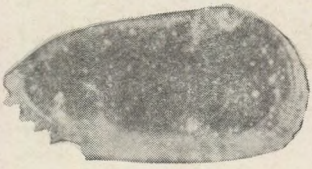

12

PLATE II.

Fig. 1. Monoceratina sp. Left valve

Figs. 2 – 4. Clithrocytheridea faboides gantensis n. ssp.

Fig. 2: Right valve

Figs. 3 – 4: Left valves

Fig. 4: Holotype

Figs. 5 – 7. Monsmirabilia triebeli (Keij)

Fig. 5: Right valve

Figs. 6 – 7: left valve

Fig. 8. Neocyprideis williamsoniana (Bosquet). Right valve

Figs. 9, 11, 13 – 14. Krithe bartonensis (Jones)

Figs. 9, 13: Left valve

Figs. 11, 14: Right valve

Fig. 10. Caudites monsmirabiliensis (Apostolescu). Right valve

Fig. 12. Paracytheridea gradata (Bosquet). Left valve

Figs. 15 – 17. Cytheridella ? gantensis n. sp.

Fig. 15: Left valve anterior, with the sulci

Fig. 16: Right valve; holotype

Fig. 17: Left valve

Fig. 18. Loxoconcha sp. Left valve

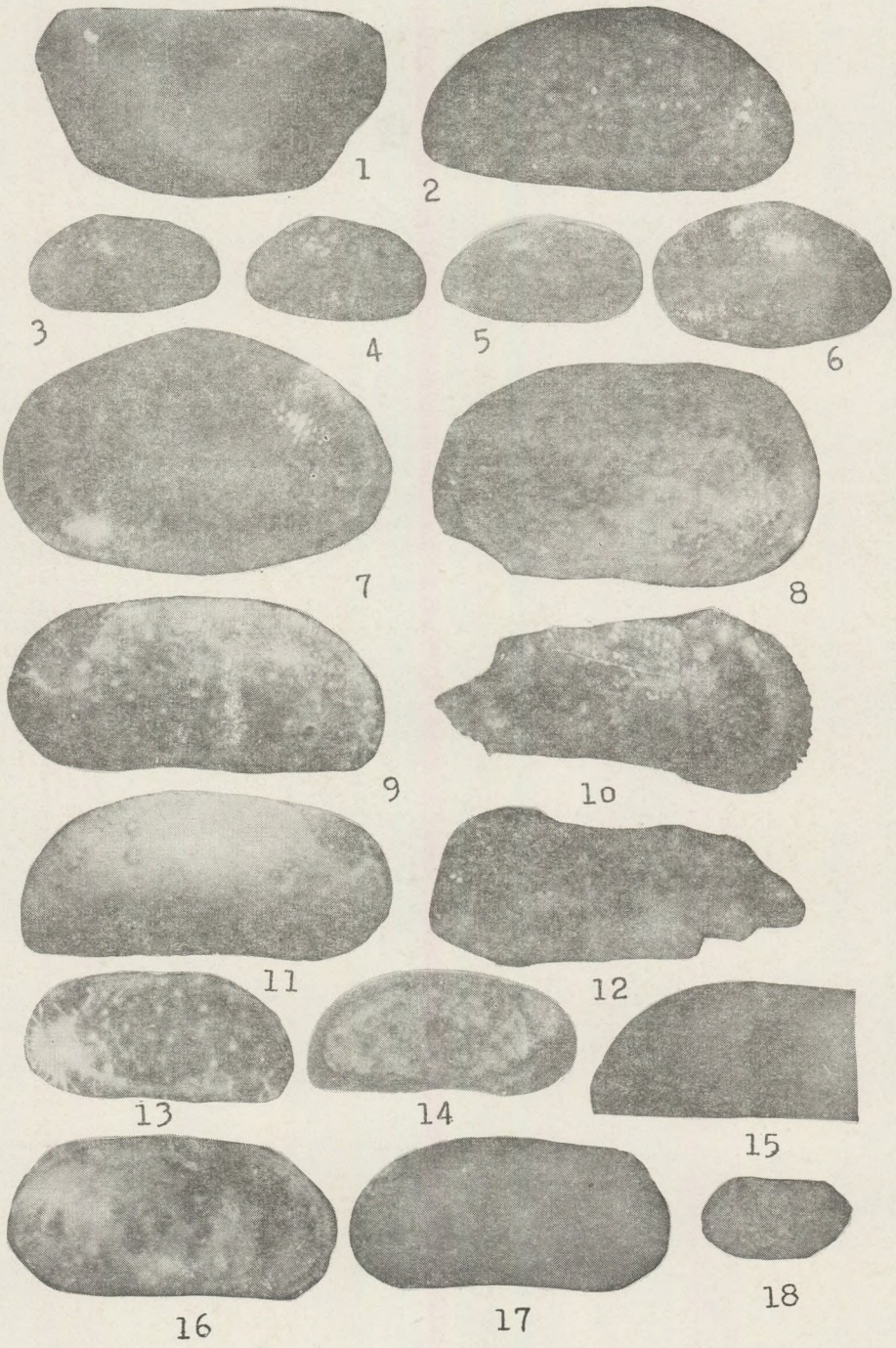
1
2
3
4
5
6
7
8
9
10
11
12
13
14
15
16
17
18

PLATE III.

Figs. 1—4. Schizocythere depressa (Méhes)

Figs. 1—3: Left valve

Fig. 4: Right valve

Figs. 5—8. Bladleya validornata hungarica n. ssp.

Figs. 1—2: Left valve

Figs. 3—4: Right valve

Fig. 1: Holotype

Figs. 9—11. Echinocythereis dadayana (Méhes)

Figs. 9—10: Left valve

Fig. 11: Right valve

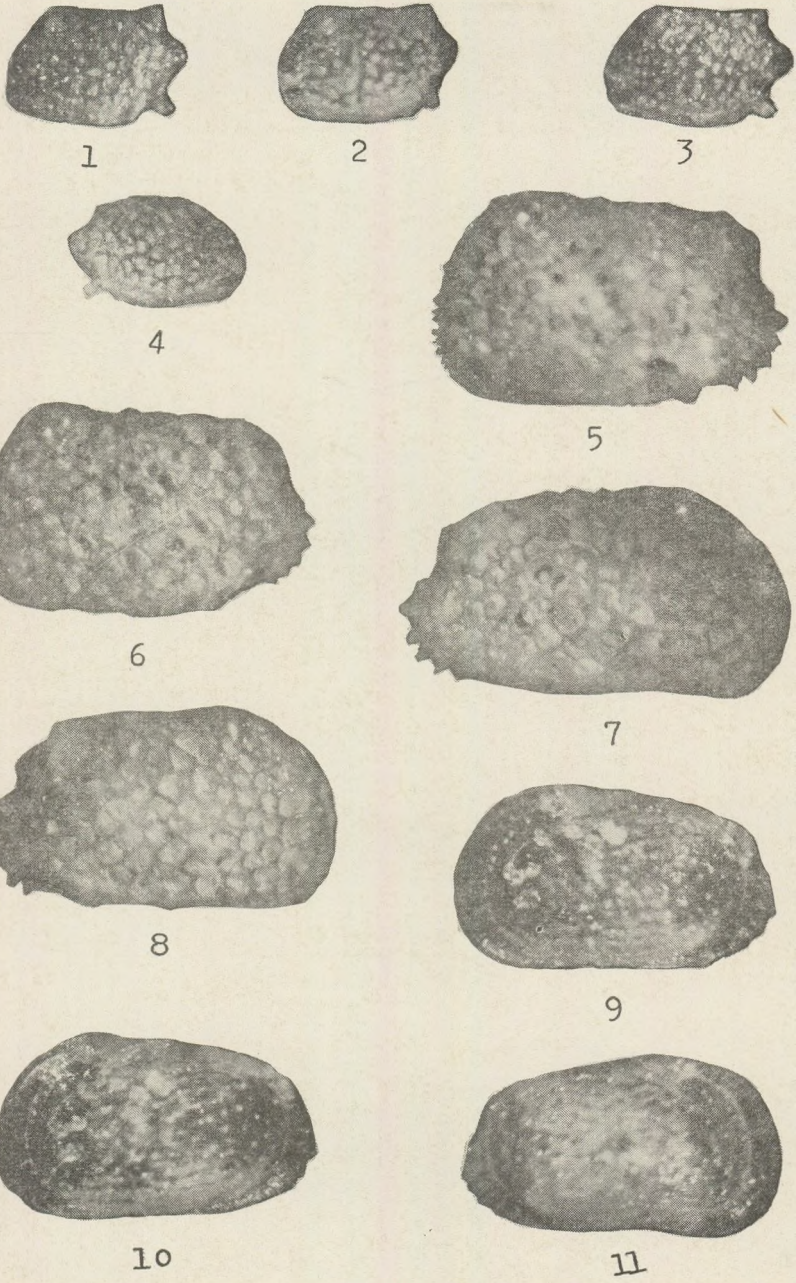
1
2
3
4
5
6
7
8
9
10
11

PLATE IV.

Figs. 1 – 2. Hermanites haidingeri paijenborchiana Keij

Fig. 1: Left valve

Fig. 2: Embryonal left valve

Figs. 3 – 6. Hermanites acuticosta gantensis n. ssp.

Figs. 3 – 4: Left valve

Figs. 5 – 6: Right valve

Fig. 3: Holotype

Figs. 7 – 10. Quadracythere angusticostata (Bosquet)

Figs. 7 – 8: Left valve

Fig. 9: Right valve

Fig. 10: Embryonal left valve

Figs. 11 – 13: Quadracythere vahrenkampi Moos

Fig. 11: Right valve

Fig. 12: Embryonal left valve

Fig. 13: Embryonal right valve

Figs. 14 – 17. Xestroleberis gantensis n. sp.

Figs. 14 – 15: Left valve

Fig. 14: Holotype

Fig. 16: Right valve

Fig. 17: Embryonal right valve

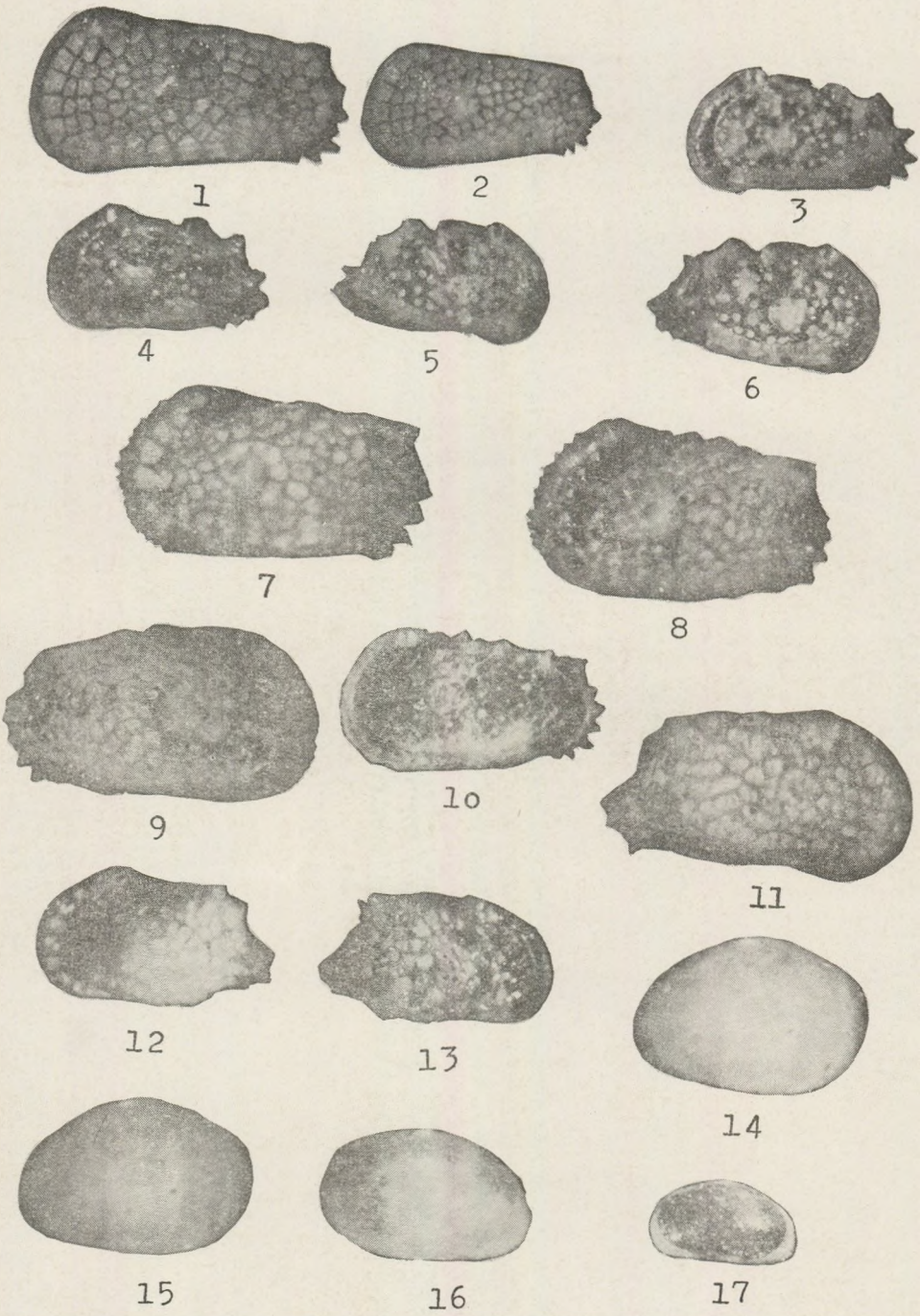
1
2
3
4
5
6
7
8
9
10
11
12
13
14
15
16
17

POSSIBILITIES AND METHODS OF INVESTIGATION OF FOSSIL RIVER BEDS

I. ORSOVAI

Department for Applied and Technical Geology, Eötvös University, Budapest

Received 15 October 1975

РЕЗЮМЕ

В системе добычи воды с береговой фильтрацией часто необходима точная локализация заполненных в недавнем геологическом прошлом русел рек, поскольку качество воды в таких местах существенно портится. Локализация положеиня русел может быть проведена с помощью следующих методов:

а) бурение по густой сетке
б) измерение геоэлектрuческого сопротивления
в) использование страрых карт
г) интерпретация крупномасштабных карт нивелирования
д) химический анализ воды
е) непосредственное исследование района при высоком уровне воды в реках и грунтовых вод
ж) детальный анализ растительности
з) исследование карт положения покрывающих слоев гравия
и) интерпретация данных аэрофотос'емок

В работе показана эффективность применения отдельных методов на примере исследования района острова Чепель, где были применены все вышеуказанные методы за исключением аэрофотос'емки.

Introduction

In the course of changes of the river bed the branches turned inactive will be disjoined and they will be filled by sediments becoming more and more fine grained going upwards from below. In the fine grained sediments much organic matter is contained, the anaerobic disintegration of which results in a reductive environment. As a consequence of this the oxigen content solved in the surrounding ground water falls below 20%, where the Fe^{2+} and Mn^{2+} ions go into solution.

It is therefore important to know precisely the places of the fossil river beds, as well as the spontaneous flow of the ground water, so that we could draw conclusion to the flow presenting itself on the occasion of a later water extraction.

Several investigation methods concerning the places of fossil river beds were studied by us on the Western side of Csepel-island and we will give here an evaluation of the methods, the possibilities and limits of their application.

The disjoined beds of the investigated area are not the disjointed mort-lakes of a meandering river, but they are the consequences of a slow flanking erosion from western direction and of the bed changes caused by floods, therefore they are mostly characteristically straight or their radii of curvature are very great.

Various methods of investigation of fossil river beds

These are:

a) By means of borings taking core-samples in a dense network one can get a very precise picture of the positions of one time beds, but the application of this method is very restricted owing to its expensivity of time and costs. It can be applied on a restricted area in the narrow surroundings of the planned water-producing project; furthermore it is practical to set up these in the early phase of the study – taking into account the traces found at the surface – for the detection of local features of the buried river beds. The basic dimension-parameter of the network can not surpasse the river width to be expected, because the borings made in a sparse net provides ill-proportionately less information, their results depend on chance and it may happen that we get a misleading paleogeographical picture.

b) On an area with known layering we can state the places of fossil river beds in general with a relatively high reliability by means of geo-electric resitivity measurements. The electric resistivity of the surrounding terrace gravel is 200 – 1000 ohmm, that of the silt filling the bed is 10 – 100 ohmm, so that the basic conditions of the resistivity mesurements are fulfilled. It may be disturbing that the smaller beds are not becoming deeply immersed into the gravel body, so that in every case one had to carry out a complete vertical electric sounding down to the depth of the impermeable substratum. A trouble difficult to be overcome is the circumstance, if the local ground water level coincides with the lower boundary of the list filling the bed. A further difficulty is that the wide bed at places can not be measured out with one central point, because the $\frac{\overline{AB}}{3}$ belonging to the $\overline{AB}$ max. equalling the bed width can surpasse by several times the depth of the impermeable substratum. In such a case it is practicable to carry out – besides the verical sounding – also a horizontal profiling and to chose the size of $\overline{AB}$ three times as long as the depth of the bottom layer. All these refer to a symmetrical Schlumberger electrode configuration.

c) Using old maps one can sometimes fix the state existing before the major human intervention (regulation of the bed), respectively one can state the natural changes from the oldest existing map (1528) up to the regulation of the bed (1850) from time to time and to clear the regularities of the variations.

Restrictions of the use of old maps are as follows: The changes of the river beds are recognisable only in broad lines, but the maps are not suitable – without other features – for the exact recognition of the past of limited areas. The cause of this lies – besides the inaccuracies of the one time surveys – in the scale and projection of the map. The scale is very small, it is not a decimal number (1 : 1440; 2880)

and it is not given explicitely in the text, and it is rarely given even graphically. The projection is very rarely given by a net and hardly mentioned in references, so that it is impossible to redraw the maps in Gauss-Krüger or stereographic projection. Thus, the ancient map is a good orientating tool for the character of the variations, but for an actual practical purpose it is only suitable together with other complementing factors.

As an example of what was said above we may mention the situation of the small islands in the branches of the Danube around the Csepel-island. In the main branch the islands did not change their position during the last 400 years (except for smaller sandbanks), only the river branches around them changed (the Háros–, Ercsi– and Rácalmás islands), while in the eastern (Ráckeve) branch – despite of the lower water transport – we encounter a vivid development, discontinuing and wandering of islands. Two major islands (Angyali and Kerek-sand bank) did not exist at all at the beginning of the XVIIIth century.

Another informative example is the case of the connection between the two branches of the Danube. On the map of Marsigli (1726) many complicated flowings through can be seen in SW direction from the Ráckeve-branch into the main branch. On the present contour maps of the gravel cover the beds show – owing to the isohypses constructed on the basis of insufficient data – just a reversed connection. Thus, using the Marsigli-map we succeeded to detect the real character of a phenomenon, while the modern, sketchy surveys were successful in determining, its exact spot.

d) Through the evaluation of large scale contour maps we are able to get useful data only on areas not having undergone topographic regularization and agricultural cultivation. This condition has been fulfilled in our case, because in the course of location of the dam trace in the last century they tried to leave the fossil beds on the flood area.

On the given length-profile we selected the contour line corresponding to the height above sea level of the highest water level and we carried out the marking off of the areas lower than this one, then for sake of checking we repeated the procedure using a contour level value lower by 1 and 2 meters: the basic bed picture has not changed in these cases. But the fixing of the local highest water level is not fully exact owing to the great distances of the water – gauges, nevertheless, if we take into account that on the given section of the Danube its mean fall is 7 cm/km and the contour lines follow each other with a height difference of 1 m, we can be sure that the error made by linear interpolation can not be too high.

e) By a local perambulation we can make more precise the picture assured by the contour map first of all in the case of a very high water level. In that case, namely, the fossil river beds will also be filled with water owing to the rule of the communicating vessels and such minute

depression of a few dm depth can be observed, which do not appear clearly on the contour map of 1 m line distance and also the local high water level can be observed with an unambiguous accuracy.
According to the observations of earlier years the water movement in the fossil beds follows the Danube level with a lag of 2 – 4 days, but it appears in all beds at the same time, independently of the distance from the Danube. According to our interpretation this indicates that the delay is not caused by the resistance of the communicating layers, but first of all by the bed-resistance of the Danube.
But because only the 1 – 2 days of the culmination can be used for such perambulation of the terrain, the method can serve only to make the picture obtained by the contour map more accurate and to clear some problematic data.

f) Water-chemical investigations may be expedient first of all on areas, where many old digged or bored wells are at disposal for taking water samples, but owing to their ancient structure the layering is not known. It is an experienced fact – it can be deducted also theoretically – that the silt of high organic content filling the fossil beds exhausts the solved oxigen-content of the water. The oxigen solved in water can be measured also directly, but it is advisable before the measurement to carry out a cleaning pumping and to make the measurement by means of an electrode which can be lowered into the well. We can draw an indirect conclusion to the presence of the fossil bed of its high mobile iron and manganese content too.
In case of water-chemical investigations we have also to take into account the direction and speed of a possible ground water flow; furthermore we have to consider that the waters of iron or manganese content can reach at a long distance by diffusion too. On the area under investigation is – according to our measurements – the ground water flow to be neglected, but the effect of diffusion is present.
A further important point of view is that during a measurement series no temperature differences during the time should be present, because these can alter in itself the oxigen content solved in the water.

g) We can obtain many useful informations also by a detailed evaluation of the biomass-production of the vegetation. The nutritive material content of the silt filling the bed is significantly greater, than that of the surrounding gravel and also its water household is better.
But it is very difficult to draw conclusions to the biomass-production – decomposed to small areal units – from forestry data, because the production data are averaging ones valid for larger territories, and the quantity of the biomass depends – besides the characteristics of the production area-largely also on the species of trees and on the cultivational methods.
According to our experience, however, a very good orientation can be obtained from the circumstance that the willow (Salix) can regenerate its wickers cut for osier culture from year to year i. e. the willow

wickers can be regularly exploited only over the fossil beds . This is an apparent phenomenon, which can be observed through a great distance.

h) From contour maps of the gravel covering (or substratum) we can get data for the area between the borings and openings by interpolation. But contour map can be constructed without ambiguity only in the possession of a sufficiently dense data network. We mentioned already the danger resulting from a conclusion drawn from insufficient data material on the occasion of the Marsigli map, which can lead to a picture contrasting the reality.

But, considering the fact that the surface of the gravel can be observed more simply and inexpensively, than other data of the layer series, therefore the contour map of the gravel covering possesses a high significance, if the fossil bed is to some extent immerged into a gravel body.

i) By the interpretation of aerial photos it is possible to detect buried river beds with great accuracy and reliability first of all on uncovered agricultural areas. On areas similar to that investigated by us, which have been afforested and intensively subjected to forestry cultivation, the simple aerial photo does not give much information.

Conclusions

For the accurate recognition of fossil beds having high organic material content and spoiling water quality several methods are at disposal, assuring different reliability and accuracy. Local conditions may decide, which of then can be applied; according to our opinion the more methods will be used in a harmony one with another, in a complex manner, the more we get a complete picture. When using several methods it is not the plurality principle that decides, whether on a given spot there was or not a river bed, but we have to accept the positive result of any method, if it is not in contradiction to our experiences. The idealized picture, namely, as outlined above does not furnish – owing to causes not to be detailed here – unequivocal result in every case. E. g. morphological elements and vegetation are not in contradiction one with another, but it happens frequently that they present themselves separately, owing to the human activity. At places an unsuccessful attempt of plant cultivation disrupted the original vegetation, on other spots, though the depressions have been filled out, the roots of the plants go down into the water and only a vegetation enduring these conditions can hold out permanently. The trials of several methods known well before as well as their coordination were carried out by us on the west-side of the Csepel-island on a flood area of 30 km^2. By the condensation of observations made at points we succeeded to make more precise the paleogeographical picture of the area, but all the methods can be extended to the east-side of the island, to the Ráckeve- branch of the Danube, where the higher urbanisation conceals to a greater extent the original state.

REFERENCES

Bayer, W. – Banscher E. (1976): Zur Erkundungsmethodik der Uferfiltratgewinnung Zeitschrift für Angewandte Geologie B. 22. H. 4.

Busch, K. F. – Luckner L. (1973): Geohydraulik, Leipzig

Gorelik, A. M. – Sacharowa M. P. (1952): Die Elektrososchürfung bei ingenieur-geologischen Untersuchungen, Berlin

Harold, L. J. (1966): Chemistry of the Iron-rich Sedimentary Rocks Data of Geochemistry 6th Ed. Chapter W.

Kovács, Gy. (1972): A szivárgás hidraulikája (Hidraulics of Filtration) Budapest

Marosi, S. (1955): A Csepel-sziget geomorfológiai problémái (Geomorphological Problems of Csepel-island) Földrajzi Értesítő IV. 3.

Orsovai, I. (1973): Study of Groundwater Replenishment in Natural Reservoirs Ann Univ. Sci. Bud. Sect. Geol Tom. XVII.

INFORMATIONSGEHALT DER NIEDERSCHLAGSREICHE VON BUDAPEST

F. RÁKÓCZI und F. SZIDAROVSZKY

Lehrstuhl für Meteorologie L. Eötvös Univ., Budapest
Lehrstuhl für Num. und Maschin Mathematik L. Eötvös Univ., Budapest
Einegegangen am 8. 4. 1976

РЕЗЮМЕ

В работе приводится разработанная авторами техника прогноза месячной величины осадка. Техника прогноза была разработана на основе использования количества информации в последовательности данных об осадке в территории Будапешта, а методика была проверена на данных, охватывающих 10-летний период. Полученные результаты указывают на то, что с помощью предложенной техники могут быть составлены прогнозы, достоверность которых больше чем случайных совпадений.

Bei der langfristigen Vorhersage der meteorologischen Elemente greift man auf die Geschehnisse der Vergangenheit zurück and man untersucht, welche Information die in der Vergangenheit beobachteten Zeitreihen für die Zukunft darbieten können [1, 3]. Der Grundgedanke solcher Versuche ist, dass in den Wettergeschehnissen gewisse Erhaltungs- und Rückkehr-Tendenzen vorhanden sind, und dass gewisse Zirkulationscharakteristiken zu denselben oder zumindest ähnlichen Resultaten führen.

Bei einer solchen Untersuchung von Zeitreihen müssen wir zuallerest feststellen, ob nicht das Einsetzen eines Ereignisses von dem Eintritt der vorangehenden Ereignissen vollständig unabhängig sei. Wenn das Vorhandensein eines Zusammenhanges, welcher in einer gewissen Anzahl der Fälle nicht zu stark sein könnte, erwiesen wird, dann können wir hoffen, dass aus einer Kenntnis der Vergangenheit für die Zukunft Wahrscheinlichkeitsaussagen gemacht werden können. Für die Erarbeitung solcher Zusammenhänge wendet man die *Korrelationsanalyse* oder andere *Methoden der Unabhängigkeitsuntersuchungen* an, es gibt aber auch solche Verfahren, die den Informationsgehalt dieser Zeitreihen untersuchen [3], bei denen eigentlich festgestellt wird, inwieweit sich das gegebene System an die Geschehnisse der Vergangenheit „zurückzuerinnern" fähig sei.

In der folgenden Studie werden die Monatssummen des Niederschlages von Budapest auf Grund der Beobachtungen der Jahre 1841–1960 untersucht [2].

Im Gange der Untersuchungen wird es erwogen, inwieweit die Niederschlagssumme eines gegebenen Monats die Niederschlagsverhältnisse

der nachfolgenden Monate beeinflusst, und wenn ja, dann in welchem Masse. Dabei wird eigentlich mit zwei Wahrscheinlichkeitsschemas X und Y gearbeitet, deren vorherige Realisationen bekannt sind. Die Auftrittswahrscheinlichkeiten der Ereignisse der Schemas X und Y sind uns bekannt, so dass wir über die endlichen Schemas

$$X = \begin{Bmatrix} X_1, & X_2, & \dots, & X_n \\ p_1, & p_2, & \dots, & p_n \end{Bmatrix}, \qquad Y = \begin{Bmatrix} Y_1, & Y_2, & \dots, & Y_n \\ q_1, & q_2, & \dots, & q_n \end{Bmatrix}$$

verfügen können. Der simultane Eintritt der Ereignisse X_i und Y_k sei mit $X_i\, Y_k$ $(1 \leqq i \leqq n,\ 1 \leqq k \leqq m)$ bezeichnet. Die Wahrscheinlichkeit des Eintretens des zusammengesetzten Ereignisses sei W_{ik}. So erhalten wir aus dem zusammengesetzten Ereignis ein neues endliches Schema

$$[X \cdot Y] = \begin{Bmatrix} X_1 \cdot Y_1, & X_1 Y_2, & \dots & X_1 Y_m \\ X_n \cdot Y_1, & X_n Y_2, & \dots & X_n Y_m \end{Bmatrix},$$

und die Matrix der entsprechenden Wahrscheinlichkeiten in der Form

$$[P(XY)] = \begin{Bmatrix} W_{11}, & W_{12}, & \dots, & W_{1n} \\ W_{n1}, & W_{n2}, & \dots, & W_{nm} \end{Bmatrix}$$

geschrieben werden kann.

Sind X uns Y unabhängig eines vom anderen, dann besteht der Zusammenhang

$$W_{ik} = p_i q_k .$$

Wenn aber die Schemas X und Y voneinander abhängig sind, dann haben wir an Stelle der obigen Produktregel folgendes zu setzen:

$$W_{ik} = p_i q_{ik} \qquad (1 \leqq i \leqq n, \quad 1 \leqq k \leqq m),$$

wobei q_{ik} die Wahrscheinlichkeit des Auftretens von Y_k im Schema Y bedeutet unter der Bedingung, dass im Ereignisraum X das Ereignis X_i erfolgte.

Auf Grund der angegebenen Schemas können die Entropien $H(X)$, $H(Y)$, $H(XY)$, sowie $H_X(Y)$ und $H_Y(X)$ abgeschätzt werden, d. h. die statistische Entropie des Ereignisses X und Y, die Entropie des zusammengesetztes Ereignisses, sowie die bedingten Entropien. Im Besitze dieser kann die Informationsgrösse $I\,(X,\ Y)$ abgeleitet werden, welche ein Mass darüber darstellt, welchen Einfluss das Ereignis X auf die Entwicklung des Ereignisses Y ausübt. Es ist bekannt, dass

$$H(X, Y) = H(X) + H_X(Y),$$

während das Informationsmass $I\,(X,\ Y)$ in der Form

$$I(X, Y) = H(Y) - H_X(Y)$$

geschrieben werden kann. Wenn man die zwei letzten Gleichungen addiert und eine Umordnung ausführt, kommt man zum Zusammenhang:

$$I(X, Y) = H(X) + H(Y) - H(X, Y),$$

welcher eine bequeme Möglichkeit für die Bestimmung der Informationsgrösse ermöglicht. Da im Unabhängigkeitsfall $H(X, Y) = H(X) + H(Y)$, die Abweichung von $I(X, Y)$ von Null stellt ein Mass der gegenseitigen Einwirkung eines der Ereignisse auf das andere dar.

Bei der Niederschlagsreihe von Budapest wurde, wie folgt, vorgegangen:

Die in jedem Monat des Jahres auftretenden Werte wurden in drei Wertgruppen: A_1, A_2, A_3 eingereiht. Im Gange der Eingliederung wurde das Intervall $A_{\min} - A_{\max}$ in 40 gleiche Teile aufgespaltet und die Warscheinlichkeit p_i der in die einzelnen Teilintervalle fallenden Werte untersucht, dann wurde die Summierung der Fälle soweit fortgesetzt, bis die Werte: $p_1 = 1/3$, $p_2 = 2/3$ und $p_3 = 1$ erreicht wurden. Die Werte der so bestimmten Konfidenzgrenzen – von Monat zu Monat – enthält die folgende Tabelle I.:

Tabelle I. Trennungspunkte der Intervalle

I	26.13 – 51.16
II	20.21 – 45.86
III	29.03 – 51.31
IV	36.78 – 63.90
V	52.64 – 86.98
VI	54.64 – 81.78
VII	38.27 – 65.74
VIII	35.44 – 62.54
IX	30.90 – 56.23
X	39.48 – 71.55
XI	41.24 – 67.62
XII.	36.43 – 57.87

Die Daten der Tabelle enthalten das mittlere Intervall, und wenn die Niederschlagswerte des betreffenden Monats sich zwischen diesen Grenzen befinden, wird der Monat als ein normaler Niederschlagsmonat betrachtet. Im Falle eines gegenüber der unteren Grenze niedrigeren Wertes haben wir es mit einem niederschlagsarmen Monat zu tun, während ein Monat mit einem Niederschlag über der oberen Grenze als niederschlagsreich angesehen wird.

Mit der Beachtung dieser Klassengrenzen haben wir Konfidenztabellen hergestellt und für jeden einzelnen Monat untersucht, welchen Einfluss ein jeder der vorangehenden Monate auf die Niederschlagsverhältnisse des in Rede stehenden Monats ausübt. Der Einflussgrad wurde durch die Informationsgrösse $I(X, Y)$ dargestellt. Die erhaltenen Werte der Informationsgrösse werden in der Tabelle II. gegeben:

Tabelle II.

Informationsgrössen I (X, Y) 10^4

	I	II	III	IV	V	VI	VII	VIII	IX	X	XI	XII
1	79	206	136	320	429	229	151	496	263	175	428	10
2	294	56	247	441	219	272	184	297	186	44	224	116
3	499	466	315	35	153	178	137	555	597	272	39	337
4	262	277	97	164	257	102	596	125	60	414	199	150
5	70	73	396	103	385	672	395	187	79	1213	36	72
6	481	209	236	633	71	191	190	258	323	230	292	351
7	310	46	148	244	18	351	177	294	384	97	381	640
8	183	307	48	248	244	348	176	53	119	82	204	225
9	244	253	70	483	901	273	141	325	124	497	169	424
10	134	74	205	138	141	233	342	982	59	340	441	356
11	131	255	238	102	86	538	29	384	157	282	239	62

Aus den Werten der Tabelle kann man feststellen, dass in der Mehrzahl der Fälle der Zusammenhang in der Zeitfolge der Niederschlagswerte zwar nicht zu eng ist, es gibt aber für jeden Monat wenigstens drei solche vorangegangene Monate, die einen Einfluss auf die Gestaltung der Niederschlagsverhältnisse des betreffenden Monats ausüben. Es ist auch ohne weiteres klar, dass sich in der Niederschlagszeitreihe auch stärkere Einflüsse, als eine einfache Erhaltungstendenz offenbaren, sonst müssten die maximalen Werte in den Kolumnen der Tabelle II. durch die Informationsgrössen der dem betreffenden Monat vorangegangenen Monate representiert werden. Es ist auch zu ersehen, dass das zeitliche System der Zusammenhänge recht kompliziert ist, aber in der etwa halber Anzahl der Fälle die Gestaltung der Niederschlagsverhältnisse am stärksten durch die Werte der dem betreffenden Monat vorangehenden 3 — 5 Monate beeinflusst wird, während in mehreren Fällen darf man auch die Verhältnisse der vorangehenden 9 — 10 Monate nicht ausser Acht lassen. In der ersten Hälfte des Jahres — bis zum Mai — verschiebt sich der die meisten Informationen bietende Monat nach rückwerts in der Zeit, während in den Monaten Juni und Juli eine Voranrückung, erfolgt, dann haben wir mit einem unregelmässigen Verhalten zu tun. Als der von der Vorgeschichte am besten beeinflusste Monat scheint Oktober zu sein, während März als am wenigstem beeinflusst erscheint.

In der Tabelle III. — nach einer Absonderung der Monate mit den grössten Informationswerten aus der Tabelle II. — wird zusammengefasst dass für betreffenden Monat die Niederschlagsverhältnisse welchen Monats im Laufe der Schätzung der Auftrittswarscheinlichkeit in Betracht gezogen werden. Die mit Stern bezeichneten Werte in der Tabelle representieren den entsprechenden Monat des vorangehenden Jahres.

Tabelle III.

Januar	(Okt.,*	Jul.,*	Jun.*)
Februar	(Nov.,*	Okt.,*	Jun.*)
März	(Okt.,*	Dez.,*	Jan.*)
April	(Okt.,*	Jul.,*	Febr.)
Mai	(Aug.,*	Apr.,	Dez.*)
Juni	(Jan.,	Jul.,*	Nov.*)
Juli	(März,	Apr.,	Nov.*)
August	(Okt.,*	Mai.,	Jul.)
September	(Jan.,	Febr.,	März.)
Oktober	(Mai.,	Jan.,	Jun.)
November	(Jan.,	Okt.,	Apr.)
Dezember	(Mai.,	März.,	Febr.)

Aus dieser Tabeller scheint es, als ob die Niederschlagsverhältnisse des Monats Oktober den grössten Einfluss auf die anderen Monate des Jahres ausübten, i. e. diese als die besten Prediktoren benutzt werden könnten. Innerhalb des Jahres scheinen die Verhältnisse des Januars die am meisten determinierenden Werte aufzuweisen. Für das Vorzeichen des Zusammenhanges gibt das Informationsmass – seiner Definition entsprechend – keine Auskunft, so dass für die Klärung der Frage noch andere Indikatoren in Betracht genommen werden müssen. In unserem Falle werden wirt im Laufe des vorzuführenden Schätzungsverfahrens die sich auf das Vorzeichen des Zusammenhanges beziehenden Kenntisse nicht berücksichtigen, da wir nur daran interressiert sind, ob der betreffende Monat für den in Rede stehenden Monat informativ sei oder nicht. Aus den Daten der Tabelle ist es zu ersehen, dass zwischen den monatlichen Niederschlagsdaten ein verwickelter, keine einfache Markov-Kette bildender Zusammenhang anzunehmen sei. Es sei bemerkt, dass die erwähnten Zusammenhänge zwar nicht zu stark sind, sie scheinen aber genügend ausgesprochen dafür zu sein, um mit ihrer Hilfe im Besitze der Vorkenntnisse Aussagen für das Eintreten des Freignisses treffen zu können.
Das hier vorzuführende klimatologische Vorhersage – Verfahren benutzt als Prediktor die in der Tabelle III. figurierenden Werte. Im Laufe der Ausarbeitung des Verfahrens wurden für jeden Monat die Grössen A_k und B_k ($1 \leqq k \leqq 12$) bestimmt, die die Daten des betreffenden Monats in drei Gruppen teilen so, dass die Intervalle $X < A_k$, $A_k \leqq X \leqq B_k$, $X > B_k$ eine gleiche Anzahl von Beobachtungsdaten aufweisen. Die entsprechenden A_k, B_k – Werte sind in der Tabelle I. enthalten.
Im Laufe des Vorhersageverfahrens strebten wir nicht nach einer numerischen Abschätzung der monatlichen Niederschlagssumme, sondern wir wollten die Wahrscheinlichkeit anzugeben dafür dass die Monatssumme des Niederschlages kleiner als A_k ausfällt, sich zwischen A_k und B_k befindet, oder aber grösser als B_k sei.
Das Verfahren kann wie folgt zusammengefasst werden. Der Index der in die Vorhersage einbezogenen Monate sei mit $i_1, i_2, \ldots, i_r$ bezeichnet, k soll den Monat angeben, für welchen die Vorhersage ausführt werden soll.

1. Wir untersuchen es für $i = i_1, i_2, \ldots, i_r$, dass die aktuelle Angabe des i-ten Monats in welches der Intervalle $(-\infty, A_i), [A_i, B_i), [B_i, \infty)$ fällt.

2. Dann werden aus der beobachteten Datenreihe die Werte von Jahren aufgesucht, bei denen die Niederschlagssummen der $i_1, i_2, \ldots, i_r$-ten Monats einer nach dem anderen in dasselbe Intervall zu liegen kommen, wie im Falle des Vorhersagemonats.

3. Auf Grund dieser Jahre errechnen wir die Anzahl jener, wo die Niederschlagssummen der k-ten Monats in die Intervalle $(-\infty, A_k)$, $[A_k, B_k)$, $[B_k, \infty)$ fallen und approximieren die gesuchten Wahrscheinlichkeiten durch die relative Häufigkeiten.

Bei der Anwendung dieses Verfahrens müssen wir bei der Wahl des Parameters r eine doppelte Tendenz in Betracht nehmen. Wenn r gross ist, dann nehmen wir die Ausführung der Vorhersage auf Grund von mehreren Informationen vor. Da im Falle von r Prediktoren gibt es 3^r Fälle für die Verteilung der Daten an die drei Teilintervalle, die Anzahl der im zweiten Schritt angetroffenen Daten zu gering ausfallen und die Abschätzung der gesuchten Wahrscheinlichkeiten mit Hilfe der relativen Häufigkeiten zu ungenau sein wird. Wenn aber der Wert von r relativ klein gewählt wird, dann verlieren wir etwas an Information, demgegenüber aber werden wir im zweiten Schritt im allgemeinen mehr entsprechende Datenreihen antreffen, so dass die Wahrscheinlichkeiten im Gegensatz zum vorigen Fall durch die relativen Häufigkeiten besser approximiert werden können. Bei der Wahl des optimalen r — wertes sollen diese zwei Gesichtspunkte beachtet werden.

Die Monatssummen des Niederschlages von Budapest wurden von 1841 bis 1960 benutzt. Unser Vorhersageverfahren wurde für den Fall der nächstfolgenden zehn Jahre angewendet, um eine Kontrolle zu erhalten, und die Vorhersagen zu verifizieren. Beim Verfahren probierten wir alle drei Werte $r = 1, 2 =$ und $r = 3$ aus. Weiterhin fürten wir die Vorhersage auch *so* aus, dass wir — die für jeden Monat berechneten Kontingenz-Tabellen anwendend — die Eintritt- wahrscheinlichkeiten der einzelnen Ereignisse in eine Rangordnung einreihten. In diesem Falle wurde als höchstwahrscheinlicher Wert diejenige Kategorie genommen, die im Laufe der 11 Vorhersagen am häufigsten den ersten Platz belegte; wenn aber so keine Entscheidung getroffen werden konnte, so beachteten wir auch den Umstand, mit welcher Häufigkeiten die betreffende Kategorie den zweiten Platz in der Rangordnung eingenommen hat.

Die Auswertung der Vorhersagen ist in der Tabelle IV. dargestellt.

Tabelle IV.

	Übereinstimmung	Fehlschlag von einer Kategorie	Fehlschlag mit zwei Kategorien
$r = 1$	42	47	31
$r = 2$	43	50	27
$r = 3$	53	43	24
	49	51	20

In der ersten Kolonne der Tabelle finden wir die Anzahl der Fälle, wo die vorhergesagten und eintreffenden Kategorien übereinstimmen. In der zweiten Kolonne wurde die Anzahl der Fälle gegeben, in welchen die vorhergesagte Kategorie in den neben der tatsächlich eingetroffenen Kategorie liegenden Ereignissraum führte. Die dritte Kolonne enthält die Anzahl der erfolglosen Vorhersagen. In der letzten Reihe der Tabelle wurden die Resultate der auf Grund der Wahrscheinlichkeitsrangordnung getroffenen Vorhersagen angeführt.

Ohne jedwede Vorhersage und ohne Benutzung der Zeitreihen sind die Wahrscheinlichkeiten eines Resultats vom ersten, zweiten, bezüglicherweise dritten Typ, eine nach der anderen: 0,333, 0,444, 0,222, da in die erste Gruppe die Ereignisse 1 – 1, 2 – 2, 3 – 3, in die zweite die Ereignisse 1 – 2, 2 – 3, 2 – 1 und 3 – 2, und in die dritte die Ereignisse 1 – 3 und 3 – 1 eingereiht wurden. Bei den von uns untersuchten 120 Fällen im Laufe der Vorhersage wächst die Anzahl der Übereinstimmungen mit dem Anwachsen der Informationsmenge, während die Anzahl der fehlgeschlagenen Prognosen abnimmt. Da bei vielen praktischen Entscheidungen als eine nützliche Information gilt die Angaben dessen, dass im gegebenen Monat eine durchschnittliche (mittlere Kategorie), eine sich unter dem Durchschnitt befindende oder aber eine überdurchschnittliche Niederschlagsmenge zu erwarten sei, so sollte die Anwendung in der langfristigen Vorhersage neben anderen, manchmal viel komplizierteren Verfahren erwogen und die Methode in die tägliche Praxis eingeführt werden.

LITERATURA

1. Nyberg, A. (1975): An experiment in forecasting monthly mean temperature in Stockholm. Tellus 27, No. 1. pp. 34 – 37.
2. Kakas, J. (Editor): Klimaatlas von Ungarn II. Publishing House of the Hung. Acad. of Sciences, Budapest.
3. Rákóczi, F. – Szidarovszky, F. (1976): Die Bedeutung von Zeitreihen bei der langfristigen Wettervorhersage Időjárás 80. 5, pp. 292 – 294

THERMAL INVESTIGATION OF SYNTHESIS OF PEROVSKITE

A. M. ABDEL REHIM*
Institute of Mineralogy, ELTE University, Budapest

S. O. KHALIL
Department of Geology, Alexandria University, Egypt.

Received: 12 March 1974

ABSTRACT

Perovskite is found in some contact metamorphosed impure limestone. Also it occurs as an accessory mineral in a wide variety of undersaturated rock types, including potassic lavas and alkali pyroxenites. Little is known concerning the thermal condition of formation of perovskite. The present work represents a thermal investigation of synthesis of perovskite by sintering of rutile with calcite in presence of graphite by using derivatograph. The data obtained indicate that complete sintering takes place at 970°C with the formation of orthorhombic perovskite. Also the results of the differential thermal analysis and *X*-ray diffractometric study of sintering products have been reported.

РЕЗЮМЕ

Нами был найден перовскит в некоторых загрязненных, метаморфозированных, известняковых образцах. Этот минерал также появляется в виде случайной компоненты в широком классе насыщенных пород, включительно калиевых лав и алкали пироксенитов. Нам мало известно относительно термических условий образования пероксита. В настоящей работе приводятся результаты по исследованию термических условий синтеза перовскита и кальцита при наличии графита. При этом нами был использован дериватограф. Данные указывают на то, что образование туфы имеет место при температуре 970°C и образуется ортохомбический перовскит. Результаты дифференциального термического анализа и дифрактометрического исследования с помощью X-лучей также приводятся.

Introduction

Perovskite occurs as an accessory mineral in basic and alkaline rocks and is often found as a deuteric mineral in such rocks, commonly in association with melilithe leucite or nepheline.

It has been recorded also from a diabase-porphyrite where it is considered to be pseudomorphous after ilmenite. Perovskite is found in some contact metamorphosed impure limestones, where often it occurs as the cerium or niobium-rich variety. At the dolerite limestone contact of Scawt Hill, Northern Ireland, perovskite occurs both in the hybrid rock formed by assimilation of carbonate and as a constituent of the exogenous contact zone, where it is associated with larnite, melilithe, spinel and wollastonite. (15).

* Present address: Geology Dept., Alexandria University.

Little is known concerning the thermal condition of formation of perovskite. This present work reports a thermal investigation of synthesis of perovskite by sintering of rutile with calcite in presence of graphite by using derivatograph. Also, the results of the differential thermal analysis and *X*-ray diffractometric study of sintering products are reported.

Rutile and anatase did not give any thermal reaction during heating. At 200 – 900°C, perovskite lattice remains rhombic, but becomes more symmetrical. It fuses congruently at 1915°C. The thermogram of calcite shows a sharp and large exothermic peak at 880°C, which represents its dissociation to calcicoxide and liberation of carbon dioxide. Several data can be found on the thermal character of rutile, anatase, perovskite and calcite in the literature (1 – 9, 13, 14, 16, 17).

Experimental Work

This research was carried out with rutile concentrate, having chemical composition and X-ray analysis as given in tables (1) and (2) respectively.

Chemical composition of Rutile concentrate

Table (1)

Chemical component	Content, %
TiO_2	95.84
SiO_2	1.80
Al_2O_3	0.78
Fe_2O_3	0.61
V_2O_5	0.32
MnO	0.05

The studied rutile is reddish-brown in colour. Rutile is associated with some mineral impurities such as zircon, quartz, garnet, corundum, amphiboles and others in fine grains and in small amount. None of the contaminants was detected by *X*-ray analysis, therefore an individual mineral may be present as a major constituent which is in good agreement with the mineralogical study.

The *X*-ray analysis of the studied rutile, table (2) shows that its parameters of crystal lattice are consistent with literature data. The *X*-ray powder diffraction data of the used calcite are given in table (3).

Table (2)

X-ray powder diffraction data of rutile

d(Å) ASTM	d(Å) Observed	I ASTM	I Observed	h k l
3.25	3.249	100	100	1 1 0
2.477	2.487	50	50	1 0 1
2.297	2.297	8	6	2 0 0
2.188	2.188	25	25	1 1 1
2.054	2.053	10	9	2 1 0
1.687	1.689	60	58	2 1 1
1.624	1.626	20	20	2 2 0
1.480	1.481	10	10	0 0 2
1.453	1.453	10	9	3 1 0
1.360	1.362	20	22	3 0 1
1.347	1.349	12	12	1 1 2

Table (3)

X-ray powder diffraction data of calcite

d(Å) ASTM	d(Å) Observed	I ASTM	I Observed	h k l
3.86	3.863	12	11	1 0 2
3.035	3.035	100	100	1 0 4
2.845	2.843	3	3	0 0 6
2.495	2 493	14	16	1 1 0
2.285	2.284	18	22	1 1 3
2.095	2.095	18	18	2 0 2
1.927	1.926	5	6	2 0 4
1.913	1.913	17	18	1 0 8
1.875	1.875	17	22	1 1 6
1.626	1.626	4	4	2 1 1
1.604	1.604	8	9	2 1 2
1.587	1.586	2	1	1. 0. 10
1.525	1.524	5	5	2 1 4
1.518	1.518	4	3	2 0 8
1.510	1.509	3	2	1 1 9
1.473	1.472	2	2	2 1 5
1.440	1.440	5	(	3 0 0
1.422	1.423	3		0. 0. 12

Techniques of Work:

Starting materials are usually consisted of rutile mixes. Calcite and graphite are used in mixes in particular amounts. Mixes were processed by repeated grinding in an automated agate morter and sieving till all the powder pass through 0.06 mm sieve and pestle for one hour to achieve homogeneity.

Apparatus:

Experiments were carried out in ceramic crucible, heated in an electrical furnace under suction of carbon dioxide. The character of the reaction of sintering of rutile with calcite in presence of graphite was studied by thermal analysis using P a u l i k F., P a u l i k J. and E r d e y L. (MOM) derivatograph (11, 12). This apparatus records simultaneously four thermal curves: (T) the change of temperature of sample, (DTA) differential thermal analysis, (TG) thermogravimetric, (quantitatively in mg) and (DTG) derivative thermogravimetric one a single sample under controlled conditions. DTA and temperature measuring thermocouples are Pt/Pt-Rh wires. Ceramic crucible and a ceramic sample holder were used. Alumina, calcined at 1000°C, was used as a reference material. The parameters during tests were as follows: weight

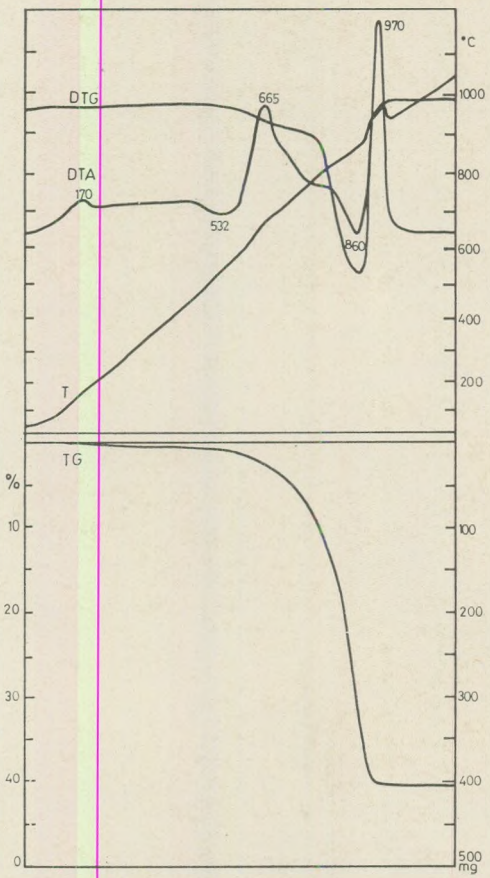

Fig. 1: Derivatogram of rutile sintering with calcite in presence of graphite. Weight of sample 1000 mg. Heating rate 10 °C/min.

of sample 1000 mg, T – 1200°C, DTA – 1/3, DTG – 1/5, TG – 500 mg and heating rate 10°C per minute. All determinations were carried out in an atmosphere under suction of carbon dioxide.

Phase Identification and Characterization:

The end products of sintering of rutile with calcite were studied both microscopically and by *X*-ray analysis. Perovskite is colourless to dark brown in thin section and has a very high relief, anisotropic.

X-ray Procedure:

A Siemens crystalloflex diffractometer was used with nickel filtered copper radiation. Exposure was one hour and scanning speed was 1° 20 per minute, at 1 cm per minute chart speed. Intensities were collected to maximum 20 = 65°. The sensitivity of the experiment, was 4×10^4 impl./min., and the statistical error was 1.5%.

Results and discussion

For studying the influence of rutile on the thermal behaviour of calcite, and the formation of perovskite, DTA experiments were carried out using calcite in amount 150% of theoretical value. The obtained derivatogram was evaluated on the basis of literature data with trial to explain the reactions which may be connected to certain peaks of DTA curve, and by comparing it with that of calcite and other components in the mix. The small and wide endothermic peak at 532°C may be due to the presence of some mineral impurities with rutile. The exothermic peak at 665°C may represent the burning of graphite and the combustion of volatiles. This is accompanied by ash arp decrease in weight (TG). The *X*-ray powder diffraction pattern shows the first appearance of perovskite above 665°C. The large endothermic peak at 860°C, represents the intensive dissociation of calcite and probably the reaction between the resulted calcium oxide and rutile. This process is connected with a remarkable decrease in weight (TG) due to the removal of carbon dioxide. According to the thermal curve of this mixture, the beginning of decomposition of calcite follows directly the end of exothermic reaction.

The sharp and large exothermic peak at 970°C may be due to the intensive reaction between rutile and the dissociated calcite. The reaction of formation of perovskite follows immediately the endothermic reaction of dissociation of calcite. The sinterting of rutile with calcite results in the production of orthorhombic perovskite. Its *X*-ray powder diffraction data are given in table (4). The *X*-ray data of synthetic mineral are consistent with those of natural perovskite.

Table (4)

X-ray powder diffraction data of Perovskite

d(Å) ASTM	d(Å) Observed	I ASTM	I Observed	h k l
3.824	3.826	14	20	1 0 1, 2 0 0
3.423	3.426	3	5	1 1 1
2.719	2.719	40	50	2 0 0
2.701	2.700	100	100	1 2 1, 0 0 2
2.563	2.565	1	2	2 1 0
2.428	2.430	1	2	2 0 1
2.413	2.412	2	4	1 0 2
2.313	2.308	4	6	2 1 1
2.303	2.304	7	10	0 3 1
2.217	2.219	6	9	2 2 0
2.201	2.204	4	8	0 2 2
2.121	2.123	2	4	1 3 1
2.050	2.049	2	4	2 2 1
2.040	2.043	1	2	1 2 2
1.911	1.911	50	80	0 4 0
1.860	1.883	2	2	2 3 0
1.856	1.858	3	4	2 1 2
1.757	1.784	1	1	2 3 1
1.752	1.752	1	1	1 3 2
1.746	1.748	1	1	0 1 3
1.719	1.719	2	3	3 0 1
1.710	1.712	3	5	2 2 2, 1 4 1
1.703	1.702	2	3	1 0 3
1.676	1.676	3	4	3 1 1
1.663	1.664	1	1	1 1 3
1.567	1.568	14	22	3 2 1
1.563	1.563	16	25	2 4 0
1.557	1.558	25	30	0 4 2
1.529	1.532	1	1	2 3 2
1.498	1.501	1	1	1 4 2, 2 0 3
1.470	1.475	1	2	0 5 1, 2 1 3
1.466	1.468	1	1	0 3 3

Determination of thermodynamic constants

Before studying the conditions of formation of perovskite from the reaction of rutile with calcite, an attempt was carried out for calculation of its thermodynamic constants. The following thermodynamic data were used in calculation: ($\Delta F°$), standard free energy of formation of perovskite, rutile and calcium oxide are − 376.517, −212.559, and − 144.352 Kcal/mol. respectively.

The reaction of formation of perovskite from its components may be represented as:

$$TiO_2 + CaO \longrightarrow CaTiO_3$$

The standard free energy of the reaction:

$$\Delta F^{\circ}_{\text{reaction}} = \Delta F^{\circ}_{\text{perovskite}} - \Delta F^{\circ}_{\text{rutile}} - \Delta F^{\circ}_{\text{CaO}}$$
$$= -376.317 + 212.559 + 144.352$$
$$= -19.606 \text{ Kcal/mol.}$$

The equilibrium constant of the reaction may be calculated from the equation at 25°C:

$$\log K = \frac{-\Delta F^{\circ}}{4.575 \times 298} = -0.000733\, \Delta F^{\circ}$$
$$= 0.000\,733 \times 19\,606 = 14.371$$
$$K = 2.35 \times 10^{14}$$

The equilibrium constant is large and the reaction of formation of perovskite may thus be practically considered as irreversible.

For studying the effect of temperature on the efficiency of perovskite formation, some runs were carried out using rutile mixes with calcite in excess amount 50% and graphite 10% of rutile charge at different temperatures, ranging from 665.700 up to 970°C during two hours.

From the obtained result (Table 5), it is shown that the efficiency of titanate formation sharply increases with temperature. The products of sintering of these runs were identified both microscopically and by *X*-ray diffractometer. By microscopic examination of this reaction of the products of sintering at 665, 700°C considerable number of rutile grains were detected with few fine grains of perovskite. This gives good idea about the incomplete sintering. As the temperature of sintering increases, the amount of perovskite increases. At 970°C the reaction between rutile and calcite takes place completely. At such temperature only few relict grains were detected in matrix of perovskite.

Table (5)

Effect of temperature on sintering

Temperature, %	Efficiency of sintering, %
700	30.9
800	72.6
860	90.2
970	98.8

The *X*-ray powder diffraction pattern of the end product of sintering at 970 °C is shown in figure (2). It can be observed that rutile peaks completely disappeared in such product representing the complete sin-

tering. The *X*-ray peaks of perovskite are narrow and intense suggesting good crystallinity. The microscopic study of the product phases of rutile sintering with calcite is in good agreement with *X*-ray diffractometric study.

From the above mentioned thermal investigation, the reaction of sintering of rutile with calcite takes place completely at temperature above 860°C. The sintering results in the formation of orthorhombic perovskite.

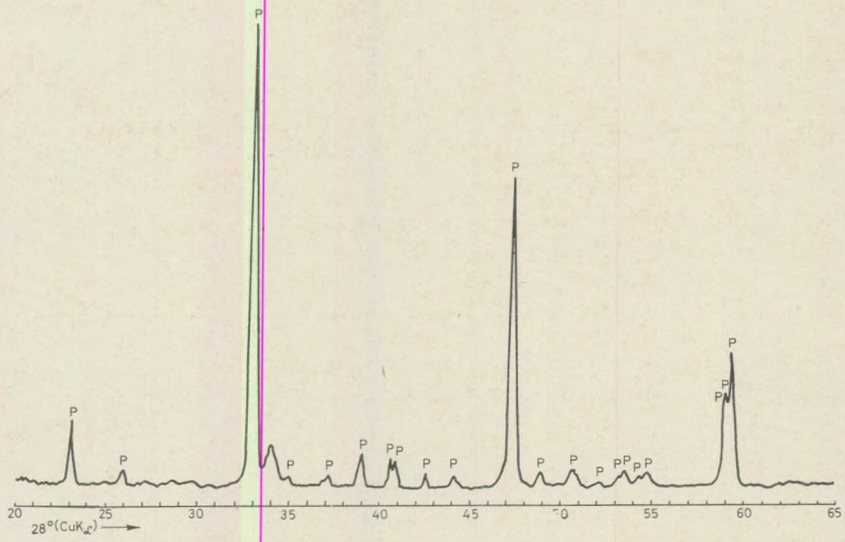

Fig. 2: *X*-ray powder diffraction pattern of the end product of sintering of rutile with calcite in presence of graphite at 970°C

Conclusion

The thermal study of the reaction between rutile and calcite has revealed that complete sintering takes place at 970°C with the formation of orthorhombic perovskite. Perovskite can also be formed at lower temperature above 700°C but it needs long time. The microscopic study and *X*-ray diffraction data of synthesised perovskite are in good agreement with the natural mineral.

Acknowledgments:

Professor Dr. J. Kiss is thanked for providing the facilities for the work to be carried out in the Institute of Mineralogy ELTE University, Budapest, All the member of the staff are also acknowledged.

REFERENCES

1. Coughanour, L. W., Roth, R. S. (1954): De Presse V. A., U. S. Nation. Bur. Stand., J. Research, V. 52, N. 1, pp. 37.
2. Deer, W. A., Howie, R. A., Zussman, J. (1965.): Rock forming minerals. V. 5, Non-silicates, Longmans.
3. Garrels, R. M., Thompson, M. E., Siever, R. (1960): Amer. Jour. Sci., N. 258, pp. 402–418.
4. Houldsworth and Cobb (1924.): Trans. Brit. Ceram. Soc, N. 22, pp. 111,, 1923 and N. 23, pp. 279.
5. Ivanova, V. P. (1961): Thermograms of minerals. Zapisky Vsiusauznova Mineralogishskova Obshestva, N. 1, pp. 50–90.
6. Kay, H. F., Bailey, P. C. (1957): Acta Cryst., N. 10., pp. 219.
7. Langmuir, D.: (1968): Geochemica Cosmochem. Acta, N. 32, pp. 835–851.
8. Mackenzie, R. C. (1970): Differential thermal analysis. V. 1, Fundamental Aspects, Academic Press, London, New York.
9. Mackenzie, R. C. (1962.): „Scifax Differential Thermal Analysis Data Index", Cleave-Hume Press, London.
10. Obrushev, S. 1(923.): Trans. Inst. Econ. Min. Petr. 2 „Lithogaea", Moscow, N. 1. (M. A. 2–397).
11. Paulik, F., Paulik, J., Erdey, L. (1958.): Z. Anal. Chem., N. 160, pp. 241.
12. Paulik, F., Paulik, J., Erdey, L. (1966): Derivatography. A complex method in thermal analysis, Talanta, V. 13, pp. 1405–1430.
13. Schuiling, R. D., Vink, V. W. (1967): Geochemica Cosmochemica Acta, V. 31, N. 22,pp. 3399– 3423,
14. Tayler, R. W., Schmalzried, H. (1964.): Jour. Phys. Chem, N. 68, pp. 2444–2449.
15. Tilley, C. E. (1929.): Antrim. Min. Mag., V. 22, pp. 77.
16. Tshokhorov, F. V. (1967): Minerals Handbook, V. II, Part 3, Multiple oxides-titanates, niobates, tantalates, antimonates and hydrozides. Izdatelstva Nauka, Moscow.
17. Van Der Manel (1956.): Amer. Min., N. 41, pp. 222.
18. Zelikman, A. N., Samsonov, G. V., Krein, O. E. (1964.): Metallurgy of rare metals. Izdatelstva Metallurgia.

INDEX

A kiadásért felelős: Az Eötvös Loránd Tudományegyetem rektora. – A kézirat nyomdába érkezett: 1976. október. – Megjelent: 1977. június – Terjedelem: 13,5 A/5 ív. – Példányszám: 800 – Készült: monószedéssel, íves magasnyomással az MSZ 5601–59 és az MSZ 5602–55 szabvány szerint
76.1092. Állami Nyomda, Budapest